Graduate Theses and Dissertations

Iowa State University Capstones, Theses and Dissertations

2010

An investigation of design alternatives for 328-ft (100-m) tall wind turbine towers

Thomas James Lewin
Iowa State University

Recommended Citation

An investigation of design alternatives for 328-ft (100-m) tall wind turbine towers

by

Thomas James Lewin

A thesis submitted to the graduate faculty
in partial fulfillment of the requirements for the degree of
MASTER OF SCIENCE

Major: Civil Engineering (Structural Engineering)

Program of Study Committee:
Sivalingam Sritharan, Major Professor
Fouad Fanous
Partha Sarkar

Iowa State University
Ames, Iowa
2010

TABLE OF CONTENTS

LIST OF TABLES

LIST OF FIGURES

ACKNOWLEDGMENTS

First and foremost, I would like to thank my beautiful wife-to-be, Charlotte Richter, for her support during my time as a graduate student. Secondly, I would like to thank my parents, Kurt and Chris Lewin, as well as my sister, Katie Tschida. I would have never made it to this point without their love and guidance. Additionally, I want to acknowledge Dr. Sri Sritharan for his expert advice during my research, as well as his excellent teaching. I would also like to recognize Dr. Fouad Fanous for his assistance during the completion of this project and Dr. Partha Sarkar for serving on my committee. Credit for all conceptual UHPC tower renderings in this thesis should be given to Doug Hartwell. This project was made possible through the support of Dr. Sritharan's Wilson Endowed Professorship.

ABSTRACT

As wind turbines are continued to be placed at higher elevations, the need for taller wind turbine towers becomes necessary. However, there are multiple challenges associated with extending the currently used 262-ft (80-m) tall tubular steel towers to greater elevations. In this context, alternative tower designs and/or construction materials, including the use of concrete and Ultra-High Performance Concrete (UHPC), are explored for a wind turbine tower with a 328-ft (100-m) hub height. Given the lack of existing documents for designing wind turbine towers, the current design practice for wind turbine towers and applicable design code of practice are examined and the characteristics of UHPC are reviewed. Designs for a 328-ft (100-m) tubular steel, concrete shell, UHPC Shell, and UHPC Lattice tower are completed and the benefits and challenges associated with these towers are discussed. Both UHPC tower designs are shown to be practical alternatives to steel towers due to their efficient use of material. Although no detailed cost evaluation was completed, the UHPC Lattice tower concept was found to be the most attractive as this design was formulated to increase the tower height while reducing construction, transportation, site development, and erection costs. Furthermore, it provides a variety of options for bracing the tower along its length. Consequently, the UHPC Lattice tower concept is further evaluated through the use of finite element analysis and its design was completed using UHPC members with hollow sections as bracing elements.

1   INTRODUCTION

1.1   "20% Wind Energy by 2030"

With the growing cost of fossil fuels and their increasingly recognized impact on the Earth's atmosphere, the production of renewable energy is on the rise (Renewable Energy Policy Network for the 21st Century, 2009). Of the current clean energy alternatives, wind energy is positioned at the forefront of the renewable energy drive as the fastest growing source of renewable energy (United States Department of the Interior, 2009), as previously noted by Lewin and Sritharan (2010).

When compared to other forms of energy, the wind energy industry is relatively new. While windmills have been used as early as 500 A.D., they weren't present in the United States until 1854 (Dodge, 2006). Even so, the first large scale use of wind turbines in the United States occurred in California, when 17,000 turbines were constructed in the 1980s, with capacities spanning 20-350 kW (Dodge, 2006). Although an early leader in wind energy, the United States allowed investment tax credits to expire, hampering the growth of the American wind energy market. Despite a federal Production Tax Credit (PTC) being put in place during 1992, this industry was largely stagnant until 1999 (Dodge, 2006). In that year, there was revitalization in wind energy, with 900 MW of energy production installed in the United States (American Wind Energy Association, 1999). However, a sense of uncertainty pervaded the market until the PTC was extended in 2004. More recently environmental concerns, fluctuation of fuel prices, and strong support from state governments has revived American interest in wind energy. In July 2008, the United States again became the international leader in wind energy, out-producing Germany (Gelsi, 2008).

In May 2008, the Department of Energy (DOE) released a report, "20% Wind Energy by 2030", detailing a scenario in which 20% of all energy in the United States would be produced through wind energy. In order to meet the projected demand for energy consumption in the year 2030, the country would need to increase its wind energy production by 300,000 MW (U.S. Department of Energy, 2008). With the U.S. wind energy capacity rated at 35,000 MW at the end of 2009 (American Wind Energy Association, 2010), this goal

is far from accomplished. With only 1.8% of total U.S. energy supplied by wind (American Wind Energy Association, 2010), continued research and development of wind turbines is necessary.

1.2 Role of Towers in Wind Energy Production

One of the largest and most visible components of a wind turbine is the support tower, as shown in Figure 1.1. While much attention is currently focused on improvement of the turbine and blade technology, wind technology stands to gain tremendously through the refinement and development of new and taller towers.

One of the major challenges identified in "20% Wind Energy by 2030" is, "…reduction in wind capital cost and improvement in turbine performance through technology advancement and improved manufacturing capabilities" (U.S. Department of Energy, 2008). While continued improvement in the durability and efficiency of the turbines themselves will aid in accomplishing this goal, it is necessary to explore other cost-effective alternatives. During a 2008 Department of Energy workshop (U.S. Department of Energy, 2008), "Significantly taller towers" coupled with "Design innovation" were identified as necessary conditions for the attainment of the 20% by 2030 goal.

Figure 1.1: Wind Turbine Tower (Wind Energy Planning, 2008)

Taller towers are favorable to the wind energy generation for multiple reasons. As power production is related to the cube of the velocity, it follows that a turbine in a faster wind environment is more efficient. Due to the effects of the atmospheric boundary layer, wind velocity increases via a power-law distribution with height. Assuming a normal wind profile, as defined by the International Electrotechnical

Commission (2007), an increase of turbine elevation from 262 ft (80 m) to 328 ft (100 m) would result in a 4.6% larger wind speed and a 14% increase in power output. An increase from 262 ft (80 m) to 394 ft (120 m) would result in an 8.5% greater wind speed and a 28% increase in power production. Hence, a logical cost-effective solution to increase wind energy production is to build taller turbines to exploit higher velocities. It is also likely that turbines would gain increased operating time from these higher wind velocities.

Besides taking advantage of increased wind speed, taller turbines are also more cost effective. As shown in Figure 1.2, given the same surface area of land, taller turbines produce more energy with fewer total turbines (Brughuis, 2004). In this scenario, 8 5MW turbines would use the same surface area as 13 1.5MW turbines. Brughuis (2004) also notes that this increased output does not increase the cost of connecting the turbines to the power grid. Additional cost savings could be realized through the reduction of maintenance costs associated with the operation of fewer turbines, as well as lessened transportation costs, as fewer blades and turbines would be needed for a wind farm.
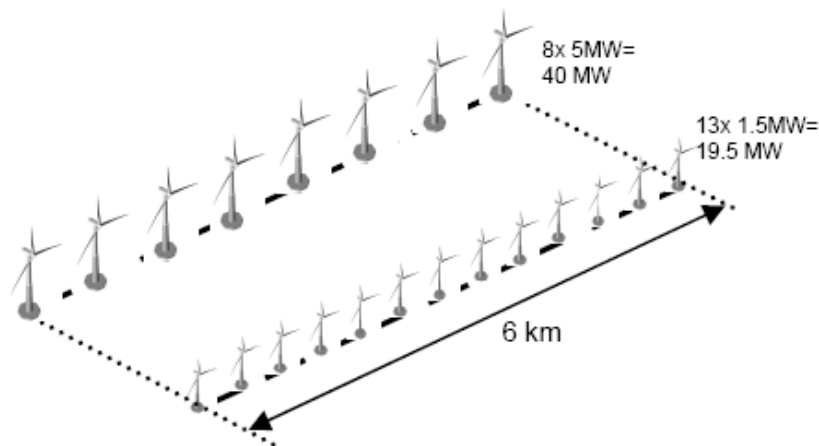
Figure 1.2: And Illustration of Power Production as a Function of Hub Height (Brughuis, 2004)

According to the WindPACT Turbine Rotor Design Study (Malcolm & Hansen, 2002), a report contracted by the National Renewable Energy Laboratory (NREL), which was further

elaborated on by LaNier (2005), the total cost for a 3.0 MW, 394 ft (120 m) tower (including rotors, drive train, nacelle, control systems, balance of station, and tower) is \$3,445,150. Of that price, \$551,415 is associated with the tower materials and \$195,160 is associated with tower transportation, representing 21.7% of the total cost of each wind turbine. Since tower research and optimization would affect more than 1/5 of the overall price, it is undeniable that tower research advancements would contribute to the DOE's goal of reducing "wind capital cost" and increase wind energy production.

1.3   Current Practice

The current state of practice for wind turbine tower design includes the use of tubular steel, regular strength concrete, and hybrid steel-concrete concepts. However, the most commonly used designs today are steel tubular towers. While current towers satisfy the design criteria for hub heights up to 80 m (262 ft), there are limitations that prevent them from being extended to taller towers.

1.3.1   Lack of Uniform Design Specifications

One of the main limitations of the current wind turbine tower industry is the lack of a unified design code, created for use in the United States. Presently, towers are engineered to a variety of specifications. Because of this practice, some towers may actually be over-designed for their task, resulting in higher than necessary costs and profligate use of materials. On the other end of the spectrum, it is also possible that current designs do not actually consider all necessary limit states for a safe structure. According to the Caithness Windfarm Information Forum (2008), structural failure is the third most common cause of "wind turbine accidents". Table 1-1 (Caithness Windfarm Information Forum, 2008) gives a yearly account of wind turbine structural failures. This table combines structural turbine and tower failures, while excluding blade failures. Table 1-1 illustrates that although failures are uncommon, they do occur and suggests that some current design criteria may be inadequate.

Table 1-1: Wind Turbine Structural Failures per Year (after Caithness Windfarm Information Forum, 2008)

Year	'00	'01	'02	'03	'04	'05	'06	'07	'08	'09
Structural Failures per Year	9	3	9	7	4	7	9	6	13	16

One the initiatives suggested by the "20% Wind Energy by 2030" is "Development of appropriate design criteria, specifications and standards" (U.S. Department of Energy, 2008). While Europe has cultivated multiple wind turbine tower design standards, such as IEC 61400-1 and DNV-RISO's "Guidelines for Design of Wind Turbines", the United States does not have its own wind turbine tower standard (Vazquez & Hagen, 2009). The result is confusion and lack of uniformity in tower design. This begs the question of why the wind turbine industry cannot merely utilize existing building standards. Wind turbine towers are unique in their functions and the environment in which they operate. Turbine towers experience different loading (corresponding to various operating states of the wind turbine) which must be specifically addressed.

One of the unique concerns for wind turbine towers is the high amount of load reversals they will experience in their design life. Although all buildings and bridges are subjected to dynamic forces, the vibratory characteristics of wind turbines, combined with constantly changing wind velocity can cause 5.29×10^8 fatigue load cycles (LaNier, 2005) for a 328-ft (100-m) tall tower with a 1.5-5.0 MW turbine. Recognized American building standards such as ACI 215R only account for fatigue of 10^4 cycles. European standards, such as the Model Code 1990 (Comite Euro-International Du Beton, 1990) for concrete or the Eurocode 3 (European Committee for Standardisation, 1992) for steel, have considered this issue. In the case of steel towers, fatigue is recognized as one of the governing limit states for design (LaNier, 2005). The absence of provisions for high cycle fatigue illustrates the inadequacy of existing American standards' for wind turbine tower design.

Another area in which existing American codes fall short is in providing the design wind speed. The ASCE 7 (Structural Engineering Institute, 2005) specifies regional wind speed through the use of its "Basic Wind Speed" map, reproduced in Figure 1.3. This map gives the 3 second wind speed at 33 ft (10 m) elevation. While the basic wind speeds change

drastically along the coasts (largely due to the occurrence of hurricanes), the map gives a reference speed that is essentially constant throughout the interior of the United States. This may be sufficient for building construction, but it is not detailed enough for wind turbines as they will be located in regions of high, and therefore favorable, wind speed.

Location	V mph	(m/s)
Hawaii	105	(47)
Puerto Rico	145	(65)
Guam	170	(76)
Virgin Islands	145	(65)
American Samoa	125	(56)

Notes:
1. Values are nominal design 3-second gust wind speeds in miles per hour (m/s) at 33 ft (10 m) above ground for Exposure C category.
2. Linear interpolation between wind contours is permitted.
3. Islands and coastal areas outside the last contour shall use the last wind speed contour of the coastal area.
4. Mountainous terrain, gorges, ocean promontories, and special wind regions shall be examined for unusual wind conditions.

Figure 1.3: ASCE 7 Basic Wind Speed Map Produced by ASCE 7 (Structural Engineering Institute, 2005)

When compared to a map of the United States' wind resources, as presented in Figure 1.4, there is a large variation in wind speed that the ASCE 7 does not account for. Other codes, such as IEC 61400-1 (International Electrotechnical Comission, 2007), specify wind speed

based on turbine class and turbulence characteristics. This is a more appropriate method, since the wind class inherently takes into account the turbine's design wind velocity.
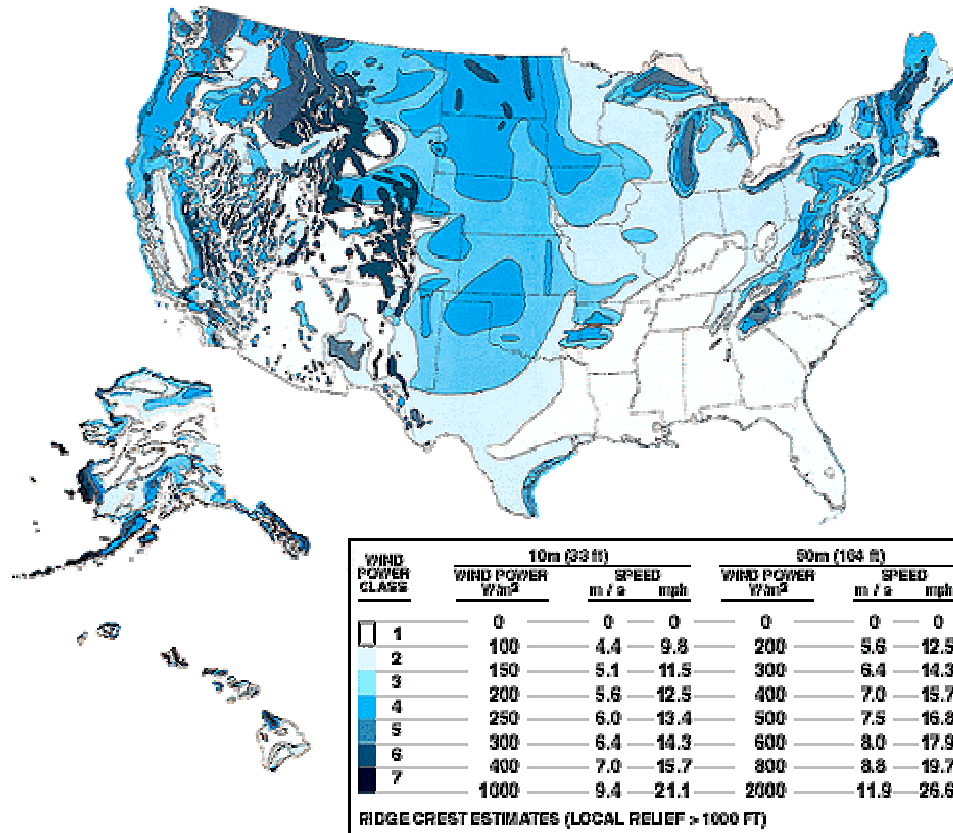
Figure 1.4: The United States' Wind Resource Map (Evolve Green, 2010)

While a unified American standard would be ideal to deal with these issues, such a document does not exist at this time. As a result, a combination of American and European standards is being used to complete the tower design today. More detail on these standards can be found in Section 2.3 of this thesis.

1.3.2   Steel Towers

The most common choice for wind turbine towers in today's market is tubular steel sections. Typical steel towers can be seen in Figure 1.5. Steel has been frequently used because of its excellent strength properties and lower weight strength to weight ratio. A tubular steel section can be continuously tapered and its wall thickness varied, resulting in a very efficient use of material. Steel, in general, is a ductile material, experiencing large deformations before failure of a section could occur. However, there are several challenges associated with the use of steel towers.

One of the most cited problems with steel is the transportation concern. Steel towers are typically composed of two or more tube sections, stacked on top of each other. These sections are bolted or welded to

Figure 1.5: Steel Wind Turbine Tower

form a complete tower. Since all steel is pre-manufactured in a rolling mill, it must be transported to the project site by truck or train. A typical transportation set-up can be seen in Figure 1.6. However, due to highway clearance issues, the diameter of a tube section is limited to 14.1 ft (4.3 m) (Brughuis, 2004), which is the approximate diameter of current 262-ft (80-m) tall towers. Demands for increased hub height require steel tubes of larger diameters. As a result, transportation limit puts a practical limit on hub heights for steel of around 328 ft (100 m) (Brughuis, 2004).

Another challenge of steel tower transportation is the long distance, and therefore the added cost associated with bringing the tower to the project site. According to a study completed by Global Energy Concepts LLC (Smith, 2000), in order to construct wind turbines within the Midwest state of South Dakota, towers may have to be transported from as far as Texas or Louisiana.

Figure 1.6: Typical Wind Turbine Tower Transportation Configuration

According to LaNier (LaNier, 2005), towers have been shipped from China or Korea to meet demand. Given these extreme distances and the specialized nature of tower construction, transportation constitutes a significant portion of the total cost for a wind turbine project. As mentioned previously, for a 3.6 MW, 328-ft (100-m) tall wind turbines, the tower could easily cost $195,160 just to transport (LaNier, 2005) to the project site. Were the diameter of steel turbine towers to increase beyond the 14.1 ft, this cost would also drastically increase because new, more complex transportation methods would need to be devised.

As mentioned earlier, wind turbines are subjected to loads that most civil engineering structures do not experience. While steel is considered a light weight building material due to its high strength, it is vulnerable to fatigue. Consequently, fatigue concerns govern the design of steel towers (LaNier, 2005). The most important factor in fatigue is the stress range that the material is expected to experience. For a smaller stress range, a structure is more damage resistant. Therefore, a thicker shell would see smaller stress variations, and be less susceptible to fatigue. It should also be noted that, for fatigue, 20 years is a common design life (DNV/Risø, 2002). In terms of civil engineering structures, this is very short.

1.3.3 Concrete Towers

While concrete is nearly ubiquitous in the world of civil engineering, it is strangely absent from the wind turbine industry. While interest in concrete has been rising in recent years, its popularity is still secondary to steel. As with any material, concrete has its pros and cons.

One of concrete's major strengths is its ready availability. There are many concrete plants throughout the United States. Where cast-in-place concrete requires long cure times, precast concrete technology facilitates a rapid construction and erection process. Additionally, precast concrete has excellent quality control, minimizing material and construction flaws. Due to the high concentration of precast concrete manufacturers, travel distances and thus transportation costs can be greatly reduced. According to the Precast Concrete Institute, most projects utilizing precast technology are located within 200 miles of the concrete plant (Shutt, 2004).

Like steel towers, precast concrete towers are typically composed of multiple sections, stacked to complete the structure. However, rather than being monolithic, the precast sections can use modular (i.e., made up of multiple pieces) construction. In this practice, modules will then be bolted or post-tensioned together to form a complete cross section. This method has several important advantages. Firstly, only several unique pieces are needed to construct the entire tower. This allows precasters to construct only a few forms in order to complete a tower. Secondly, since each individual piece is small, they can be stacked on a truck and transported using conventional means. This eliminates the need for specialized trailers and reduces transportation costs. The simplified transportation, as well as modular construction technique, can be seen in Figure 1.7.

Another beneficial aspect of concrete is its ability to be prestessed. Prestressed concrete members are more slender than those constructed from reinforced concrete. They are lighter and optimize the use of both steel reinforcement and concrete. Moreover, prestressed concrete is designed to remain uncracked and is typically subjected to constant compression under service loads. This greatly enhances the fatigue life of the concrete (LaNier, 2005). The tendons used in these members are also more resistant to fatigue than welded tubular steel (LaNier, 2005).

Figure 1.7: Precast Concrete Tower Transportation and Erection (Grupo Inneo, 2008)

One disadvantage of concrete compared to steel is the necessity of using thicker shell members. This implies increased structural weight. Heavier structures require a larger foundation and added cost. In seismic areas, heavier structures may lead to larger forces in an earthquake than a lighter structure. These challenges can be handled through design, but they add cost to the project. Although a greater volume of material would need to be brought to the project site for concrete as compared to steel towers, this cost could be mitigated through the use of conventional transportation means due to the modular nature of precast design.

1.3.4 Hybrid Towers

The third option that has been practiced in the wind energy industry is the hybrid wind tower. For the purposes of this thesis, the definition of hybrid will refer to a tower composed partially of tubular steel at the top and partially of concrete at the base. An example of a hybrid tower can be seen in Figure 1.8. As previously mentioned, economical steel section size is limited by transportation concerns. To overcome this problem, hybrid towers employ a concrete base or pedestal. The conventional steel tower is then placed on top of the base. This serves to increase hub height while avoiding unwieldy large steel sections.

Figure 1.8: Illustration of the Tindall Atlas CTB Hybrid Tower (Tindall Corporation, 2009)

This hybrid tower design seeks to capitalize on both the advantages of concrete and steel. Compared to concrete, the hybrid tower has a lighter weight. This is favorable because it reduces seismic weight. Additionally, a smaller foundation is necessary due to the decreased dead load as compared to an all-concrete tower. LaNier (2005) suggests the erection of a hybrid tower could also be quicker and cheaper than that of a full precast concrete alternative. However, this would likely depend on the tower height and the proportion of the tower utilizing concrete. Compared to a full steel tower, the transportation cost would be decreased where greater than 80 m (262 ft) heights are needed. Although a crane would be needed to erect the precast sections and steel tube, it would be smaller than one needed to erect a very large steel section. There is also the possibility that the top steel section could be jacked into place (LaNier, 2005).

Hybrid towers also have their challenges. As with steel towers, the tubular steel top could potentially need to be transported over long distances to the project site. Also, the use of two

materials means additional coordination and two lead times, from the contractor's point of view.

1.4   Ultra-High Performance Concrete Towers

Due to the multitude of tower options available, it is clear that the wind turbine market is constantly evolving. While the current practice of using steel turbine towers has helped to shore-up U.S. wind energy production, there is still room for improvement and innovation. New tower construction materials have great potential to advance the state of the wind industry. One such material is Ultra-High Performance Concrete (UHPC).

1.4.1   Introduction to UHPC

Ultra-High Performance Concrete (UHPC) has been defined by the FHWA as concrete meeting eight performance characteristics: "freeze-thaw durability, scaling resistance, abrasion resistance, chloride penetration, compressive strength, modulus of elasticity, shrinkage, and creep" (Tang, 2004). A simpler definition is rendered by Shah and Weiss: concrete with 28-day compressive strength of 21.8 ksi (150 MPa) (Shah & Weiss, 1998). This impressive strength is achieved through the elimination of defects in the concrete micro-structure. What results is an extremely dense product, capable of compressive strengths in the range of 21.8 to 30 ksi (150-207 MPa) (Vande Voort et al., 2008). One benefit of UHPC is its increased durability. More importantly, from the standpoint of concrete structures, a large level of prestressing can be applied safely to UHPC. The design implications of increased prestressing are elegant, slender structures and substantial material savings as compared to regular strength concrete. Due to the harsh environments and high transportation costs typically associated with wind turbines, the above advantages make UHPC an ideal candidate for tower design.

1.4.2   Benefits of UHPC for Wind Turbine Towers

One of the most impressive characteristics of UHPC is its extremely high compressive strength. The advantage of prestressing in regular strength concrete towers has already been discussed in Section 1.3.3. UHPC would retain and amplify those benefits. Since much more prestressing can be applied, a reduced quantity of UHPC can be used, as compared to regular

strength concrete towers. Although, like normal strength concrete, UHPC's tensile capacity is small in comparison to its compressive strength, prestressing neatly side-steps this issue.

With the modular construction techniques already employed by the industry, UHPC sections would be even more transportation friendly. Many sections could be stacked on a single truck, and the associated transportation costs would be significantly reduced.

While UHPC has a slightly higher weight (155 lb/ft^3 [24.4 kN/m^3]) (Vande Voort et al., 2008) regular strength concrete (150 pcf [23.6 kN/m^3]), with the material reductions, UHPC structures would weigh much less than regular strength concrete structures. In fact, UHPC members are comparable in size to steel (Vande Voort et al., 2008). Smaller cranes would be needed to lift the lighter pieces into place.

1.4.3   Challenges of UHPC for Wind Turbine Towers

While UHPC is a material with great potential, it does have several challenges that a new design would need to overcome. UHPC is a new material, and therefore more expensive than regular strength concrete on a per unit basis. Any new design would need to compensate for this through the use of less material and optimized transportation.

While UHPC is not as widely-available as regular strength concrete, UHPC wind turbine towers represent a potential opportunity for precasters everywhere. Were a viable UHPC design presented, local precasters could become certified to handle UHPC, allowing them to tap into the wind turbine tower market.

1.4.4   UHPC Shell Towers

One option for the use of UHPC would be to create a shell out of UHPC, similar to tubular steel or current concrete towers. The shell tower would utilize prestressing, thereby taking advantage of UHPC's high compressive strength. The prestressing could consist of pre- or post-tensioning. By post-tensioning the tower together, intermediate connections between tower cross sections could be eliminated, as post-tensioning would form these connections.

In terms of wall thickness, UHPC would be somewhere between steel and regular strength concrete shells. The structure would be modular, consisting of multiple sections

longitudinally and perhaps circumferentially. As discussed in Section 1.4.2, modularization would contribute to simplified transportation and thus reduce transportation costs. This design would not represent a significant departure from current concrete tower construction methods, so contractors should be able to easily incorporate the concept.

1.4.5 UHPC Lattice Towers

The most effective use of a completely new material is not necessarily to replicate existing design concepts. According to Tang (2004), "ultra high performance concrete …is a new material. It is not really concrete anymore. It also has to establish its empire of applications". Other possibilities do exist for UHPC towers besides shells. One alternative is the UHPC "Lattice" tower. The Lattice tower would consist of six or more UHPC columns, oriented in a circular arrangement. Each of these columns would be pre- or post-tensioned (bonded or unbonded), in order to employ UHPC's high compressive strength. The columns would be braced (using steel, concrete, or UHPC members) to each other at intermediate heights in order to increase rigidity, tie the structure together, and prevent buckling. Alternatively, thin concrete panels could span between the columns, eliminating the need for bracing. Another variation on this concept would be for the columns to be confined in thin-walled steel shells, thereby drastically increasing the concrete's compressive capacity. This is commonly done in seismic and seismic retrofit of existing structures.

The lattice tower would represent several significant advantages over conventional designs. Since UHPC is used more efficiently than in a shell structure, there could be a considerable reduction in material. The lattice sections would also be easily stacked and shipped, resulting in the further reduction of transportation and site development costs. While it could be argued that the lattice concept is not as aesthetically pleasing, it could easily be covered with structural fabric.

1.4.6 UHPC Sustainability

In today's construction environment, sustainability is an important consideration for any project. UHPC has the potential to bring further sustainability to wind turbine tower design. Because concrete production constitutes 4% of all CO_2 released annually (Sritharan, S., 2009), it is important to use the material as efficiently as possible. Since UHPC reduces the

amount of concrete needed for each tower, it could be considered more sustainable than normal strength concrete.

UHPC is also a very durable material and towers design with this material would easily last much longer than the 20 year design life typical to turbines. With proper maintenance it is not unreasonable to expect UHPC towers to last 60+ years. Therefore, at the end of a turbine life, the tower could be fitted with a new turbine and continue to harvest wind energy. Alternatively, the tower could be sold, disassembled, and used elsewhere were wind conditions to change significantly. Both of these options have the potential to drastically increase the total value of a UHPC tower. In contrast, a steel tower's lifespan is effectively matched to its original turbine. After 20 years, the steel tower can no longer be used and must be disassembled due to fatigue governing the design.

Additionally, the rapid construction associated with modular, precast design techniques would reduce construction time. The impact on surrounding areas during construction, including noise, dust, and traffic delays would thereby be minimized.

1.5   Scope of Research

The research goals of this thesis include:

- Investigate the applicability of UHPC in wind turbine tower design
- Complete detailed designs using a UHPC circular shell tower and a UHPC lattice tower
- Further investigate and validate the UHPC Lattice design using Finite Element computer software

1.6   Thesis Content

The remainder of this thesis investigates the applicability of UHPC as a viable material for wind turbine towers. The thesis is organized as follows:

- Chapter 1: An introduction in the rise of wind energy as a viable power source, the need for taller wind turbine towers, the limitations of current steel towers, and alternative options for taller tower designs.

- Chapter 2: Complete literature review of UHPC as a building material and wind turbine tower design, including loading, limit states, applicable specifications, and a design study.

- Chapter 3: A preliminary design of a 328-ft (100-m) steel and regular strength concrete wind turbine tower.

- Chapter 4: A preliminary design of a 328-ft (100-m) UHPC Shell and UHPC Lattice Tower.

- Chapter 5: Finite element analysis verification of the 3228-ft (100-m) UHPC Lattice Tower at service-level loading.

- Chapter 6: A summary of the completed research, conclusions that were drawn, and suggestions for future research.

2 LITERATURE REVIEW

2.1 Overview

The following is a discussion concerning the material properties, behavior, and past uses of UHPC as a structural building material. This is necessary as UHPC is currently establishing itself as an alternative construction material. As a result, there is no U.S. UHPC equivalent to the ACI 318 (2008) for concrete and design information must be collected from multiple sources. Similarly, as no U.S. document exists concerning all of the issues necessary to design wind turbines, information regarding loading, limit states, and strength has been collected. Since designs will be completed for steel, concrete, and UHPC towers, design information has been compiled for all three building materials.

2.2 UHPC

Although the name Ultra-High Performance Concrete is used broadly to define concrete possessing compressive strength greater than 21.8 ksi (150.3 MPa) (Ma & Schneider, 2002), the type of UHPC described within this document is more specific. More precisely, UHPC is defined as a "densified system with ultra fine particles (DSP)" (Vande Voort et al., 2008).

Additionally, UHPC can be separated into categories based on the manufacturer: "Ceracem/BSI, compact reinforced composites (CRC), multi-scale cement composite (MSCC), and reactive power concrete (RPC) (Vande Voort et al., 2008). Between these mixes, the main differences are the inclusion or exclusion of coarse aggregates and the amount of steel fibers used in the mix. The only type of UHPC that uses coarse aggregates is Ceracem/BSI. As Iowa State University (ISU) has previous experience with RPC mix and it is readily available, the literature review focuses on this UHPC variety.

2.2.1 Material Composition

The typical components of a UHPC mix design include sand, cement, silica fume, crushed quartz (quartz flour), superplasticizer, water, and fiber reinforcement. Typical ranges for the above components can be seen in Table 2-1 and Table 2-2. It should be noted that coarse aggregate has been eliminated from the RPC mix design, and therefore does not appear in the tables.

As mentioned by Vande Voort et al. (2008), the strength of the material is derived from its increased density. Therefore, the particles should not be expected to be packed in the same manner as regular strength concrete. In order to achieve this density, UHPC uses "space packing", as opposed to Apollonian packing. This is achieved by having a well-graded distribution of particles (Vernet, 2004). All particles used within the mix are separated into classes. Each consecutive class has a mean particle diameter of at least 13 times the previous class (Cheyrezy & Richard, 1995).

Table 2-1: Component Ranges for a Typical UHPC Mix (Vande Voort et al., 2008)

Component	Typical Range of Weight (Mass) per ft^3 (m^3)
Sand	31 – 87 lb (490 – 1390 kg)
Cement	38 – 67 lb (610 – 1080 kg)
Silica Fume	3.1 – 21 lb (50 – 334 kg)
Crushed Quartz	0 – 26 lb (0 - 410 kg)
Fibers	2.5 – 15.5 lb (40 – 250 kg)
Superplasticizer*	0.6 – 4.5 lb (9 – 71 kg)
Water	7.9 – 16.3 lb (126 – 261 kg)

*Superplasticizer is expressed as the weight of the solid fraction; the liquid fraction is included in the water weight

Table 2-2: A Typical UHPC Mix Design (Cheyrezy & Behloul, 2001)

Component	Weight per Cubic Foot (Meter)	Mass Ratio/Cement	Volume Fraction
Sand	61.9 lb (991 kg)	1.430	38.8%
Cement	42.3 lb (693 kg)	1.000	22.7%
Silica Fume	14.0 lb (225 kg)	0.325	10.6%
Crushed Quartz/Fly Ash	13.0 lb (208 kg)	0.300	8.1%
Fibers	9.4 lb (151 kg)	0.218	2%
Superplasticizer*	0.90 lb (14.4 kg)	0.021	1.4%
Water	9.9 lb (159 kg)	0.229	16.5%

*Superplasticizer is expressed as the weight of the solid fraction; the liquid fraction is included in the water weight

The following is a discussion of the common constituents of UHPC.

Sand

In UHPC, sand is the largest aggregate size used. This is typically quartz sand, due to its low price and excellent strength characteristics (Cheyrezy & Richard, 1995). The use of sand serves to increase the homogeneity of the concrete, creating a mixture with a relatively constant Young's modulus. Additionally, since micro-cracking within the cement paste is dependent on aggregate size, the use of sand significantly reduces the size of micro-cracks compared with regular strength concrete (Cheyrezy & Richard, 1995). The sand used has a typical mean diameter size of 0.00984 in. (250 μm).

Cement

UHPC does not require any specialized cement. Alternative cements, such as high-silica modulus, have been shown to have superior "rheological characteristics and mechanical performance" (Cheyrezy & Richard, 1995) and require less water. However, they necessitate significantly longer curing periods. Cheyrezy (1995) also notes that cement with low C_3A content performs better than that with high concentrations.

Unlike regular concrete, as much as 50% of the cement (Vernet, 2004) within the UHPC remains anhydrous, even after curing is complete. Later in the service life of the structure, this cement could become hydrate and self-repair micro-cracks that have formed throughout the structure. Additionally, the anhydrous cement has a much higher elastic modulus than the hydrated portion: 17,400 ksi (120 GPa) (Vernet, 2004) versus 7,250 ksi (50 GPa) (Cheyrezy & Richard, 1995). The result is a stronger matrix than if all of the cement was hydrated. However, this must be balanced against the need for cohesion of the mix, provided by the hydrated portion.

Silica Fume

Silica fume is necessary in UHPC for multiple reasons, as identified by Cheyrezy and Richard (1995). The space packing utilized by UHPC requires a particle size smaller than cement, around 7.9 μ in. (0.2 μm) in order to fill the matrix. Silica fume also improves the

rheological characteristics of UHPC because of its spherical shape, allowing for enhanced workability. Finally, it provides secondary hydrates, through the reaction of silica hydrates with $CA(OH_2)$ (Vande Voort et al., 2008). As a percent of concrete, 25% silica fume to cement is often used. This exceeds the 18% needed to carry out the pozzolanic reactions (Vande Voort et al., 2008), as well as provides for a very dense mix. Cheyrezy and Richard (1995) also note that since some cement remains anhydrous, the pozzolanic reaction will actually require less than 18%. Compacted silica fume cannot be used in conjunction with UHPC, in order to ensure the absence of aggregates. Additionally, the use slurry is not possible since its high water content would significantly affect the concrete strength (Cheyrezy & Richard, 1995).

Crushed Quartz (Quartz Flour)

Crushed quartz is added to UHPC primarily as filler. As mentioned previously, much of the cement remains anhydrous in UHPC. Some of this can be substituted with crushed quartz, decreasing the quantity of cement needed (Vande Voort et al., 2008). The quartz used typically has a particle size of 393.7 μ in. (10 μm). This is in the same class as cement, which has a mean particle size of 433 – 591 μ in. (11 – 15 μm). Heat-treating demands this similarity because it requires cement (or cement fillers) to have mean particle diameters of 197 – 984 μ in. (5 – 25 μm) in order to be effective (Cheyrezy & Richard, 1995).

Superplasticizer

Superplasticizer is used within UHPC in order to increase the workability of the material. As mentioned previously, many of the cement particles remain anhydrous. While this increases the strength of the mix, it has a detrimental effect on the fluidity of the concrete. When superplasticizer is added to the mix, the surface tension of the water is lowered (Morin et al., 2001), allowing for a better distribution of water. In turn, this enhances the fluidity of the mix. According to Richard and Cheyrezy (1995), a superplasticizer solid content of 1.6% of cement content is most favorable.

<u>Water</u>

For DSP concrete, the goal of the mix design is to ensure a very dense product. To accomplish this, water content is chosen to provide the maximum relative density (defined as the ratio of the density of the cured concrete to the density of the granular mixture without air or water). This is achieved when the water replaces all of the entrapped air in the mixture. Further addition of water serves to only increase the overall mix volume. According to Vande Voort et al. (2008), this optimum is a water-to-binder (binder is defined as cement and silica fume) ratio of 0.13. In practice, there is an acceptable range, both above and below the optimum content. However, the portion of the range above the optimum has increased workability versus the range below. Therefore, an ideal mix has a water-to-binder ratio of 0.13-0.14. This is well above the minimum recommended water-to-binder of 0.08 necessary for workability (Cheyrezy & Richard, 1995).

<u>Fiber Reinforcement</u>

A commonly cited concern of UHPC is its decreased ductility when compared to regular concrete. Plain UHPC exhibits only linear and elastic behavior (Cheyrezy & Richard, 1995). Without an inelastic behavioral region, UHPC would fail in a very brittle manner. In order to overcome this challenge, the addition of steel fibers to the UHPC mix is a commonly accepted practice. The fibers increase the toughness of the material by bridging the micro-cracks within the

Figure 2.1: An Image of a Ruptured Carbon Fiber (Reda, Shrive, & Gillot, 1999)

concrete. Additionally, fibers improve the tensile performance of UHPC. A bridging of a micro-crack can be seen in Figure 2.1.

Orgass and Klug (2004) list the following fiber types, along with uses:

• "Steel Fibres:

    - Increase of fracture energy, subsequent improvement of ductility

    - Increase of strength (both compressive and tensile strengths)

    - Reduction of tendency for cracking"

• "Polypropylene Fibres (PP fibres):

    - Decrease of microscopic crack growth with high loading

    - Enhanced fire resistance

    - Decrease of early shrinkage"

• "Glass Fibre:

    - Reduction of internal stresses within young concrete"

Multiple studies have been done to determine the ideal percentage of steel fibers in a UHPC mix. Cheyrezy and Richard (1995) propose that 2% by volume is the optimum amount. Orgass and Klug (2004) agree with this result, proposing 2% as the upper limit for ductile behavior.

Typical fiber sizes include 0.25 in. (6 mm) long, 0.006 in. (0.15 mm) diameter and 0.5 in. (13 mm) long, 0.006 in (0.15 mm) diameter fibers. Orgass and Klug (2004) observed excellent ductility using half 0.25 in. fibers and half 0.5 in. fibers. Cheyrezy and Richard (1995) noted that longer fibers influence ductility, while shorter fibers influence compressive and tensile strength. It is suggested a mix of the two would provide both ductility and enhanced mechanical characteristics.

2.2.2   Material Behavior

Compressive Behavior

A typical range for compressive strength of unconfined UHPC is 21.8-31.9 ksi (150-220 MPa) (Fehling et al., 2004). Without fibers, UHPC exhibits nearly pure linear-elastic behavior under compression. When 70-80% of the peak stress is reached, the modulus becomes nonlinear (Fehling et al., 2004). At failure, no strength loss occurs. This results in a sudden, explosive failure with little warning. A representative stress-strength diagram can be seen below.
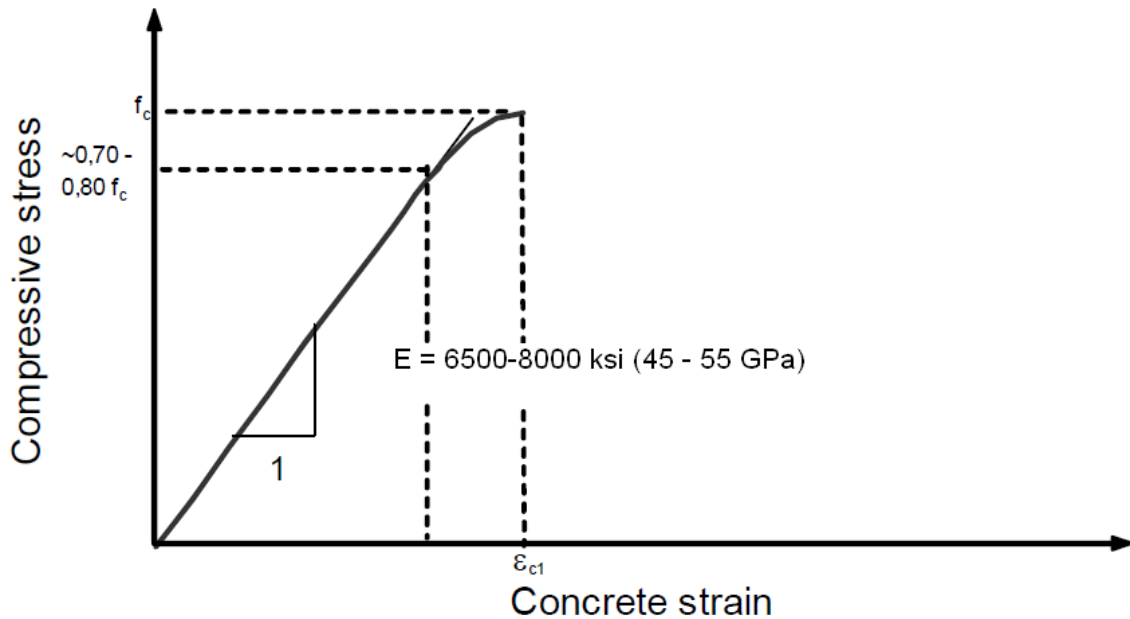
Figure 2.2: Stress-Strain Relationship of Non-fiber Reinforced UHPC (after Fehling, Bunje, & Leutbecher, 2004)

The compressive strength of UHPC is largely gained by its dense matrix and low water-to-binder ratio. However, several other factors affect the compressive strength as well. These factors, discussed below, include the addition of steel fibers, heat treatment, and confining pressure.

While fibers are typically added to concrete in order to increase its ductility, they can also have an impact on its compressive strength. However, the actual gain seems to have a large range. According to Vande Voort et al. (2008), the average strength gain is 30% for the addition of fibers. Others report a strength gain of only 15% (Fehling et al., 2004). Vande Voort et. al (2008) also note that steel fibers have more of an effect than organic fibers.

Heat treatment is another technique used to increase the compressive strength of UHPC. Strength is gained primarily through the reduction of the UHPC's porosity (Vande Voort et al., 2008). With a standard heat treatment of 190 °F (90 °C) for 48 hours, an average gain of 33% compressive strength is obtained, based on 15 different studies (Vande Voort et al., 2008). Graybeal (2006) reports a gain of 53% for 190 °F (90 °C) for 48 hours and a gain of

35.5% for 140 °F (60 °C) for 48 hours. According to Fehling et al. (2004), heat treatment also increases the rate of strength gain for UHPC.

Of all methods to improve compressive strength, confinement is currently the most effective. Confinement can either be applied during curing of the concrete, as well as through the use of steel tubes. The two can be combined for large increases in strength. According to Vande Voort et al. (2008) the use of 7.3 ksi (50 MPa) confining pressure is adequate to improve the strength qualities. Both of these techniques were used in the diagonal members of the Sherbrooke Bridge (see Section 2.2.3), resulting in 50 ksi (350 MPa) compressive strength. This represents a 67% increase versus the non-confined portions of the bridge.

<u>Tensile Behavior</u>

As with regular concrete, UHPC without fibers exhibits a very brittle tension failure. According to Fehling et al. (2004), the tensile strength of UHPC without fibers ranges from 1.0 to 1.5 ksi (7 to 10 MPa). The addition of fibers somewhat improves the strength, increasing to as much as 2.2 ksi (15 MPa). Based on direct tensile tests, Graybeal (2006) reports the strength of fiber reinforced, steam-treated (190 °F, 90 °C, for 48 hours) UHPC in the range of 1.4-1.6 ksi (9.7-11.0 MPa). Without the steam-treatment, Graybeal reports the tensile strength of UHPC as 0.8-1.0 ksi (5.5-6.9 MPa). From these results, it can be inferred that steam-treatment benefits the tensile strength, as well as the compressive strength.

While increasing tensile strength, the biggest benefit of the fibers is to introduce ductile behavior to the concrete. After cracking, the fibers bridge the micro-cracks, preventing brittle fracture. However, this is also associated with a loss in strength. This is discussed in more detail in the following section.

<u>Flexural Behavior</u>

In general, flexural tests are performed on concrete sections as an alternative, albeit indirect, way to characterize tensile behavior. Flexural tests provide valuable insight into post-cracking behavior of UHPC. Figure 2.3 shows the stress versus displacement behavior of fiber-reinforced UHPC, including the effect of different fiber orientations. It is clear from the

graph that the flexural behavior of fiber-reinforced UHPC is initially linear elastic until cracking begins to occur. The behavior then becomes nonlinear and load continues to increase. After the ultimate load is reached, there is a gradual drop in strength until fiber fracture occurs. The strain-hardening and the drop-off phases are due to the inclusion of fibers in the matrix. As mentioned previously, they bridge micro-cracks and allow for loading past the cracking point. As expected, flexural strength is dependent somewhat on fiber orientation.
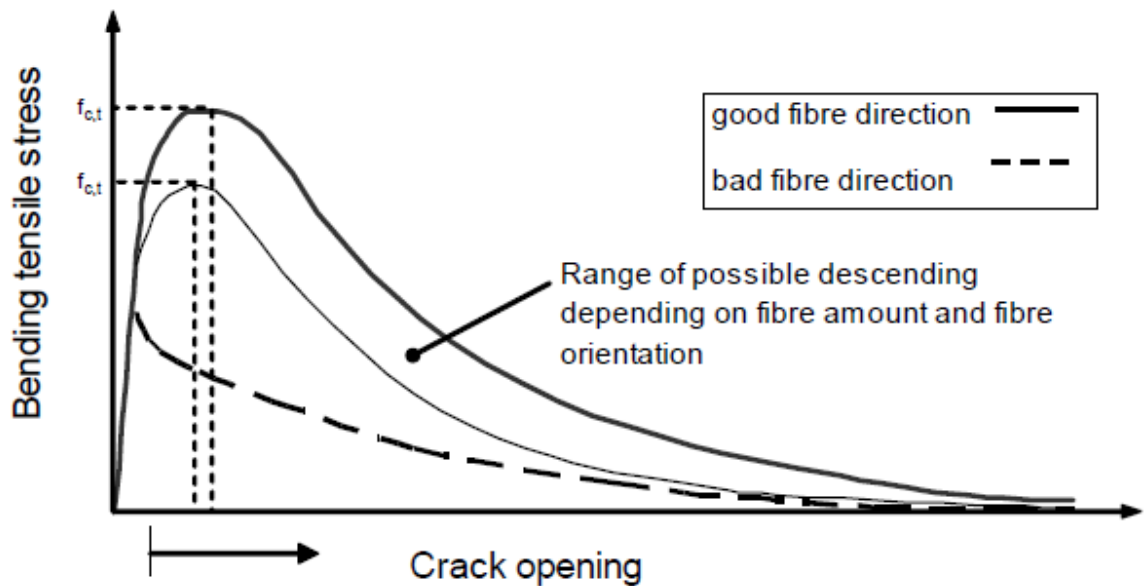
Figure 2.3: Bending Stress vs. Displacement for Fiber-Reinforced UHPC (after Fehling, Bunje, & Leutbecher, 2004)

Elastic Modulus

As UHPC is a cutting edge material, standardized equations do not exist to describe its modulus of elasticity, such as those found in ACI-318 for regular strength concrete. However, research has been done to characterize this aspect of UHPC. Several of these equations are listed below, collected by Vande Voort et al. (2008).

$$E = 50{,}000\sqrt{f_c'(psi)} \qquad\qquad \text{(Sritharan, Bristow, \& Perry, 2003)} \qquad \textbf{(2-1)}$$

$$E = 4150\sqrt{f_c'(MPa)}$$

$$E = 46{,}200\sqrt{f_c'(psi)} \qquad\qquad \text{(Graybeal B. , 2006)} \qquad \textbf{(2-2)}$$

$$E = 3840\sqrt{f_c'(MPa)}$$

$$E = 2{,}373{,}400 \ln f_c' - \qquad\qquad \text{(Ma \& Schneider, 2002)} \qquad \textbf{(2-3)}$$
$$468{,}910 \ (psi)$$

$$E = 16{,}364 \ln f_c' - 34{,}828 \ (MPa)$$

where E = elastic modulus; and

$\qquad f_c'$ = 28-day compressive strength.

Based on analysis done by Vande Voort et al. (2008), the equation proposed by Graybeal has the best correlation with tested values. For the calculations done throughout this report, Graybeal's equation will be used to determine the modulus of elasticity of UHPC with 2% steel fibers.

Poisson's Ratio

Multiple researchers have established a range for Poisson's ratio of UHPC. Vande Voort et al. (2008) report a range from 0.15 to 0.22. Gowripalan and Gilbert (2000) and a report by the Japan Society of Civil Engineers (2006) suggest a value of 0.2 is appropriate for design purposes when no test data is available.

Stress-Strain Characterization

The stress-strain behavior of UHPC is still the subject of ongoing evaluation. However, a model of the compressive behavior has been suggested by Gowripalan and Gilbert (2000). Their proposed model is tri-linear, with elastic behavior until a stress level of 0.85f'$_c$, a perfectly plastic region extending until a strain of 0.004, and a linearly decreasing strength until an ultimate strain of 0.007. This relationship is graphed in Figure 2.4.
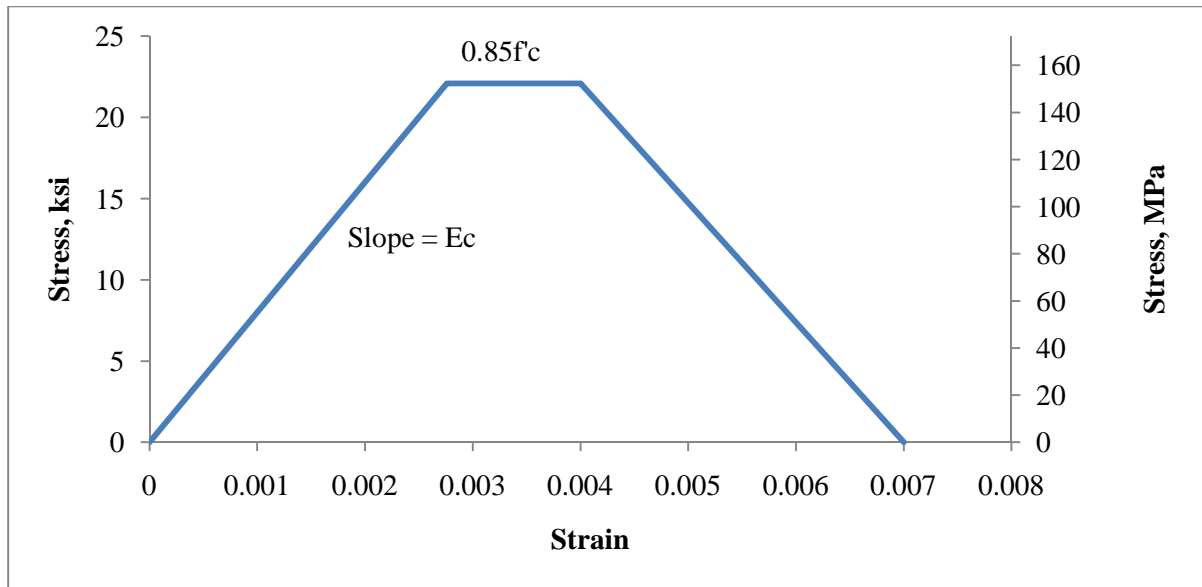
Figure 2.4: Fiber-Reinforced UHPC Compressive Stress-Strain Model (Gowripalan & Gilbert, 2000)

A model has been developed by Bristow and Sritharan (to be published) to characterize the tensile behavior of UHPC. This model has four distinct regions of behavior. Each region is defined by an equation and applies to the given strain limits.
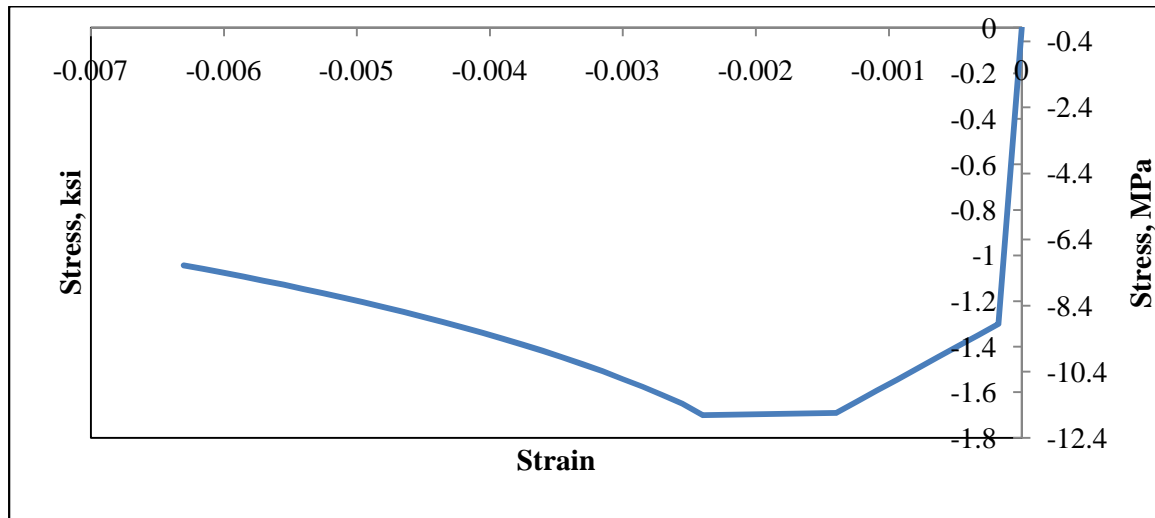
Figure 2.5: Fiber-Reinforced UHPC Tensile Stress-Strain Model (Bristow and Sritharan, to be published)

$$f_t = E_c\varepsilon \qquad\qquad\qquad for\ \varepsilon \le f'_{te}E_c \qquad\qquad\qquad \textbf{(2-4)}$$

$$f_t = f'_{te} + \frac{(f'_{teMAX} - f'_{te})(\varepsilon - f'_{te}/E_c)}{0.00125} \quad for\ f'_{te}E_c < \varepsilon < 0.0014 \qquad \textbf{(2-5)}$$

$$f_t = f'_{teMAX} \qquad\qquad\qquad for\ 0.0014 < \varepsilon < 0.0024 \qquad\qquad \textbf{(2-6)}$$

$$f_t = f'_{teMAX} - 0.672\ln\varepsilon - 4.062 \qquad \varepsilon > 0.0024\ until\ f_t = 0\ ksi \qquad \textbf{(2-7)}$$

Where f_t = tensile stress;

E_c = the Elastic Modulus, recommended as 8000 ksi (55,000 MPa);

ε = tensile strain;

$f'_{te=}$ elastic tensile strength, recommended as 1.3 ksi (9.0 MPa); and

$f'_{t,MAX}$ = maximum tensile strength, recommended as 1.7 ksi (11.7 MPa).

In Figure 2.4 and Figure 2.5, the value of E_c was taken as 7450 ksi (51,400 MPa), from Equation (2-2). The recommended tensile strain limits were utilized in Figure 2.5.

2.2.3   *Applications*

Although UHPC is generally a new material, there have been multiple uses of it in the United States and throughout the rest of the world. As previously mentioned, UHPC is most effectively used when new concepts are created that take advantage of its unique strengths. In fact, UHPC members have been created that match not only the capacity, but the overall dimensions of steel members (Vande Voort et al., 2008). The applications detailed below demonstrate both the successful applications of UHPC, as well as the creative way in which it was employed. All figures for the corresponding projects are presented at the end of this section.

Sherbrooke Footbridge

The Sherbrooke footbridge was completed in Quebec, Canada, in 1997. Figure 2.6 demonstrates how UHPC can be effectively utilized in new ways, rather than revising old designs. The bridge was constructed with RPC, with a total span length of 197 ft (60 m). The bridge is designed as open truss. RPC's high strength allows the deck to serve as the top chord of the truss. The bottom truss chord consists of two identical beams, each containing two prestressing tendons (Vande Voort et al, 2008). The RPC used in the deck and bottom chord has a compressive strength of 29 ksi (200 MPa). The diagonal members connect the top and bottom chord of the bridge, and are constructed of 0.08 in (2 mm) thick steel tubes containing RPC (Blais & Couture, 1999). Vande Voort et al. (2008) report use of these tubes increased the effective compressive strength of the RPC to 50 ksi (350 MPa). Each diagonal contains two ½ in. (13 mm) diameter unbonded tendons.

Seonyu Footbridge

The Seonynu Footbridge, or Bridge of Peace, was constructed across the Han River, in Seoul South Korea and completed in 2002 (Williams, 2002). The bridge uses a 394 ft (120 m) arch, consisting of 6 pi-shaped RPC precast segments. These segments were then joined using grouted post-tensioning (Ricciotti, 2005). As noted by Vande Voort et al. (2008), the use of UHPC allowed for the creation of a very slender arch, as seen in Figure 2.7, something that could not be accomplished using regular strength concrete.

Sakata Miraï Footbridge

This bridge (seen in Figure 2.8) was completed in Japan in 2002 and was the first use of UHPC in the country. It uses a 7.9 ft (2.4 m) wide, 164 ft (50 m) long beam that is externally prestressed. The bridge was constructed using pre-cast segments, and the use of UHPC allows it contain no "passive reinforcement" (Resplendino, 2004). As compared to a regular strength concrete bridge, the innovative design resulted in a 25% reduction of self-weight (Tanaka et al., 2009). This lead to a decrease in required foundation sizes and provided a cost savings of 8%.

Bourg-lès-Valence Bypass Bridges

The Bourg-lès-Valence Bypass bridges were the first ever road bridges to be constructed of UHPC (specifically the Béton Spécial Industriel UHPC). They were built during 2000-2001 by Eiffrage through a contract with the French government. The design consists of two side-by-side bridges, each with two span lengths of 72.2 ft (22 m). Each bridge is supported by 5 pi-shaped UHPC girders, seen in Figure 2.9. The pi-girders are pre-tensioned, and are linked with longitudinal, cast-in-place UHPC joints (Hajar Ziad, Simon, & Petitjean, 2004).

This bridge is significant because it is a first step towards the use of UHPC in major bridge projects. Although pedestrian bridges were constructed before the Bourg-lès-Valence Bypass Bridges, this bridge leads the way for UHPC as a major building material.

Mars Hill Bridge

The Mars Hill Bridge represents a major step for UHPC in the United States, as it was the first UHPC bridge used on a public road. The bridge was completed in 2006 and utilizes bulb-tee girders. The bridge spans 108 ft (33 m) with three girders. By using UHPC, the flanges and webs of the girders were able to be reduced in size (Graybeal B. A., 2009). No transverse shear reinforcement was used, as the girders were steel fiber reinforced. Ductal/RPC was used to complete the project.

Jakway Bridge

Built in Buchanan County, Iowa, the Jakway Bridge is a three-span structure, with a total length of 112 ft 4 in (34.2 m). Each span has three girders. The bridge can be seen in Figure 2.11 and Figure 2.12. The center span of the bridge is constructed using UHPC, while the others use regular strength concrete. This bridge represents a further optimization of UHPC through the use of innovative sections. While the Mars Hill Bridge uses girder shapes that have been modified for UHPC, the Jakway Bridge uses pi-girders specifically developed for UHPC applications. The particular pi-girder used is a 2nd generation design. The 2nd generation shapes have been modified for improved load distribution and increased transverse deck strength (Berg, 2010).

Figure 2.6: Comparison of the new UHPC Sherbrooke Footbridge (left) and a Steel Truss Crossing (Blais & Couture, 1999)

Figure 2.7: View of the Seonyu UHPC Bridge in South Korea (Lafarge, 2009)

Figure 2.8: View of UHPC Sakata Miraï Footbridge in Japan (Tanaka et al., 2009)

Figure 2.9: UHPC Pi-Girders in the Bourg-les-Valences Road Bridge in France (Vergoossen, 2008)

Figure 2.10: UHPC Mars Hill Bridge in Wapello County, Iowa (Keierleber et al., 2007)

Figure 2.11: Installation of the Second Generation UHPC Pi-Girder on the Jakway Bridge in Buchanan County, Iowa (Bierwagen, 2009)

Figure 2.12: View of the Completed UHPC Jakway Bridge in Buchanan County, Iowa (Bierwagen, 2009)

The previously mentioned designs indicate the potential for UHPC, and demonstrate how designs are evolving in order to fully exploit its strengths. The fact that it has been used in bridge validates it as a safe, viable construction material. However, there many avenues yet unexplored for UHPC beyond the scope of bridge construction. Wind turbines towers are one such avenue.

2.3   Wind Turbine Tower Design

As with large structures, wind turbines towers must be designed for a combination of loads, satisfying both strength and serviceability limit states. The following section details the sources of loading for wind turbine towers, necessary design limit states, applicable specifications for determining loads and strength, and example design studies.

2.3.1   Sources of Loading

Wind turbines are subjected to a multitude of loading conditions throughout their service life. These loads can be grouped into two categories: turbine loads and tower loads. Turbine loads

are defined as loads caused by the operation of the turbine, and are applied to the tower at the hub height. Turbine loads can be further separated into the following categories (LaNier, 2005):

- "Aerodynamic loads from a uniform, steady wind speed and centrifugal forces generate a stationary load";
- "A stationary, but spatially uneven flow field over the swept area causes cyclic load changes on the turning rotor";
- "The mass forces that result from the rotating rotor blade weight cause periodic, nonstationary loads"; and
- "In addition to the stationary and cyclic loads, the rotor is exposed to nonperiodic and random loads caused by wind turbulence."

As these loading conditions are not all static by nature, it is important to know both the amplitude of the loading as well as the excitation frequency.

Tower loads include the self-weight of the tower, the dead-weight of the wind turbine, the direct wind force on the tower, and seismic acceleration of the system if applicable. The direct wind force can be calculated as a static equivalent force (see more details in Section 1.1.1).

These forces give rise to the limits states discussed in the following section.

2.3.2   Limit States

In order to complete the design of a wind turbine tower, all necessary limit states must be identified. A limit state failure can have multiple definitions, but implies the structure has reached the limit of its usefulness. This includes, but is not limited to a collapse of the tower. Therefore, some limit states are evaluated at factored load levels, and some at service load levels.

<u>Strength</u>

Strength limit states can either be satisfied by evaluating service level stresses and limiting them to "relatively small fractions of the characteristic strength of the component materials"

(Naaman, 2004), or by evaluating a member's ultimate capacity compared to factored-level loads. With prestressed concrete, it is common to design the structure using the former approach. One method is to prevent the development of tension anywhere in the structure. Alternatively, a limited amount of tension is allowed, such that cracking does not occur.

If the structure satisfies the strength limit state for service level conditions, factored level loads are applied and its ultimate strength can be checked. However, since the service level loads typically govern the design, the ultimate strength is usually left as a check. LaNier (2005) identifies the following as pertinent strength limit states for prestressed concrete design:

- "Resistance to the design earthquake or wind load";
- "Zero-tension stress in the concrete under the service wind loads"; and
- "No failure during construction for temporary wind loads".

For steel, Allowable Stress Design (ASD) or Load and Resistance Factor Design (LRFD) can be used. For ASD, sections are limited to elastic behavior and are designed for service level loads. Therefore, the applicable limit states define yielding and buckling as the failure modes. For LRFD, factored level loads are applied. Limits states would include excessive yielding, fracture, and buckling. In the case of steel, buckling refers to both global buckling of the tower due to compressive loads, as well as local buckling of slender steel elements.

For both steel and concrete design, shear strength must be satisfied as well.

Fatigue

Due to the high number of cycles occurring during the lifetime of a wind turbine, fatigue becomes a necessary concern in tower design. For both concrete and steel towers, this limit state needs to be addressed through a fatigue analysis. For this analysis, the total number of cycles and corresponding stress range in the structural elements needs to be known. A detailed analysis or codified approach can then be used to evaluate the fatigue strength of the material. A method of high cycle fatigue is contained with CEB-FIP Model Code 1990, and

is discussed further in Section 1.1.1. Additionally, the Damage Equivalent Load Method is described in Section 2.3.7.

Serviceability

In the context of wind turbine towers, the limit state of serviceability refers to a limiting deflection. As there are no specifications currently in the U.S. devoted to wind turbine towers, there are no standardized deflection limits. However, industrial chimneys have been built of concrete for years, and have similar design considerations. ACI 307-98 is one such specification, which includes recommendations on deflection limits in order to "reduce effects of secondary bending moments" (ACI Committee 307, 1998) that could be used for the design fo concrete chimneys. Additionally, some deflection control would be needed to allow technicians to access and service the turbine without excessive discomfort. Code deflections limits are discussed further in Section 2.3.6.

Dynamic Effects

Since wind turbines have multiple excitation frequencies, the natural frequency of the tower is an important design consideration. The most important of these excitation frequencies are the blade rotational frequency, known as 1P, and the blade passing frequency known as 2P or 3P, for a 2-bladed or 3-bladed turbine, respectively. "Soft towers" are typically designed somewhere in between these frequencies, in what is termed as a "working range" (LaNier, 2005). It is suggested that this working range is bounded by 1P +/-10% and 2P/3P +/- 10% (DNV/Risø, 2002), resulting in a range of 1.1P-2.7P. Figure 2.13 illustrates working ranges for various turbine ratings, as well as the tower natural frequencies for designs developed by LaNier (2005). It can be seen that as the power output of the turbine increases, the working range of the natural frequency decreases. A stiffer tower could be designed with a natural frequency greater than 3P (or 2P for a 2-bladed turbine); however this would increase its cost considerably, making it uneconomical.
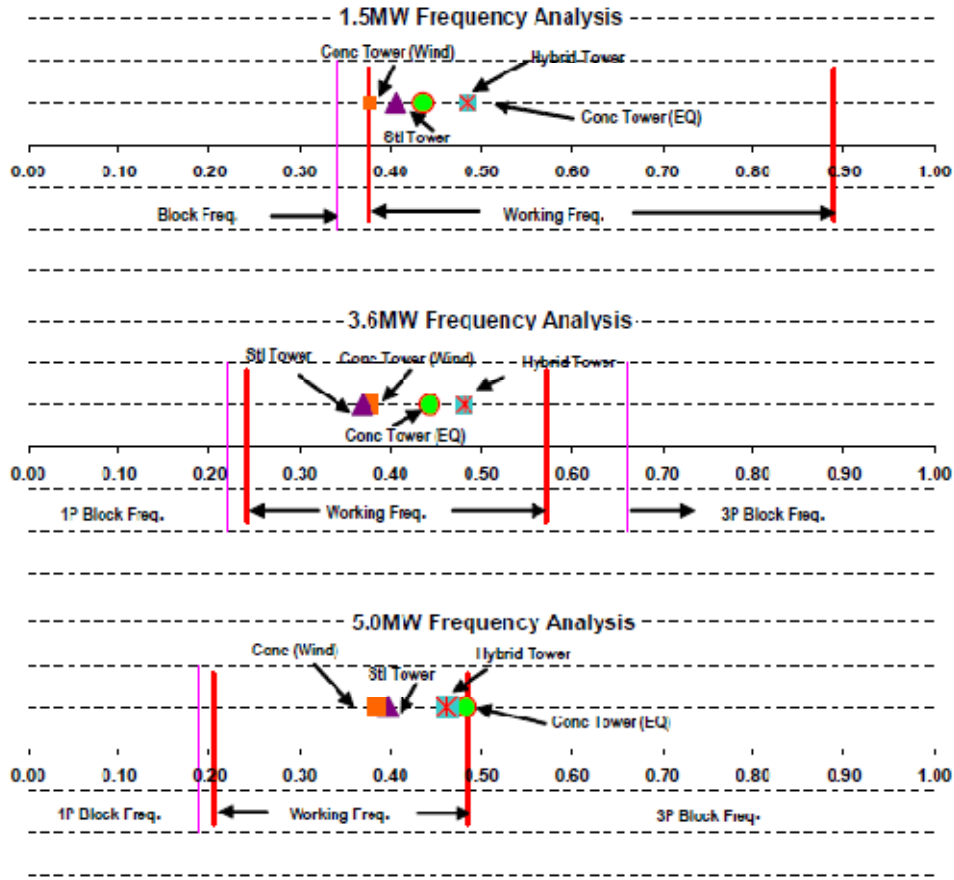
Figure 2.13: Acceptable Working Range for Fundamental Natural Frequency for Different Tower Types and Turbine Ratings by LaNier (2005)

Additionally, the effect of vibrations induced by vortex shedding must be accounted for (DNV/Risø, 2002). Vortex shedding is an aeroelastic phenomenon that involves the creation of "areas of negative pressures on either side of a structure normal to the wind direction" (Chang, 2007). Its occurrence is dependent on the cross section of the structure, as well as the design wind speed. ACI 307-98 addresses this concern for circular cross sections. The use of this specification is discussed in Section 2.3.6.

2.3.3 Load Cases

The load cases for design can, in general, be derived from the ASCE 7-05, but several modifications are suggested by LaNier (2005). The first is that for wind turbine loads, a load

factor of 1.35 be used. This corresponds to the International Electrotechnical Commission (IEC) partial load factor for wind turbines (International Electrotechnical Commission, 2007). For direct wind loads on the tower, the factor of 1.6 is retained. LaNier's rationale for two different factors is that the tower will always be subjected to the direct wind load. However, the turbine wind load can be controlled somewhat through the operation of the rotor. This measure of control over the wind turbine load is justification for reduction in the load factor. Additionally, since the turbine wind loads are often based on the load cases specified by the IEC, using the IEC's load factor lends consistency to the design. For ultimate loads, this results in the following load combinations, as load cases involving primarily live load, snow, and roof live can be neglected:

$$1.4D \tag{2-8}$$

$$1.2D + (1.6W + 1.35TL) \tag{2-9}$$

$$1.2D + 1.0E \tag{2-10}$$

For service level load conditions, the following load combination is recommended by LaNier (2005):

$$1.0D + 1.0W + 1.0TL \tag{2-11}$$

For fatigue evaluation, the following load combination is recommended (LaNier, 2005):

$$1.0D + \Delta TL \tag{2-12}$$

where D = Dead Load;

$\quad W$ = Direct Wind Load;

$\quad TL$ = Turbine Wind Load;

$\quad E$ = Earthquake Load; and

$\quad \Delta TL$ = Turbine Fatigue Load Range.

Equation (2-12) results in a range of loads, and therefore a range of stresses. This range can be evaluated with an applicable specification, as discussed in Section . It should be noted that direct wind loads are not included in the fatigue load case, which remains consistent with

industry methods (LaNier, 2005). LaNier's recommended load factor of 1.0 for wind turbine loads was judged adequate, as specifications dealing with fatigue typically include their own load factors.

2.3.4 *Applicable Loading Provisions*

As mentioned previously, it is necessary to use a combination of design standards to complete a wind turbine tower design. As there is no all-inclusive design document available in the United States for this purpose, designers use a combination to satisfy all necessary requirements. The following are documents used for determining loading for the design of wind turbine towers in this report.

<u>IEC 61400-1</u>

The IEC 61400-1 is a design standard published by the International Electrotechnical Commission (IEC), which is an organization founded in London, UK that provides design standards concerning "electrotechnical industries" (Electrotechnical Commission). The IEC 61400-1 concerns "Wind Turbine Safety and Design" (International Electrotechnical Commission, 2007). This standard is specifically useful for American wind turbine tower design because of its method for specifying design wind speed. Although the ASCE 7-05 specifies a basic design wind speed based on the location within the United States, this does not take into account the actual power rating of the design turbine. IEC 61400-1 does this by grouping wind turbines into classes (I, II, or III), based on typical wind speeds within their intended operating environment. Additionally, each class has a sub-category (A, B, or C) for wind turbulence characteristics, allowing for the wind turbine operating environment to be more accurately described. IEC also presents a special class, S, for use in regions with "tropical storms, such as hurricanes" (International Electrotechnical Commission, 2007). Each class has its own reference wind speed and turbulence intensity. The reference speed is given as a 10 minute average, at hub height, as shown in Table 3-2.

Table 2-3: International Electrotechnical Commission's Reference Wind Speed (2007)

Wind turbine class		I	II	III	S
V_{ref} , mph (m/s)		111.8 (50)	95.1 (42.5)	83.9 (37.5)	Values specified by the designer
A	I_{ref}(-)	0.16			
B	I_{ref}(-)	0.14			
C	I_{ref}(-)	0.12			

The values apply at hub height and

V_{ref} is the reference wind speed average over 10 min,

A designates the category for higher turbulence characteristics,

B designates the category for medium turbulence characteristics,

C designates the category for lower turbulence characteristics and

I_{ref} is the expected value of the turbulence intensity at 15 m/s.

This reference speed and turbulence can then be used in wind speed models detailed in the standard, including: Normal Wind Profile (NWP), Normal Turbulence Model (NTM), Extreme Wind Model (EWM), Extreme Operating Gust (EOG), Extreme Turbulence Model (ETM), Extreme Direction Change (EDC), Extreme Coherent Gust with Direction Change (ECD), and Extreme Wind Shear (EWS). In order to fully evaluate a wind turbine with this standard, a variety of load cases should be examined. The American Institute of Aeronautics and Astronautics (AAIA) has compiled a list of these loads cases, shown in Table 2-4. In the third column of this table, V_r stands for V_{ref}, the reference velocity from Table 2-3. In the case of many of the operating condition load cases, a design cut-out velocity (i.e. the highest velocity at which the turbine is designed to run) would ideally be used to determine the wind load. However, as stated in the caption of Table 2-4 it is permissible to use V_{ref} if a cut-out velocity is unknown. The basic wind speed calculated with specification can then be used in conjunction with the ASCE7-05 (Structural Engineering Institute, 2005) to calculate a direct wind load. It would also be used an input to a simulation or code to obtain wind turbine loads. As only turbine loading is available for the EOG50 and EWM50 wind speeds, as discussed later in this Chapter, only these wind speeds will be discussed further.

Table 2-4: IEC Load Cases Compiled by Veers and Butterfield (2001)

Design Situation	Load Case	Wind condition*		Analysis Type**
1) Power production	1.1	NTM	$V_{hub}=V_r$ or V_{out}	U
	1.2	NTM	$V_{in} < V_{hub} < V_{out}$	F
	1.3	ECD	$V_{hub}=V_r$	U
	1.4	NWP	$V_{hub}=V_r$ or V_{out}	U
				U
	1.5	EOG1	$V_{hub}=V_r$ or V_{out}	U
	1.6	EOG50	$V_{hub}=V_r$ or V_{out}	U
	1.7	EWS	$V_{hub}=V_r$ or V_{out}	U
	1.8	EDC50	$V_{hub}=V_r$ or V_{out}	U
	1.9	ECG	$V_{hub}=V_r$	U
2) Power production + fault	2.1	NWP	$V_{hub}=V_r$ or V_{out}	U
	2.2	NWP	$V_{hub}=V_r$ or V_{out}	U
	2.3	NTM	$V_{in} < V_{hub} < V_{out}$	F
3) Start up	3.1	NWP	$V_{in} < V_{hub} < V_{out}$	F
	3.2	EOG1	$V_{hub}=V_r$ or V_{out}	U
	3.3	EDC1	$V_{hub}=V_r$ or V_{out}	U
2) Normal shut down	4.1	NWP	$V_{in} < V_{hub} < V_{out}$	F
	4.2	EOG1	$V_{hub}=V_r$ or V_{out}	U
5) Emergency shut-down	5.1	NWP	$V_{hub}=V_r$ or V_{out}	U
6) Parked	6.1	EWM	$V_{hub} = V_{e50}$	U
	6.2	NTM	$V_{hub} < 0.7(V_{ref})$	F
7) Parked+Fault	7.1	EWM	$V_{hub} = V_{e1}$	U

*If cut-out wind speed, V_{out}, is unknown, V_{ref} should be used

** U designates ultimate and F designates fatigue

For the EWM50 wind speed, the turbulent wind speed with 3 second averaging time can be calculated through the following steps:

1) Calculate the 50 year mean recurrence interval (MRI), 10 minute wind speed:

$$V_{e50} = 1.4V_{ref} \left(\frac{z}{z_{hub}}\right)^{0.11} \qquad \textbf{(2-13)}$$

where V_{ref} is given in Table 2-3:
   $z =$ height of interest; and
   $z_{hub} =$ turbine hub height.

2) Convert the wind speed to a 3 second gust at 33 ft (10 m) Equations (2-19) and (2-20).

For the EOG50 wind speed, the following steps should be followed to calculate the wind speed with a 3 second averaging time:

1) Calculate the 1 year MRI, 10 min. wind speed from the EWM wind model at 33 ft (10 m):

$$V_{e1} = 1.12V_{ref} \qquad \textbf{(2-14)}$$

where V_{ref} is given in Table 2-3;
   $z =$ height of interest; and
   $z_{hub} =$ turbine hub height.

2) Calculate the turbulence standard deviation from the Normal Turbulence Model (NTM);

$$\sigma_{1,NTM} = I_{ref}(0.75V_{hub} + b) \qquad \textbf{(2-15)}$$

where I_{ref} is given in Table 2-3;
   $V_{hub} =$ cut-out wind speed, and is specified by turbine manufacturers; and
   $b = 12.53$ mph (5.6 m/s).

3) Calculate the 10 minute average wind gust speed at 33 ft (10 m):

$$V_{gust} = Min \left\{ 1.35(V_{e1} - V_{hub}), 3.3 \left(\frac{\sigma_{1,NTM}}{1 + 0.1 \left(\frac{D}{\Lambda_1} \right)} \right) \right\} \qquad \textbf{(2-16)}$$

where V_{hub} = 10 min. cut-out wind speed, and is specified by turbine manufacturers;

   D = turbine rotor diameter; and

   Λ_1 = 137.8 ft (42 m) for hub heights greater than 196.9 ft (60 m).

4) Calculate the 50 year MRI, 10 minute, extreme operating gust:

$$V(z,t) = V(z) - 0.37V_{gust} \sin(3\pi t/T)(1 - \cos(2\pi t/T)) \qquad \textbf{(2-17)}$$

$$V(z) = V_{hub}(z/z_{hub})^{0.2} \qquad \textbf{(2-18)}$$

where t =time; and

   T = 10.5 seconds.

The evaluation of Equation (2-17) results in a wind speed distribution, due to its inclusion of time as a variable. The approximate time associated with the maximum wind speed in this equation is 5.125 seconds. It should also be noted that this Equation (2-17) is only valid from 0-10.5 seconds.

5) Convert the 10 minute extreme operating gust, $V(z,t)$, to a 3 second wind speed using Equations (2-19) and (2-20).

In order to change wind speed averaging time from 10 minutes, as given in the IEC 61400-1 (International Electrotechnical Comission, 2007), to the 3 seconds, as required by the ACE 7-05 (Structural Engineering Institute, 2005), the following procedure should be followed:

1) Convert the wind speed from a 10 minute averaging time to a mean-hourly averaging time (Simiu & Scanlan, 1996):

$$V_{mean-hourly}(z) = \frac{V_{10\,minutes}(z)}{\left(1 + \frac{\beta^{0.5} c(10\,minutes)}{2.5 \ln(z/z_0)} \right)} \qquad \textbf{(2-19)}$$

where $c(10\,minutes) = 0.36$;

$z_0 =$ 0.0164 ft (0.005 m) (Simiu & Scanlan, 1996) which approximately corresponds to ASCE 7-05 (Structural Engineering Institute, 2005) exposure category D, and is the surface roughness height; and

$\beta = 6.5$ (Simiu & Scanlan, 1996) which approximately corresponds to ASCE 7-05 (Structural Engineering Institute, 2005) exposure category D.

2) Convert the wind speed from a mean-hourly averaging time to a 3 second averaging time:

$$V_{3-second}(z) = V_{mean-hourly}(z)\left(1 + \frac{\beta^{0.5}c(3\ seconds)}{2.5\ln(z/z_0)}\right)$$ **(2-20)**

where $c(10\ minutes) = 2.85$ (Simiu & Scanlan, 1996); and

z_0 and β as in Equation (2-19).

ASCE 7

Minimum Design Loads for Buildings and Other Structures, also known ASCE/SE 7-05 (Structural Engineering Institute, 2005), is an American design standard that, as the title implies, specifies loading for various structures. In the case of wind turbines towers, wind and seismic loading directly apply.

The ASCE 7-05 describes the overall wind region characteristics through the use of a basic wind speed. This speed is specified as a 3 second gust at 33 ft elevation. It is then used to determine a pressure, which varies with height and can be modified based on terrain and return period. For all calculations, the exposure category of "D" was used by default. This exposure category is for wide-open spaces, with few obstructions to block wind. This was a conservative choice, as it is the most harsh wind speed environment. The actual wind speed environment would depend on the turbine location and the terrain characteristics, however, it was felt typical wind turbine locations would fall within this exposure category. Additionally, this exposure category is consistent with that chosen by LaNier (2005), and was also used so that direct comparisons could be made with the study by that author.

The direct wind load applied to the wind turbine tower is given as:

$$F(z) = q_z(z)GC_f A_f \qquad \text{(2-21)}$$

where $q_z(z)$ = wind velocity pressure;

G = gust-effect factor;

z = elevation of interest

C_f = force coefficient; and

A_f = solid projected tower area.

The equation that defines the velocity wind pressure from wind speed is as follows (SEI, 2005):

$$q_z(z) = \begin{cases} 0.00256 K_z K_{zt} K_d V^2 I \ (U.S. units) \\ 0.613 K_z K_{zt} K_d V^2 I \ (S.I. Units) \end{cases} \qquad \text{(2-22)}$$

where

$$K_z = \begin{cases} 2.01(z/z_g)^{2/\alpha} for\ 15\ ft \le z \le z_g \\ 2.01(15\ ft/z_g)^{2/\alpha} for\ z < 15 ft \end{cases} (U.S. Units)$$

$$\qquad \text{(2-23)}$$

$$K_z = \begin{cases} 2.01(z/z_g)^{2/\alpha} for\ 4.57\ m \le z \le z_g \\ 2.01(4.57\ m/z_g)^{2/\alpha} for\ z < 4.57\ m \end{cases} (S.I. Units)$$

and is an exposure coefficient that depends on elevation above the ground;

z = elevation of interest;

$\alpha = 11.5$ for exposure category "D";

$z_g = 700$ ft (213.36 m), and is the gradient height for exposure category "D";

$K_{zt} = 1.0$ for flat terrain;

$K_d = 0.95$ for round towers and truss towers that have non-square, triangular, and rectangular cross-sections, and is a directionality factor;

V = basic wind speed, mph or m/s, with a 3 second averaging time, obtained in this study from the IEC 61400-1 (International Electrotechnical Comission, 2007); and

$I = 1.0$ and is the Importance Factor, altering mean recurrence interval of wind speed.

Since a typical wind turbine farm can have 100 or more turbines, the loss of any single turbine does not represent the total failure of the wind farm. Therefore, a single turbine loss does was judged not to represent a "mass disruption of day-to-day civilian life" (Structural Engineering Institute, 2005), and an importance factor of 1.0 was judged adequate. LaNier's work agrees with this factor (2005), citing the low human occupancy of wind turbines as justification.

The gust-effect factor value is dependent on the tower's fundamental natural frequency. The equation for this factor is given as:

$$G_f = 0.925 \left(\frac{1 + 1.7 I_{\bar{z}} \sqrt{g_Q^2 Q^2 + g_R^2 R^2}}{1 + 1.7 g_V I_{\bar{z}}} \right)$$

(2-24)

where $g_Q = 3.4$, the peak factor for background response;
$\quad g_v = 3.4$, the peak factor for wind response;

$$g_R = \sqrt{2 \ln(3600 n_1)} + \frac{0.577}{\sqrt{2 \ln(3600 n_1)}}$$

(2-25)

and is the peak factor for resonance;

$\quad n_1 =$ tower fundamental natural frequency, Hz;

$$I_{\bar{z}} = \begin{cases} c \left(\frac{33 \ ft.}{\bar{z}} \right)^{1/6} & (U.S. \ Units) \\ c \left(\frac{10 \ m.}{\bar{z}} \right)^{1/6} & (S.I. \ Units) \end{cases}$$

(2-26)

and is the turbulence intensity at 33 ft (10 m);

$\quad c = 0.15$, the turbulence intensity for exposure "D";

$$\bar{z} = 0.6h$$

(2-27)

$h =$ the structure height;

$$R = \sqrt{\frac{1}{\beta} R_n R_h R_B (0.53 + 0.47 R_L)} \tag{2-28}$$

and is the resonance response factor;

$\beta = 0.02$, and is the assumed structural damping ratio;

$$N_1 = \frac{n_1 L_{\bar{z}}}{\bar{V}_{\bar{z}}} \tag{2-29}$$

$$R_n = \frac{7.47 N_1}{(1 + 10.3 N_1)^{5/3}} \tag{2-30}$$

$$L_{\bar{z}} = \begin{cases} l\left(\dfrac{\bar{z}}{33\,ft.}\right)^{0.125} (U.S.\,Units) \\ l\left(\dfrac{\bar{z}}{10\,m.}\right)^{0.125} (S.I.\,Units) \end{cases} \tag{2-31}$$

for exposure category "D";

$l = 650\,ft\ (198.2\,m)$, for exposure category "D";

$$\bar{V}_{\bar{z}} = \begin{cases} 0.8\left(\dfrac{\bar{z}}{33\,ft.}\right)^{0.11} V\left(\dfrac{88}{60}\right) (U.S.\,Units) \\ 0.8\left(\dfrac{\bar{z}}{10\,m.}\right)^{0.11} V\ (S.I.\ Units) \end{cases} \tag{2-32}$$

with V in mph or m/s for exposure category "D";

$$R_h = \frac{1}{4.6 n_1 \frac{h}{\bar{V}_{\bar{z}}}} - \frac{\left(1 - e^{-2\left(4.6 n_1 \frac{h}{\bar{V}_{\bar{z}}}\right)}\right)}{2\left(4.6 n_1 \frac{h}{\bar{V}_{\bar{z}}}\right)^2} \tag{2-33}$$

$$R_B = \frac{1}{4.6 n_1 \frac{B}{\bar{V}_{\bar{z}}}} - \frac{\left(1 - e^{-2\left(4.6 n_1 \frac{B}{\bar{V}_{\bar{z}}}\right)}\right)}{2\left(4.6 n_1 \frac{B}{\bar{V}_{\bar{z}}}\right)^2} \tag{2-34}$$

where B = width of the tower, measured normal to the wind direction;

$$R_L = \frac{1}{15.4 n_1 \frac{L}{\overline{V}_{\bar{z}}}} - \frac{\left(1 - e^{-2\left(15.4 n_1 \frac{L}{\overline{V}_{\bar{z}}}\right)}\right)}{2\left(15.4 n_1 \frac{L}{\overline{V}_{\bar{z}}}\right)^2}$$

(2-35)

where L = tower length, measured parallel to the wind direction; and

$$Q = \sqrt{\frac{1}{1 + 0.63 \left(\frac{B + h}{L_{\bar{z}}}\right)^{0.63}}}$$

(2-36)

and is the background response factor.

C_f is the force coefficient that is determined by the tower cross-sectional shape and surface roughness. For circular sections with,

$$D\sqrt{q_z} > 2.5 \ (U.S. Units)$$

(2-37)

$$D\sqrt{q_z} > 5.3 \ (S.I. Units)$$

where $D =$ is the diameter of the tower, in ft. (m); and
q_z = the basic wind pressure as defined in Equation (2-22), in psf (N/m^2).

$$C_f = \begin{cases} 0.5 \ for \ h/D = 1 \\ 0.6 for \ h/D = 7 \\ 0.7 for \ h/D = 25 \end{cases}$$

(2-38)

for moderately smooth towers.

For values of h/D between those given in (2-38), linear interpolation can be used. Although not explicitly stated in the specification, it was assumed that linear extrapolation is conservative, as opposed to using 0.7 as an upper bound. For square or triangular trussed or

lattice towers, Figure 6-23 in the ASCE 7-05 can be used to calculate C_f. The way this figure was utilized in this report is detailed in Section 4.3.1 of this report.

2.3.5   Applicable Design Standards for Steel

The following are the applicable standards for evaluating the limit states for steel towers.

ANSI/AISC 360-05

AISC 360-05 can be used to evaluate the strength of the steel shell, using either Load and Resistance Factor Design (LRFD) or Allowable Strength Design (ASD). As LRFD is more versatile than ASD, its use will be described in detail. While AISC 360-05 does not specifically address large cylindrical shells, it does have provisions for round Hollow Structural Steel (HSS) sections. As round HSS are similar in shape and D/t ratios (where D is the diameter of the shell and t is the thickness thickness of the shell) to steel wind turbine tower shells, the provisions would apply.

For compression, the AISC sets limits for D/t in order to classify a section as noncompact or slender. For sections with a D/t ratio greater than the specified limit, the section is classified as slender. If the D/t ratio falls below the limit, the section is classified as noncompact. The limit is given as:

$$D/t \lessgtr 0.11E/F_y \qquad \text{(2-39)}$$

where D = diameter of the shell;

t = thickness of the shell;

E = modulus of elasticity; and

F_y = yield strength of the steel.

For noncompact sections, the strength of the section in pure compression is given as:

$$P_n = F_{cr}A_g \qquad \text{(2-40)}$$

where P_n = nominal design strength in compression; and

F_{cr} = critical buckling stress.

F_{cr} requires the calculation of the elastic buckling stress, F_e, given by:

$$F_e = \frac{\pi^2 E}{\left(\frac{KL}{r}\right)^2} \tag{2-41}$$

where $\frac{KL}{r}$ = slenderness ratio; and

$k = 2$ for a cantilever.

When $F_e \geq 0.44 F_y$, inelastic buckling occurs, and the critical buckling stress is given as:

$$F_{cr} = \left[0.658^{\frac{F_y}{F_e}}\right] F_y \tag{2-42}$$

When $F_e < 0.44 F_y$, elastic buckling occurs, and the critical buckling stress is given as:

$$F_{cr} = 0.877 F_e \tag{2-43}$$

For slender sections, F_y is replaced by QF_y in Equation (2-42). Additionally, the stress F_e is compared to a limit of $0.44QF_y$ to determine whether elastic or inelastic buckling occurs. For stiffened elements Q is given is Equation (2-44) as:

$$Q = Q_a = \frac{0.038E}{F_y \left(\frac{D}{t}\right)} + \frac{2}{3} \tag{2-44}$$

when $0.11\frac{E}{F_y} < \frac{D}{t} < 0.45\frac{E}{F_y}$.

Equation (2-44) accounts for local buckling occurring due to compression applied to slender sections. The resistance factor for compression is taken as $\phi_c = 0.9$.

For bending, the following is the limit for a compact section:

$$D/t < 0.07E/F_y \tag{2-45}$$

The limit for noncompact sections is:

$$D/t < 0.31E/F_y \tag{2-46}$$

The bending strength of a compact round HSS is given as:

$$M_n = M_p = F_y Z \tag{2-47}$$

where Z = plastic section modulus.

The bending strength of noncompact round HSS is given as:

$$M_n = \left(\frac{0.021E}{\frac{D}{t}} + F_y \right) S \tag{2-48}$$

where S = elastic section modulus.

The bending strength of slender round HSS, accounting for the occurrence of local buckling is given as:

$$M_n = F_{cr} S \tag{2-49}$$

$$F_{cr} = \frac{0.33E}{\frac{D}{t}} \tag{2-50}$$

The resistance factor for bending is taken as $\phi_b = 0.9$.

For torsion, the nominal strength is given as:

$$T_n = F_{cr} C \tag{2-51}$$

$$C = \frac{\pi(D - t)^2 t}{2} \tag{2-52}$$

F_{cr} for torsional buckling is the larger of:

$$F_{cr} = \frac{1.23E}{\sqrt{\frac{L}{D}} \left(\frac{D}{t} \right)^{\frac{5}{4}}} \tag{2-53}$$

$$F_{cr} = \frac{0.60E}{\left(\frac{D}{t} \right)^{\frac{3}{2}}} \tag{2-54}$$

where L = length of the section.

The resistance factor for torsion is taken as $\phi_t = 0.9$.

The nominal shear strength of round HSS is given as:

$$V_n = F_{cr}A_g/2 \tag{2-55}$$

where A_g = gross section area; and

    F_{cr} = critical shear buckling stress, and can be calculated as the larger of:

$$F_{cr} = \frac{1.60E}{\sqrt{\frac{L_v}{D}}\left(\frac{D}{t}\right)^{\frac{5}{4}}} \tag{2-56}$$

$$F_{cr} = \frac{0.78E}{\left(\frac{D}{t}\right)^{\frac{3}{2}}} \tag{2-57}$$

where L_v = length from maximum to zero shear force.

This stress cannot be taken larger than $0.6F_y$. The resistance factor for shear is taken as $\phi_v = 0.9$.

The combination of forces should meet the following condition:

$$\left(\frac{P_u}{\phi_c P_n} + \frac{M_u}{\phi_b M_n}\right) + \left(\frac{V_u}{\phi_v V_n} + \frac{T_u}{\phi_t T_n}\right)^2 \leq 1.0 \tag{2-58}$$

where P_u = required, factored-level axial force;

    M_u = required, factored-level bending moment;

    V_u = required, factored-level shear force; and

    T_u = required, factored-level torsional moment.

European Convention for Constructional Steelwork (ECCS)

Local buckling of the steel shell can be evaluated using the method laid out in *Recommendations on Buckling of Shells* (European Convention for Constructional Steelwork,

1988), as discussed in *The Wind Energy Handbook* (Burton, Sharpe, Jenkins, & Bossanyi, 2001). The elastic buckling stress for a cylindrical tube is given as,

$$\sigma_{cr} = \frac{0.605Et}{r} \tag{2-59}$$

where E = elastic modulus;

  t = wall thickness; and

  r = radius of the cylinder.

Due to imperfections caused by welding, a reduction to the buckling strength is introduced assuming the length of the imperfection is less than 1% of the total height. Equation (2-60) is a version of the ECCS reduction factor which has been modified for tapered cylinders (Chryssanthopoulos et al., 1998):

$$\alpha_0 = \begin{cases} \dfrac{0.83}{\sqrt{1 + 0.01(R_{1e}/t)}} & for \ \ R_{1e}/t \leq 212 \\ \dfrac{0.70}{\sqrt{0.1 + 0.01(R_{1e}/t)}} & for \ \ R_{1e}/t > 212 \end{cases} \tag{2-60}$$

where

$$R_{1e} = R_1/cos\rho \tag{2-61}$$

and ρ = semi-vertex angle of the conical shell;

  R_1 = smaller of the two end radii; and

  t = shell thickness.

However, since a steel wind turbine tower is typically subjected to bending and compression due to the combination of dead loads and lateral wind loads, the bending reduction factor is introduced:

$$\alpha_B = 0.1887 + 0.8113\alpha_0 \tag{2-62}$$

The buckling stress is then given as,

$$\sigma_u = \begin{cases} f_y \left[1 - 0.4123 \left(\dfrac{f_y}{\alpha_B \sigma_{cr}} \right)^{0.6} \right] & for\ \alpha_B \sigma_{cr} > f_y/2 \\[3mm] 0.75 \alpha_B \sigma_{cr} & for\ \alpha_B \sigma_{cr} < \dfrac{f_y}{2} \end{cases} \tag{2-63}$$

where f_y = yield strength of the steel.

According to LaNier (2005), the buckling stress can then be compared to the maximum applied stress,

$$\sigma_{app} = \sqrt{(f_a + f_b)^2 + 3f_v^2} \tag{2-64}$$

Where f_a = applied axial stress;

f_b = applied bending stress; and

f_v = applied shear stress.

As the AISC (American Institute of Steel Construction, Inc., 2005) specification includes slenderness as a design criterion, this local buckling calculation serves as a second check in design. However, it was felt that this check was valuable, as the AISC method does not account for imperfections due to welding. The computation of this buckling strength as a portion of the elastic buckling strength implies stresses are limited to less than residual stresses caused by differential cooling in steel sections. Factored-level forces are expected to cause inelastic behavior in members, hence the use of the plastic section modulus in Equation (2-47). Therefore, the stresses f_a, f_b, and f_v should be calculated for service-level loading.

2.3.6 Applicable Design Standards for Concrete

The following are applicable standards for evaluating the various limit states for concrete towers.

<u>CEB-FIP Model Code 1990</u>

The Model Code 1990 (MC90) is a document created through the collaboration of the Euro-International Committee for Concrete (CEB) and the Federation of Prestressing (FIP) regarding the design of concrete structures. It is intended to cover "the description of the

mechanical behavior of reinforced concrete, the materials' and their composite behavior" and "a coherent framewok for the subsequent chapters with appropriate simplifications of the basic models" (Comite Euro-International Du Beton, 1993). In the context of concrete wind turbine towers, it is particularly useful because it addresses low amplitude, high cycle fatigue with more than 10^8 cycles.

Chapter 6.7 of the MC90 presents several methods for the evaluation of fatigue for concrete, reinforcing steel, and prestressing steel. The first method, known as "Verification by the simplified procedure", is applicable for fatigue design of structures subjected to between 10^4 and 10^8 load cycles. As wind turbines are predicted to experience around 5.29×10^8 load cycles, this approach cannot be used.

The second method, "Verification by means of a single load level" can be used for any number of cycles, and therefore is applicable.

For reinforcing and prestressing steel, the following requirement is set:

$$\gamma_{Sd} max \Delta\sigma_{Ss} \leq \Delta\sigma_{Rsk}(n)/\gamma_{s,fat} \qquad \text{(2-65)}$$

where $max\Delta\sigma_{Ss}$ = maximum fatigue stress range for steel;

n = predicted number of fatigue cycles over the lifetime;

$\Delta\sigma_{Rsk}(n)$ = stress range relevant to n cycles obtained from a characteristic fatigue function;

$\gamma_{Sd} = 1.1$, and is a fatigue load factor; and

$\gamma_{s,fat} = 1.15$, and is a fatigue material safety factor for steel.

$\Delta\sigma_{Rsk}(n)$ is determined by plotting the stress (S) versus cycles (N) curve and comparing the allowable stress range at the predicted number of cycles with the measured stress range due to the fatigue load case. An illustrative example of an S-N curve can be seen in Figure 2.14.
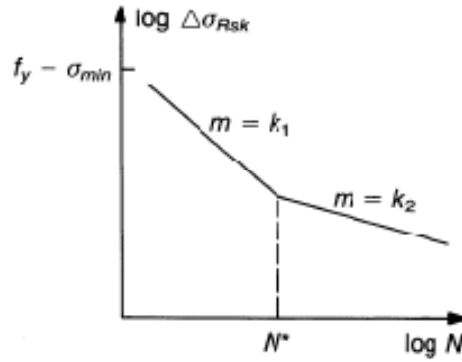
Figure 2.14: Example S-N Curve (Comite Euro-International Du Beton, 1993)

The S-N curve is a bi-linear curve when plotted on a log-log scale. In Figure 2.14, -1/m is the slope of each part of the curve. N* represents the number of cycles at which the curve transitions from slope $-1/k_1$ to $-1/k_2$. The values of N^*, k_1, and k_2 for prestressing steel can be obtained from Table 2-5 provided in the MC90.

Table 2-5: MC90 Steel Fatigue Parameters (Comite Euro-International Du Beton, 1993)

	N*	Stress Exponent		$\Delta\sigma_{Rsk}$ (Mpa)		$\Delta\sigma_{Rsk}$ (ksi)	
		k_1	k_2	At N* cycles	At 10^8 cycles	At N* cycles	At 10^8 cycles
Pretensioning Straight Steels	10^6	5	9	160	95	23.21	13.78
Post-tensioning Curved Tendons[a]	10^6	3	7	120	65	17.40	9.43
Straight Tendons	10^6	5	9	160	95	23.21	13.78
Mechanical Connectors	10^6	3	5	80	30	11.60	4.35

[a]In cases where the S-N curve intersects that of the straight bar, the fatigue strength of the straight bar is valid.

It can be seen in Table 2-5 that N*=10^6 for all prestressing steel types. As the towers in this study are subjected to 5.29×10^8 load cycles, the portion of the S-N curve with the slope $-1/k_2$ should used. Therefore, $\Delta\sigma_{Rsk}(n)$ can be calculated as:

$$\log[\Delta\sigma(n)_{Rsk}] = \log[\Delta\sigma(N^*)_{Rsk}] - \frac{1}{k_2}\log\left(\frac{n}{N^*}\right) \tag{2-66}$$

$$\Delta\sigma_{Rsk}(n) = 10^{\log[\Delta\sigma(n)_{Rsk}]} \tag{2-67}$$

For concrete, the following fatigue requirement applies,

$$n \leq N \tag{2-68}$$

where n = required number of cycles (lifetime); and

N = allowable number of load cycles.

For concrete in compression only, N based on $S_{cd,min}$, $S_{cd,max}$, and ΔS_{cd} as detailed below.
For $0 < S_{cd,min} < 0.8$

$$logN_1 = \left(12 + 16S_{cd,min} + 8S_{cd,min}^2\right)\left(1 - S_{cd,max}\right) \tag{2-69}$$

$$logN_2 = 0.2logN_1(logN_1 - 1) \tag{2-70}$$

$$logN_3 = logN_2(0.3 - \frac{3}{8}S_{Sd,min})/\Delta S_{cd} \tag{2-71}$$

If $logN_1 \leq 6$, then $logN = logN_1$

If $logN_1 > 6$ and $\Delta S_{cd} \geq 0.3 - \frac{3}{8}S_{Sd,min}$, then $logN = logN_2$

If $logN_1 > 6$ and $\Delta S_{cd} < 0.3 - \frac{3}{8}S_{Sd,min}$, then $logN = logN_3$

where

$$S_{cd,max} = \gamma_{Sd}\sigma_{c,max}\eta_c/f_{cd,fat} \tag{2-72}$$

$$S_{cd,min} = \gamma_{Sd}\sigma_{c,min}\eta_c/f_{cd,fat} \tag{2-73}$$

$$\Delta S_{cd} = S_{cd,max} - S_{cd,min} \tag{2-74}$$

$\sigma_{c,max}$ = maximum compressive stress; and

$\sigma_{c,min}$ = minimum compressive stress.

$S_{cd,max}$ and $S_{cd,min}$ involve the factor η_c, which is the gradient factor, accounting for non-uniform stress levels in a cracked concrete section. This factor is calculated as follows,

$$\eta_c = \frac{1}{1.5 - 0.5|\sigma_{c1}|/|\sigma_{c2}|} \tag{2-75}$$

where $|\sigma_{c1}|$ = lower absolute value of the compressive stress within a distance of no more

than 11.81 in. (300 mm) from the surface under the relevant load combination; and

$|\sigma_{c2}|$ = larger absolute value of the compressive stress within a distance no more than

11.81 in. (300 mm) from the surface under the same load combination as for $|\sigma_{c1}|$.

$S_{cd,max}$ and $S_{cd,min}$ also involve the reference compressive fatigue strength, $f_{cd,fat}$, which can

be calculated according to the following equation,

$$f_{cd,fat} = 0.85\beta_{cc}(t) \left[f_{ck} \left(1 - \frac{f_{ck}}{25 f_{ck0}} \right) \right] / \gamma_c \tag{2-76}$$

where $\gamma_c = \gamma_{c.fat} = 1.5$;

$f_{ck0} = 1.450$ ksi (10 MPa).

f_{ck} is approximated as the 28-day strength, ksi (MPa).

$\beta_{cc}(t)$ is a factor accounting the for aging of concrete, and was calculated from the following

formula:

$$\beta_{cc}(t) = e^{s\left[1 - \left(\frac{28}{t}\right)^{1/2}\right]} \tag{2-77}$$

where $s = 0.2$ for rapidly aging concretes; and

t = age of concrete, days.

In the BergerABAM study, LaNier (2005) used a concrete age of 60 days in calculating fatigue resistance, as well as assumed the use of rapidly aging concrete. Given the common use of heating treating in prestressed concrete, and the delay between when the concrete sections would be cast, and when the turbine would actually become operational, these assumptions were judged reasonable.

ACI 307-98

ACI 307-98 (ACI Committee 307, 1998) is a standard discussing the design of reinforced concrete chimneys. In many regards, these chimneys are very similar to concrete wind turbine towers. They are of similar height, designed as a shell structure, and experience comparable direct wind loading. Therefore, several aspects of this specification can be directly applied to wind turbine towers. While no standard was found to specifically identify a limit for lateral deflection on wind turbine towers, ACI 307-98 sets out deflection limits to reduce P-Δ effects. This following formula defines the allowable maximum deflection for concrete chimney:

$$Y_{max} = 0.04h \qquad \text{(2-78)}$$

Where Y_{max} = maximum allowable deflection, in.; and

h = the tower height, ft.

For a 328 ft (100 m) tall tower, Equation (2-78) yields an allowable lateral deflection of 13.12 in. (0.333 m).

ACI307-98 also addresses vibration effects on concrete chimneys arising from vortex shedding. The criterion for consideration of vortex shedding involves comparing the critical excitation speed with the mean hourly design speed $(\overline{V})$ at 5/6 of the total tower height (z_{cr}). The critical speed is given as,

$$V_{cr} = \frac{fd(u)}{S_t} \qquad \text{(2-79)}$$

where f = first frequency mode, Hz; and

$d(u)$ = mean outside diameter of upper third of the tower.

S_t = Strouhal Number, and can be calculated based on the following formula:

$$S_t = 0.25F_1(A) \qquad \text{(2-80)}$$

where

$$F_1(A) = 0.333 + 0.206 \log_e \left(\frac{h}{d(u)}\right) \tag{2-81}$$

where h = tower height.

If $0.5\overline{V}(z_{cr}) \leq V_{cr} \leq 1.30\overline{V}(z_{cr})$, then vortex shedding must be considered as a design criterion.

<u>ACI 318-08</u>

ACI 318-08 is an American standard that addresses materials, design, and construction of structural concrete (ACI Committee 318, 2008). It is the predominant standard for concrete building construction in the United States. It can be used to design prestressed and non-prestressed members subject to the combination of flexure, compression, tension, and shear. However, it is not generally applicable to UHPC.

For prestressed flexural members, service-level loads typically govern the design. The following limit is set the following allowable compressive stress limit for prestressed concrete (ACI Committee 318, 2008) under service-level loading:

$$f_a \leq \begin{cases} 0.45 f_c' \; for \; prestress \; plus \; sustained \; loads \\ 0.60 f_c' \; for \; prestress \; plus \; total \; load \; (including \; transient) \end{cases} \tag{2-82}$$

where f_c' = the 28-day compressive strength of the concrete.

For post-tensioning steel, the following permissible values are given for service-level loading:

$$f_t \leq \begin{cases} minimum(0.94 f_{py}, 0.8 f_u) \; for \; jacking \; force \\ minimum \; (0.70 f_{pu}, 0.82 f_{py}) \; immediately \; after \; transfer \end{cases} \tag{2-83}$$

where f_{py} = post-tensioning yield stress; and

f_{pu} = post-tensioning ultimate stress.

For ASTM A 416 prestressing tendons with f_{pu}= 270 ksi (1862 MPa) and f_{py}= 243 ksi (1675 MPa), this translates to an allowable jacking stress of 216 ksi (1489 MPa) and an allowable transfer stress of 189 ksi (1303 MPa).

To define the concrete shear strength of prestressed members, ACI specifies two applicable limit states: Flexure-shear cracking (V_{ci}) and Web-shear cracking (V_{cw}). The limiting strength is defined as follows:

$$V_{ci} = \begin{cases} \left(0.6\sqrt{f_c'(psi)}\right)b_w d + \dfrac{V_i M_{cre}}{M_{max}} \not< 1.7\sqrt{f_c'(psi)}b_w d \\ \left(0.049821\sqrt{f_c'(MPa)}\right)b_w d + \dfrac{V_i M_{cre}}{M_{max}} \not< 0.14112\sqrt{f_c'(MPa)}b_w d \end{cases} \tag{2-84}$$

where

$$M_{cre} = \begin{cases} \left(\dfrac{I}{y_t}\right)\left(6\sqrt{f_c'} + f_{pe}(psi)\right) \\ \left(\dfrac{I}{y_t}\right)\left(0.49821\sqrt{f_c'(MPa)} + f_{pe}\right) \end{cases} \tag{2-85}$$

and f_c' = 28-day compressive strength of the concrete;

I = moment of inertia of the section;

y_t = distance from the centroid to the extreme tension fiber;

f_{pe} = effective stress due to prestress where tension is expected due to external load;

V_i = factored level shear demand;

M_{max} = factored level moment demand;

b_w = width of the section; and

d = depth of the section.

$$V_{cw} = \begin{cases} \left(3.5\sqrt{f_c'(psi)} + 0.3f_{pc}\right)b_w d + V_p \\ \left(0.29062\sqrt{f_c'(MPa)} + 0.3f_{pc}\right)b_w d + V_p \end{cases} \tag{2-86}$$

where f_c' = 28-day compressive strength of the concrete, psi

f_{pc} = stress due to prestressing at the centroidal axis; and

V_p = vertical component of effective prestress force.

One noticeable aspect of the ACI equations is their predisposition to rectangular sections. An alternative recommendation is to replace the $b_w d$ term in the above equations with $0.8A_{gross}$ (Priestly, Seible, & Calvi, 1996) for circular sections.

For any ultimate strengths calculated, ACI specifies strength reduction factors based on the type of limit state. These are listed below:

$$\phi_{bending} = 0.90 \text{ for tension controlled sections}$$

$$\phi_{shear/torsion} = 0.75$$

ACI also makes recommendations for the adequacy of hollow concrete sections for shear and torsion interaction. A section subjected to a combination of torsion and shear force is considered adequate if the following condition is met:

$$\left(\frac{V_u}{b_w d}\right) + \left(\frac{T_u p_h}{1.7A_{oh}^2}\right) \le \phi\left(\frac{V_c}{b_w d} + 8\sqrt{f_c'(psi)}\right) \tag{2-87}$$

$$\left(\frac{V_u}{b_w d}\right) + \left(\frac{T_u p_h}{1.7A_{oh}^2}\right) \le \phi\left(\frac{V_c}{b_w d} + \frac{2}{3}\sqrt{f_c'(MPa)}\right)$$

where V_u = factored-level shear demand;

T_u = factored-level torsional moment demand;

b_w = width of the section;

d = depth of the section;

p_h = perimeter of the centerline of the outermost closed transverse torsional reinforcement;

A_{oh} = area enclosed by the centerline of the outermost closed transverse torsional reinforcement;

V_c = nominal concrete shear strength; and

ϕ = 0.75, a safety factor for torsion

f_c' = 28-day compressive strength of concrete, psi.

These recommendations are predisposed for used with rectangular sections. Therefore, the term in Equation (2-94) should be replaced with $0.8A_{\text{gross}}$ (Priestly, Seible, & Calvi, 1996) for use with circular sections.

2.3.7 Applicable Design Standards for UHPC

While UHPC design standards are continuing to evolve, no one standard seems to cover every limit state necessary for UHPC turbine tower. As a result, it is necessary to utilize multiple standards to complete a design.

AFGC Ultra High Performance Fibre-Reinforced Concretes: Interim Recommendations

This document is a French design standard for UHPC (Association Française de Génie Civil/SETRA, 2002). It was created between 1999 and 2002, and includes information on UHPC's material properties, design methods, and durability. The equations for the shear strength of UHPC members have been adapted for use with American Customary Units by Degen (2006). UHPC's shear strength can be split into two distinct portions: that provided by the concrete, V_c, and that provided by the fibers, V_f. These equations are given below:

$$V_c = \begin{cases} 1.7b_w d\sqrt{f_c'(psi)} \\ 0.14116 b_w d\sqrt{f_c'(MPa)} \end{cases} \tag{2-88}$$

$$V_f = \frac{0.9b_w d|f_{t,max}|}{\gamma_{bf}\tan(\beta)} \tag{2-89}$$

where b_w = the section width, in.;

d = section depth, in.;

f_c' = 28-day compressive strength, psi;

$f_{t,max}$ = maximum UHPC tensile strength;

γ_{bf} = partial safety factor, 1.3; and

β = shear crack angle.

Additionally, these equations are calibrated for use with rectangular sections. For circular sections, the $b_w d$ term could be replaced with $A_e = 0.8A_{gross}$ (Priestly, Seible, & Calvi, 1996). The crack angle can be calculated based on the nominal concrete strength, V_c:

$$\beta = \frac{1}{2}\tan^{-1}\left(\frac{2}{\sigma_x}\left(\frac{V_c Q}{It}\right)\right) \qquad \textbf{(2-90)}$$

where Q = second moment of area;

I = moment of inertia;

t = thickness of the concrete shell; and

σ_x = axial stress at the point of interest.

Design Guidelines for RPC Prestressed Concrete Beams

This document was prepared for VSL, and specifically addresses Reaction Powder Concrete. In addition to providing the assumed compressive strain behavior discussed in Section 2.2.2, it is one of the few documents that discusses torsion as an ultimate limit state. The torsional ultimate strength of a section is given as (Gowripalan & Gilbert, 2000):

$$T_{uc} = \begin{cases} J_t\left(725.19\ (psi) + 1.5656\sqrt{f_c'}\right)\sqrt{1 + 10s_{cp}/f_c'} \\ J_t\left(5.0\ (MPa) + 0.13\sqrt{f_c'}\right)\sqrt{1 + 10s_{cp}/f_c'} \end{cases} \qquad \textbf{(2-91)}$$

where $J_t = 2A_m b_w$, for circular hollow sections only;

A_m = area enclosed by the median lines of the walls of a hollow section;

b_w = wall thickness;

f_c' = 28-day compressive strength, psi (MPa); and

s_{cp} = average effective prestressing force, psi (MPa).

In Equation (2-91), the term in parenthesis immediately after J_t represents the tensile cracking strength of UHPC.

Guidelines are also given for the interaction of shear and torsion as an ultimate limit state:

$$\frac{T^*}{\phi T_{uc}} + \frac{V^*}{\phi V_{uc}} \leq 0.75 \qquad \textbf{(2-92)}$$

Where T^* = factored level torsional moment demand;

V^* = factored level demand;

T_{uc} = ultimate torsional moment capacity;

V_{uc} = ultimate shear capacity; and

$\phi = 0.7$, a strength reduction factor for torsion.

<u>Recommendations for Design and Construction of Ultra High Strength Fiber Reinforced Concrete Structures, JGC No. 9</u>

JGC No. 9 (2006) is a draft guideline based on the lessons learned from the Sakata-Mirai Bridge and French standards. One of the areas that was addressed was the fatigue life of UHPC in both tension and compression. As set out in the guideline, the compressive fatigue strength of UHPC is as follows:

$$f_{rd} = 0.85 f_d \left(1 - \frac{\sigma_p}{f_d}\right)\left(1 - \frac{\log(N)}{17}\right) \tag{2-93}$$

Where f_{rd} = design fatigue strength of UHPC in compression/flexural compression;

σ_p = permanent stress that the section is subjected to;

f_d = design compressive strength, taken as the 28-day strength of concrete (f_c'), divided by a safety factor of 1.3; and

N = number of load cycles.

Although these recommendations are intended for loading less than 2×10^6 cycles, the commentary states that the equation is a conservative estimate, and Equation (2-93) remains valid beyond 2×10^6 cycles. It is also specified to apply a safety material factor of 0.76923. Additionally, it is stated that for reversed cyclic loading, σ_p is typically set to zero. For a 20 year turbine life, or 5.29×10^8 cycles, when σ_p is set to zero, the allowable stress range for UHPC with a 26 ksi (179.3 MPa) compressive strength is 6.37 ksi (43.9 MPa).

2.3.8 *Additional Design Criteria*

In addition to code specified criteria, some limit states require the use of non-code methods to complete the design. These include classical analysis methods and industry standard design practices.

Shear Cracking for Concrete

Although it usually does not govern, shear cracking in concrete under service conditions is undesirable. Therefore, it should be used as a limit state for prestressed concrete design. From engineering mechanics, the principal tensile stress, caused by interaction of shear and axial stresses should be limited to the tensile strength of concrete:

$$\sqrt{\left(\frac{f_{pc}}{2}\right)^2 + (\tau)^2} - \frac{f_{pc}}{2} \leq f_t \tag{2-94}$$

where f_{pc} = axial stress at the centroid due to prestressing and external loads;

$f_t = 3.5\sqrt{f_c'(psi)}, 0.29062\sqrt{f_c'(MPa)}$ and is the tensile strength of concrete;

τ = service-level required shear stress; and

f_c' = 28-day compressive strength of concrete.

Rayleigh Method for Natural Frequency

In order to evaluate the dynamic amplification of the structure, as well as calculate direct wind loading on the tower using the ASCE 7 specification (SEI, 2005), the first natural frequency of the tower needs to be estimated (including both the tower and the turbine). The Rayleigh method uses energy concepts to estimate the 1st natural frequency of the tower. The equation for the first natural angular frequency is given as (after LaNier, 2005)

$$\omega_n^2 = \frac{\int_0^h E(z)I(z)[Y''(z)]^2 dz}{\int_0^h m(z)[Y(z)]^2 dz + \sum_i m_i Y(z_i)^2} \tag{2-95}$$

where z = vertical length along the tower;

h = total tower height;

$m(z)$ = distributed mass along the tower;

$I(z)$ = moment of inertia along the tower;

$E(z)$ = modulus of elasticity along the tower;

$Y(z)$ = assumed displacement function for the tower deformation;

m_i = a concentrated mass at some point along the tower height; and

z_i = location of a concentrated mass, m_i.

In order to account for the effect of the concentrated mass at the tower top due to the turbine, the summation term in the denominator of Eq. (2-95) accounts for the effect of the turbine weight at the tower top. The accuracy of ω_n depends on how well the displacement function fits the actual tower's deflected shape. According to Chopra (2007), several applicable displacement functions for uniform and non-uniform towers with distributed mass and elasticity are:

$$Y(z) = a\left[1 - cos\left(\frac{\pi z}{2h}\right)\right] \tag{2-96}$$

$$Y(z) = a\left[\frac{3}{2}\frac{z^2}{h^2} - \frac{1}{2}\frac{z^3}{h^3}\right] \tag{2-97}$$

where a = constant describing the maximum deflection.

The constant a is divided out of Eq. (2-95), and therefore is left as a constant during evaluation of Equation (2-95).

Rayleigh-Ritz Method for Buckling Load

The Rayleigh-Ritz method may be used to determine the global buckling load for a system that has complicated geometry (i.e. varying cross sectional area and moment of inertia). It is based on the principal that the smallest buckling load occurs when the change in potential energy is a minimum. The buckling load of the system is obtained in the following steps (after LaNier, 2005):

1) Choose a displacement function, such as Equations (2-96) and (2-97).

2) Calculate the strain energy of bending in the system:

$$U = \frac{1}{2}\int_0^h E(z)I(z)[Y''(z)]^2 dz \tag{2-98}$$

where $E(z), I(z), Y(z), z$, and h are the same variables as in the natural frequency calculation.

3) Calculate the potential energy in the system due to the buckling load:

$$V = -\frac{P}{2}\int_0^h [Y'(z)]^2 dz$$

(2-99)

where P is the critical buckling load at the top of the tower. Alternatively, this can be described as $V = P\lambda$ or $\lambda = {}^V/_P$.

4) Calculate the potential energy of the self-weight of the system:

$$W_{self} = W_{turbine+}W_{tower}$$

(2-100)

$$W_{turbine} = -\frac{1}{2}\int_0^h P_{turbine}[Y'(z)]^2 dz$$

$$W_{tower} = -\frac{1}{2}\int_0^h W(z)z[Y'(z)]^2 dz$$

where $P_{turbine}$ = weight of the turbine; and
$W(z)$ = distributed tower weight.

5) Calculate P through the use of :

$$P = \min \left[\frac{U + W_{self}}{\lambda}\right]$$

(2-101)

However, when a displacement function is chosen with only one unknown (e.g., a), only one solution exists to Eq. (2-101), simplifying the answer.

Damage Equivalent Load Method for Steel Fatigue

The Damage Equivalent Load (DEL) Method is a method used to evaluate fatigue strength of steel structures. In this method, the entire load history for a structure is represented by a damage equivalent load and a number of cycles. This load is applied to the structure, and the corresponding stress range is determined through an analysis of the structure. This stress range is then compared to a calculated allowable stress range. For welded steel towers (LaNier, 2005), the allowable stress range is given as:

$$\log[\Delta\sigma_s(n)] = \log(\Delta\sigma_{max}) + \frac{\left[\log\left(\frac{2E6}{n}\right)\right]}{m} \tag{2-102}$$

where $\Delta\sigma_{max} = 11.60$ ksi (80 MPa) and is the allowable stress range associated with 2×10^6
cycles;

$\Delta\sigma_s(n) =$ allowable stress range for the material;

$n =$ expected number of cycles in the structure's lifetime; and

$m = 4$, and is the representative slope for the material fatigue strength.

Based on a comparison by LaNier (2005), this S-N is very similar to the fatigue design curve specified by Eurocode 3 (European Committee for Standardisation, 1992). Therefore it was judged to be adequate for use in this report. The structure's stress range, as caused by the DEL, is then compared to this allowable stress range, and is safe for fatigue loading if:

$$\gamma_{Sd}\gamma_S\Delta\sigma_{DEL} \leq \Delta\sigma_s \tag{2-103}$$

where $\Delta\sigma_{DEL} =$ stress range caused by the DEL;

$\gamma_{Sd} = 1.15$, and is the consequence failure factor; and

$\gamma_S = 1.1$, and is the material factor for steel.

These material factors correspond to those used in the MC90 (Comite Euro-International Du Beton, 1993) for fatigue analysis. While not specifically calibrated for the use with the DEL load method, it was judged conservative to apply this safety factor to the design.

2.3.9 BergerABAM Design Study

In January 2005, NREL published a study completed by BergerABAM Engineers Inc. entitled "LWST Phase I Project Conceptual Design Study: Evaluation of Design and Construction Approaches for Economical Hybrid Steel/Concrete Wind Turbine Towers" (LaNier, 2005). The purpose of this study was to evaluate the possibility of constructing economical hybrid wind turbine towers. As a part of this study, complete designs were prepared for 328 ft (100 m) steel, prestressed concrete, and steel/concrete hybrid towers for 1.5, 3.6, and 5.0 MW turbines. Throughout this report, explicit details are supplied for applicable turbine and tower loads, limit states, design specifications, and design

methodologies. The wind turbine loading data used by BergerABAM will be addressed, and results of the steel and prestressed concrete towers will be briefly discussed as they will provide useful comparisons to the designs presented in Chapters 1-5 of this report.

WindPACT Design Loads

The turbine loads that BergerABAM used to complete the tower designs were simulated by Global Energy Concepts (GEC), for another NREL study (Global Energy Concepts, 2002). Loads were given for two IEC wind conditions, Extreme Wind Model (EWM50) and Extreme Operating Gust (EOG50) (mentioned in Section 2.3.4), and the program outputs maximum and minimum shears, moments, and torsional moments. The EWM50 wind speed used was a 59.5 m/s 3s gust, and the EOG50 was a 35 m/s 3s gust for hub height elevations. Additionally, a Damage Equivalent Load was specified and fatigue loads were simulated.

The loads in Table 2-6 and Table 2-7 represent an envelope, meaning that they are maximums. In Table 2-6, the thrust and moment values are vector summations of loads in the X (along-wind) and Y (across-wind) directions. These values are separated into their constituent directions, and are listed in Table 2-7. The x-direction fatigue moments are assumed to be independent of the fatigue load moments in the y-direction. Therefore, both fatigue moments are examined as separate load cases.

Ideally, a study interested in tower design would use field measured loads from the design turbine or simulated turbine loading using computational fluid dynamics (CFD). Most turbine manufacturers consider load data for their turbines proprietary information and few companies are willing to distribute this information freely. Generic loads, such as those listed in Table 2-6 and Table 2-7, provide a starting point for tower design. However, a final tower design would need to be designed for a specific turbine using manufacturer-approved turbine loading, and would need to address more than the EWM50 and EOG50 load cases.

In general, the turbine loads are larger in magnitude than the direct wind load. This results in significantly different tower designs for 1.5 MW, 3.6 MW, and 5.0 MW turbines placed at the same elevation.

Table 2-6: WindPACT Service-Level Load Envelope at Tower Top, Vector Summations (after Global Energy Concepts, 2002)

		Thrust	Moment	Tower Axial Force (causing tower compression)	Torsional Moment (about tower longitudinal axis)
		F_T, kips (kN)	M_T, kip-ft (kN-m)	F_z, kips (kN)	M_z, kip-ft (kN-m)
1.5 MW	EWM50	86.3 (384)	2810 (3805)	187.0 (832)	1450 (1966)
	EOG50	90.6 (403)	1083 (1468)	187.0 (832)	171.1 (232)
3.6 MW	EWM50	244 (1,086)	12,370 (16,767)	709 (3155)	4397 (5961)
	EOG50	270 (1,199)	7310 (9913)	703 (3129)	1178 (1597)
5 MW	EWM50	129.9 (578)	21,070 (28,568)	1124 (4998)	4300 (5834)
	EOG50	239 (1065)	14,260 (19,337)	1097 (4879)	2740 (3714)

Table 2-7: WindPACT Service-Level Detailed Thrust and Moment Envelope at Tower Top (after Global Energy Concepts, 2002)

		Thrust		Moment	
		F_x, kips (kN)	F_y, kips (kN)	M_x, kip-ft (kN-m)	M_y, kip-ft (kN-m)
1.5 MW	EWM50	42.7 (190)	75.1 (334)	2506 (3398)	1263 (1713)
	EOG50	90.2 (401)	8.77 (39)	656 (889)	861 (1168)
	Fatigue Load	12.81 (57)	-	89.2 (121)	409 (554)
3.6 MW	EWM50	143.0 (636)	198.1 (881)	10,460 (14,179)	6600 (8950)
	EOG50	269 (1196)	18.21 (81)	3140 (4262)	6600 (8950)
	Fatigue Load	32.1 (143)	-	319 (432)	1601 (2170)
5 MW	EWM50	44.7 (199)	122.1 (543)	16,090 (21,820)	13,600 (18,440)
	EOG50	238 (1057)	28.8 (128)	4294 (5822)	13,600 (18,440)
	Fatigue Load	44.3 (197)	-	533 (722)	2670 (3616)

328 ft (100 m) Steel Tower

BergerABAM completed the design of the steel tower using Allowable Stress Design, assuming 50 ksi yield-strength steel. Additionally, they considered the effects of fatigue as well as the dynamic properties of the tower in the design, keeping the tower natural frequency within the working frequency range. The results of the steel tower designs for 1.5, 3.6, and 5.0 MW are summarized in Table 2-8. In all cases, steel tower fatigue governed their design (LaNier, 2005) at some point along the tower governed the tower geometry. While the actual location of the maximum demand-to-capacity ratio (DCR) for fatigue is not specified for any of their tower designs, it can be seen from a design example in the report that for the 5.0 MW tower this point occurs at around 230 ft (70.1 m) elevation. As discussed in Section 1.3.2, BergerABAM used a design life of 20 years for their towers. The DCR's listed in Table 2-8 suggest that the towers' service lives could exceed 20 years, as they are approximately 20% below unity. However, this DCR is not small enough for the tower to be re-used with another turbine. It is probable that a final design would be further optimized, bringing the fatigue DCR's closer to unity, and thus matching the design life of the tower to that of the turbine.

As mentioned previously, turbine size has a significant effect on the required tower dimensions. For a 328 ft (100 m) turbine height, BergerABAM's 5.0 MW requires more than double the volume of steel as compared to the their 1.5 MW tower.

All three of BergerABAM's steel tower designs experience significant sidesway under direct and turbine wind loading. While BergerABAM identified no lateral deflection restrictions in their report, it is likely turbine manufacturers specify a limiting value for deflection.

Table 2-8: BergerABAM 328 ft (100 m) Steel Tower Characteristics (after LaNier, 2005)

	1.5 MW	3.6 MW	5.0 MW
Rotor Diameter, ft (m)	231.2 (70.5)	355.6 (108.4)	419.8 (128)
Total Head Weight, kips (kg)	187 (84,800)	694 (314,912)	1058 (480,076)
Outside Diameter at Base for Steel Tower, in. (m)	228 (5.791)	300 (7.62)	348 (8.839)
Wall Thickness at Base for Steel Tower, in. (m)	1 (0.0254)	1.25 (0.03175)	1.438 (0.03651)
Outside Diameter at Midheight of Steel Tower, in. (m)	168 (4.267)	222 (5.639)	264 (6.706)
Wall Thickness at Midheight of Steel Tower, in. (m)	1 (0.0254)	1.25 (0.03175)	1.375 (0.03492)
Outside Diameter at Top of Steel Tower, in. (m)	114 (2.896)	156 (3.962)	180 (4.572)
Wall Thickness at Top of Steel Tower, in. (m)	0.375 (0.009525)	0.75 (0.01905)	0.875 (0.02222)
Steel Tower Weight, kips (kN)	516.1 (2296)	899.2 (4000)	1188 (5282)
Steel Tower Volume, ft^3 (m^3)	1053 (29.8)	1835 (52.0)	2420 (68.6)
Deflection at Top of Tower for Wind Load, ft (m)	3.013 (0.9185)	3.013 (0.9183)	1.994 (0.6078)
Tower Natural Frequency (Hz) [Rayleigh-SAP]	0.4059, 0.3669	0.3693, 0.3341	0.3973, 0.3605
Max. Stress DCR for Steel (Wind)	0.492	0.575	0.494
Max. Buckling DCR of Steel (Wind)	0.37	0.449	0.379
Max. Fatigue DCR of Steel Tower	0.758	0.803	0.78
Controlling Loading Case	Fatigue (20 years)	Fatigue (20 years)	Fatigue (20 years)

328 ft (100 m) Prestressed Concrete Tower

The prestressed concrete design consists of a bonded, post-tensioned, circular shell design. The concrete has a 28-day strength of 7 ksi (48.3 MPa). As with the steel design, the concrete tower is designed for fatigue and strength, with the consideration of dynamic effects. One difference between the designs is the local buckling is not considered in the design of the concrete tower.

For the 1.5 MW tower, Tower Natural Frequency is the governing limit state. For BergerABAM's 1.5 MW turbine, the bottom of the working natural frequency range is specified as 0.376 Hz, with a 1P value equal to 0.342. In general, the tower natural frequency can be increased when the stiffness to mass ratio of the tower in increased. While BergerABAM does not detail how the natural frequency of the tower was tuned, it is possible the diameter or wall thickness was increased along the tower height to increase the stiffness.

The 3.6 MW tower cites concrete fatigue as the limit design constraint. For the 3.6 MW, the concrete DCR's listed in Table 2-9 do not support this conclusion. In fact, they are much less than unity, implying a tower service life greatly exceeds 20 years. It is possible the critical location for fatigue occurs at another location on the tower, but this is unlikely, given the extremely low DCR values for the base and midheight. The most critical DCR for this tower would appear to be the moment demand DCR, which is still significantly less than unity.

The 5.0 MW lists concrete fatigue as the main design limitation. It can be seen that the concrete fatigue DCR is 0.886 at midheight, suggesting that the tower has a service life only slightly longer than the 20 year turbine life. This result is interesting, as the fatigue effects appear to be negligible on the 1.5 MW and 3.6 MW tower designs.

The lateral deflections for the 1.5 MW and 3.6 MW concrete towers are approximately 50% larger than their steel counterparts. The 5.0 MW concrete tower deflection is approximately 30% less than the 5.0 MW steel tower. This wide range of deflections further suggests that no limit has been set by this author. However, in general the concrete towers appear to be stiffer, while maintaining a natural frequency within the working range. It should be noted that neither the concrete nor the steel tower designs meet the deflection criteria suggested by ACI (ACI Committee 307, 1998) for concrete chimneys, 0.333% drift.

Table 2-9: BergerABAM 328 ft (100 m) Prestressed Concrete Tower Characteristics (after LaNier 2005)

	1.5 MW	3.6 MW	5.0 MW
Rotor Diameter, ft (m)	231.2 (70.5)	355.6 (108.4)	419.8 (128)
Total Head Weight, kip (kg)	187 (84,800)	694 (314,912)	1058 (480,076)
Outside Diameter at Base for Concrete Tower, in. (m)	228 (5.791)	264 (6.706)	300 (7.62)
Wall Thickness at Base for Concrete Tower, in. (m)	24 (0.6096)	27 (0.6858)	30 (0.762)
Outside Diameter at Midheight of Concrete Tower, in. (m)	156 (3.962)	204 (5.182)	222 (5.639)
Wall Thickness at Midheight of Concrete Tower, in. (m)	21 (0.5334)	24 (0.6096)	27 (0.6858)
Outside Diameter at Top of Concrete Tower, in. (m)	114 (2.896)	144 (3.658)	144 (3.658)
Wall Thickness at Top of Concrete Tower, in. (m)	18 (0.4572)	18 (0.4572)	18 (0.4572)
Concrete Tower Weight, kip (kN)	3254 (14,470)	4579 (20,370)	5502 (24,470)
Tendon Weight, kip (kg)	78.49 (35,600)	104.60 (47,470)	130.50 (59,180)
Deflection at Tower Top, Wind, ft (m)	1.256 (0.3828)	1.656 (0.5046)	1.361 (0.4148)
Number of Tendon at Base and Mid Section (12-strand bundle)	30, 24	40,32	56,34
Tower Natural Frequency (Hz) [Rayleigh-SAP]	0.3774, 0.3557	0.3768, 0.3419	0.384, 0.3564
Moment DCR of Tower at Base (Wind)	0.453	0.669	0.470
Shear DCR of Concrete at Base (Wind)	0.265	0.390	0.240
Concrete Fatigue DCR, Midheight	9.884E-3	0.099	0.886
Steel Fatigue DCR, Midheight	9.451E-9	4.073E-7	2.868E-5
Concrete Fatigue DCR, Base	1.84E-7	0.016	0.139
Steel Fatigue DCR, Base	2.426E-11	1.863E-7	1.791E-6
Controlling Load Case	Tower Freq.	Concrete Fatigue	Concrete Fatigue/Ten. Str.

3   TALLER TOWERS

3.1   Overview

In Chapter 2, the strengths and weaknesses of concrete and steel turbine towers were discussed. It was indicated that for steel, the required base diameter for a 328 ft (100 m) or taller tower would exceed transportation limits, resulting in increased transportation and erection costs. In order to validate that claim, as well as establish a baseline for comparison of towers made with different materials, designs of both steel and regular strength concrete were first developed.

In order to complete consistent towers designs using different materials, a representative turbine size and wind environment were chosen. The turbine used for design is an ACCIONA Windpower AW-109/3000 (3 MW) because of readily available information on this next generation turbine. This turbine was designed by ACCIONA for an IEC Class IIa environment. For this particular turbine, the tower height is specified as 322 ft (98.2 m), which results in a hub height of 328 ft (100 m). The nominal rotational speed of the rotor is 13.2 rpm, with a 3-blade rotor diameter of 358 ft (109 m) and a cut-out speed of 25 m/s.

3.2   Steel Towers

3.2.1   Loading

The design of the steel tower was performed using a combination of loads, utilizing the sources discussed in Chapter 2. The turbine loads were obtained from LaNier (2005) and ACCIONA literature (ACCIONA Windpower, n.d.). While LaNier (2005) did not specify loads for a 3MW turbine, simulated loads for 1.5, 3.6, and 5.0 MW at 328 ft (100 m) hub height were given. In order to estimate turbine loads for a 3MW turbine at 328 ft (100 m) hub height, a 2nd order polynomial was fitted for turbine thrust vs. power rating, turbine moment vs. power rating, and the turbine torsion vs. power rating. The loads for a 3 MW turbine were then estimated from these equations. The plots, as well as the fitted-curves for the loading are shown in Figure 3.1 through Figure 3.6. Two IEC (International Electrotechnical Comission, 2007) load cases were considered for design: an Extreme Operating Gust with a 50 year

return period (EOG50), and the Extreme Wind Model with a 50 year return period (EWM50).
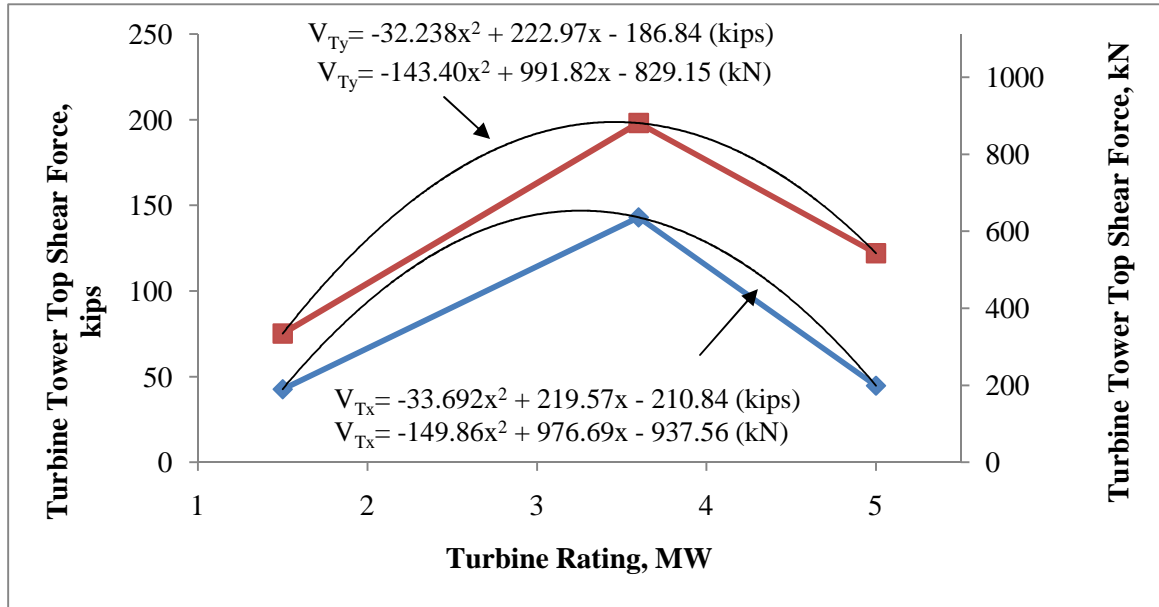
Figure 3.1: EWM50 Tower Top Service-Level Turbine Thrust
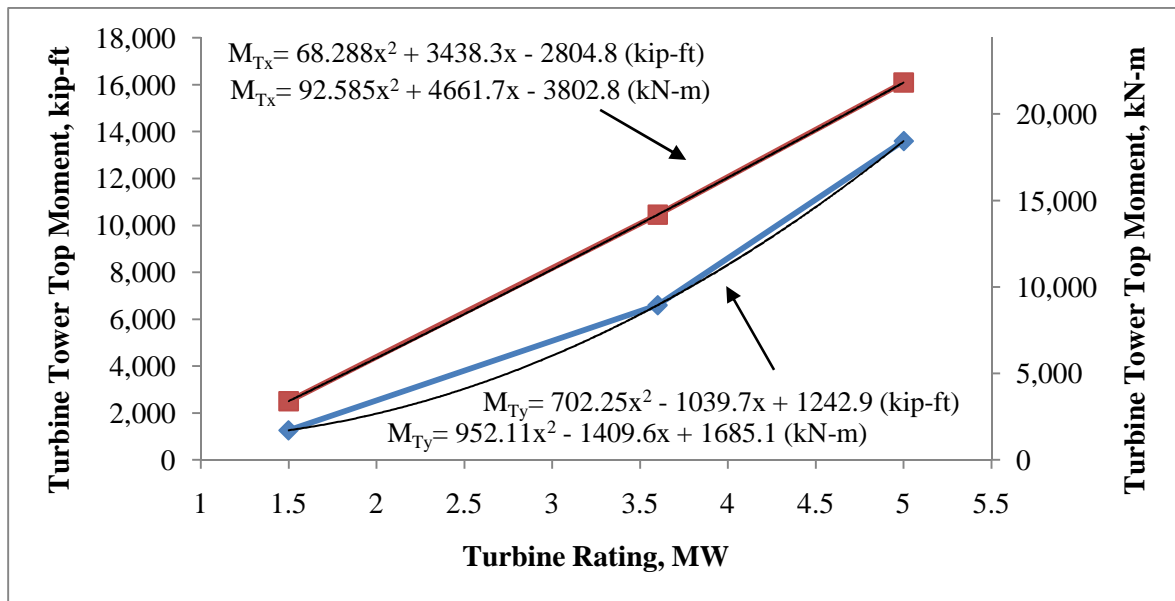
Figure 3.2: EWM50 Tower Top Service-Level Turbine Moments
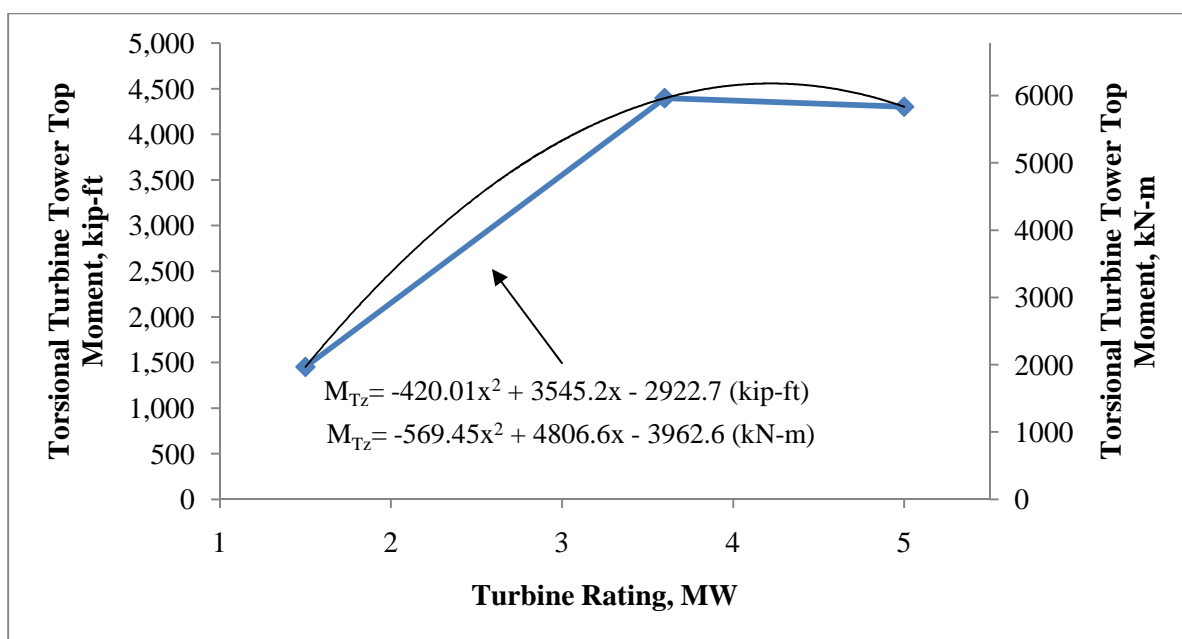
Figure 3.3: EWM50 Turbine Tower Top Service-Level Torsional Moment

$M_{Tz}= -420.01x^2 + 3545.2x - 2922.7$ (kip-ft)

$M_{Tz}= -569.45x^2 + 4806.6x - 3962.6$ (kN-m)
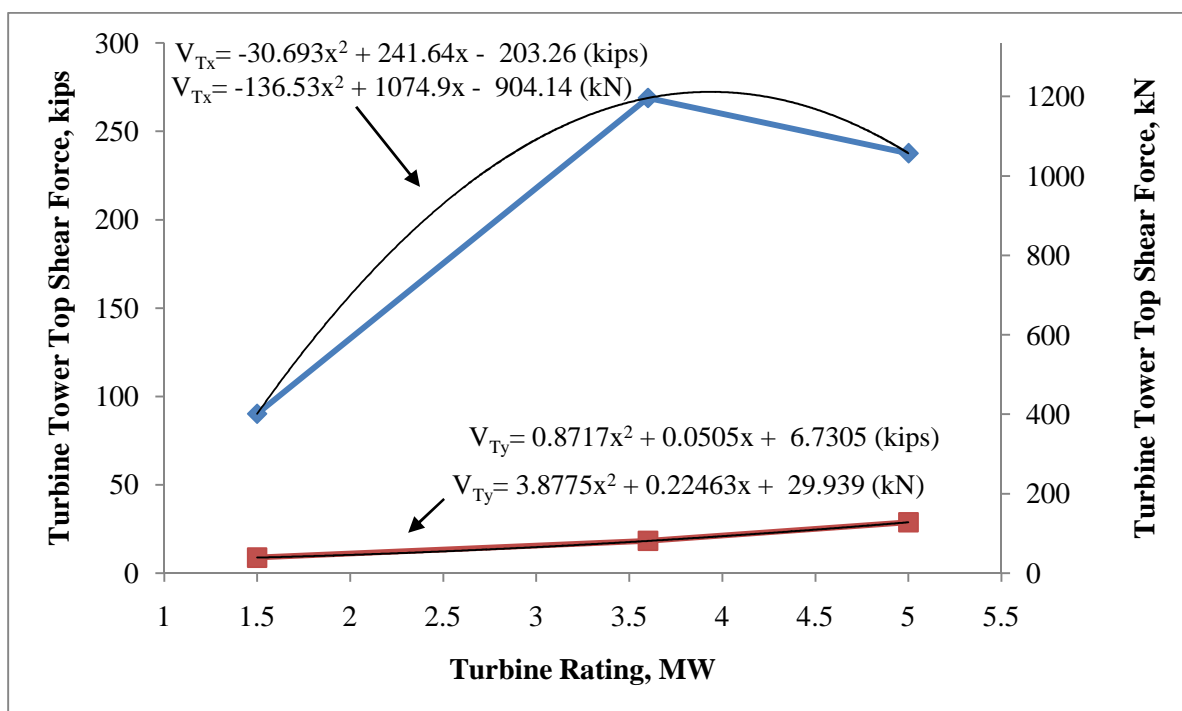
Figure 3.4: EOG50 Tower Top Service-Level Turbine Thrust

$V_{Tx}= -30.693x^2 + 241.64x - 203.26$ (kips)

$V_{Tx}= -136.53x^2 + 1074.9x - 904.14$ (kN)

$V_{Ty}= 0.8717x^2 + 0.0505x + 6.7305$ (kips)

$V_{Ty}= 3.8775x^2 + 0.22463x + 29.939$ (kN)
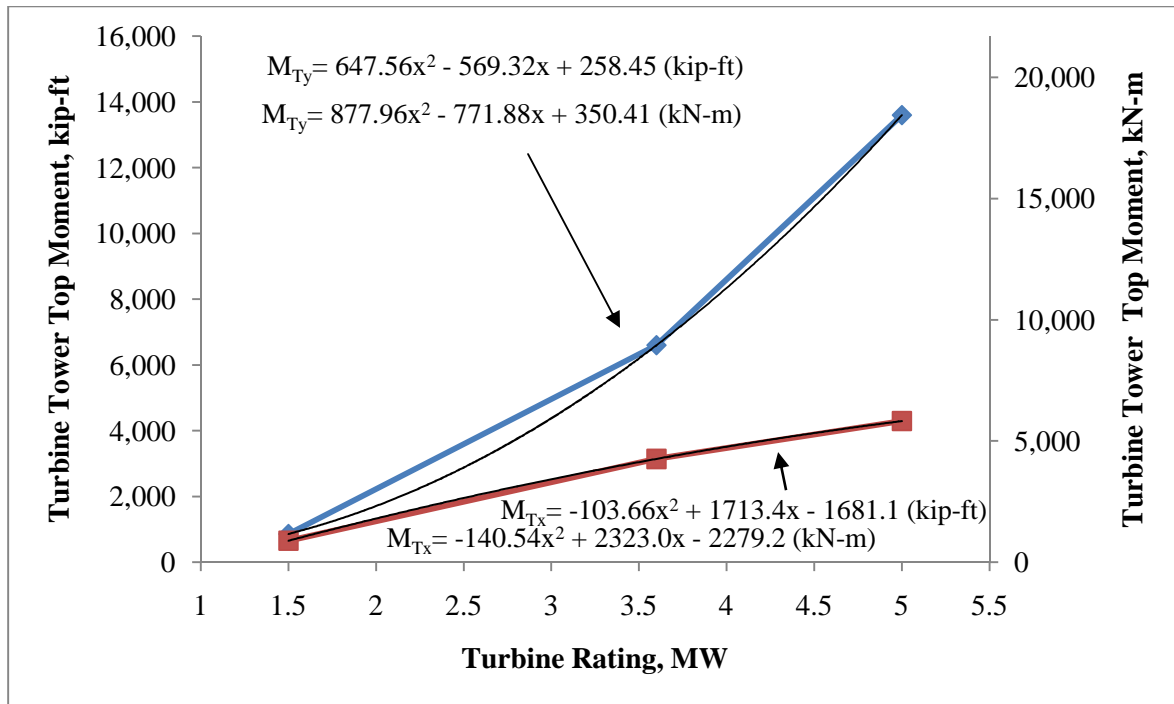
Figure 3.5: EOG50 Turbine Tower Top Service-Level Moments

The figure shows plotted data with the following fitted equations:

$$M_{Ty} = 647.56x^2 - 569.32x + 258.45 \text{ (kip-ft)}$$
$$M_{Ty} = 877.96x^2 - 771.88x + 350.41 \text{ (kN-m)}$$

$$M_{Tx} = -103.66x^2 + 1713.4x - 1681.1 \text{ (kip-ft)}$$
$$M_{Tx} = -140.54x^2 + 2323.0x - 2279.2 \text{ (kN-m)}$$
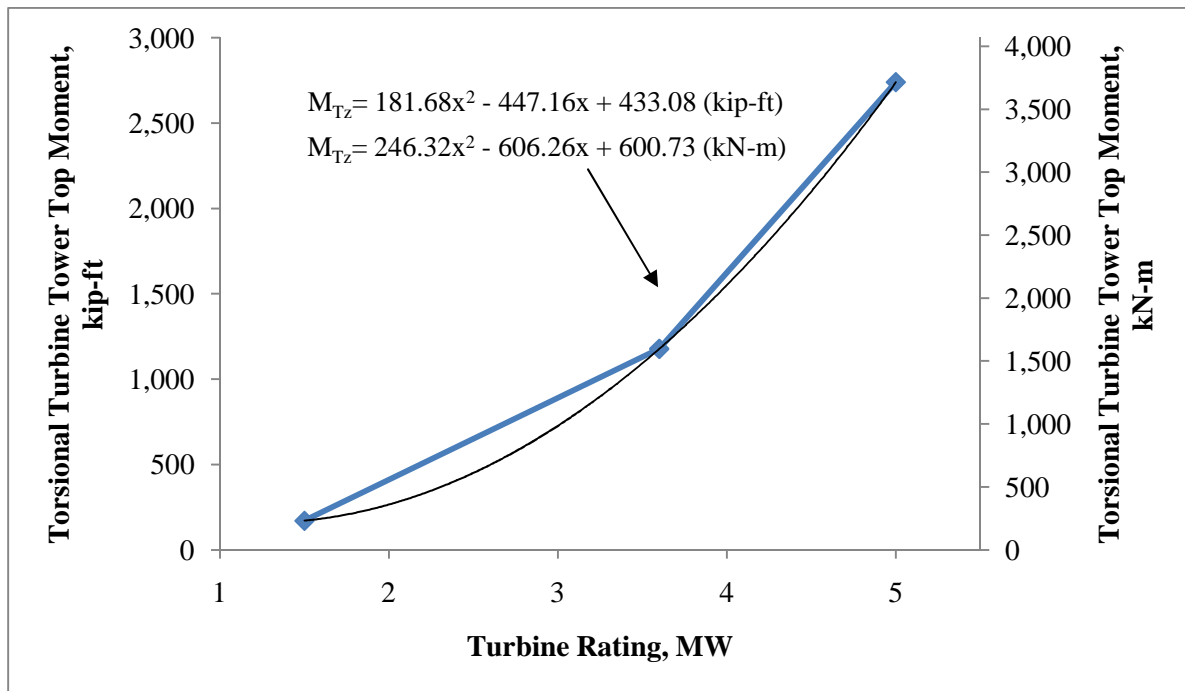
Figure 3.6: EOG50 Turbine Tower Top Service-Level Torsional Moment

The figure shows plotted data with the following fitted equations:

$$M_{Tz} = 181.68x^2 - 447.16x + 433.08 \text{ (kip-ft)}$$
$$M_{Tz} = 246.32x^2 - 606.26x + 600.73 \text{ (kN-m)}$$

The tower top loads estimated for a 3 MW turbine from Figure 3.1 through Figure 3.6 can be seen in Table 3-1. It should be noted that for the forces listed in Table 3-1 the x-direction is the along-wind direction, and the y-direction is the across-wind direction.

Table 3-1: Turbine Top Loads at Service-Level Estimated for a 3 MW ACCIONA AW-109/3000 Wind Turbine

EWM50	V_{Tx} kips (kN)	V_{Ty} kips (kN)	M_{Tx} kip-ft (kN-m)	M_{Ty} kip-ft (kN-m)	M_z kip-ft (kN-m)
	144.6 (643)	191.9 (854)	8120 (11,020)	4440 (6030)	3930 (5330)
EOG50	V_{Tx} kips (kN)	V_{Ty} kips (kN)	M_{Tx} kip-ft (kN-m)	M_{Ty} kip-ft (kN-m)	M_z kip-ft (kN-m)
	245 (1092)	15.00 (65.5)	2530 (3420)	4380 (6820)	727 (985)

V_T is the horizontal thrust applied to the top of the tower by the turbine, in the x or y direction;
M_T is the moment applied at the top of the tower by the turbine, in the x or y direction; and
M_Z is the torsional moment applied to the top of the tower by the turbine, in the z direction.

These turbine loads have been already amplified for dynamic effects (LaNier, 2005) and are to be treated as equivalent static loads. It was assumed that the dynamic properties (i.e., damping and natural frequency) of the tower designed here were similar to that designed by LaNier's 328 ft (100 m) tower designs (2005), and therefore the dynamic amplification of the loading is similar. Were a detailed design to be completed for a steel tower, this assumption would need to be validated.

The turbine also causes an axial load on the tower due to its self-weight. The axial compression used by LaNier (2005) includes both the self-weight of the hub and rotor, as well as an axial force caused by turbine operation. However, for this study a different turbine than that considered LaNier was used. Therefore, the ACCIONA turbine weight combined with the additional wind force caused by operation was used in this design. This force ranges from 0 (for a 1.5 MW turbine, EOG/EWM50) to 65 kip (14.61 kN) (for a 5.0 MW, EWM50). That fact that it is zero suggests that it may be negligible. However, in the interest of conservatism, an additional axial load of 70 kips (15.74 kN) was added to account for this variable operational force. The axial loads are given in Table 3-2.

Table 3-2: Turbine Axial Loads at Service-Level for a 3 MW ACCIONA AW-109/3000 Wind Turbine

Weight/blade*, kips (kN)	25.4 (113.2)
Nacelle+hub*, kips (kN)	340 (1510)
Additional axial compression, kips (kN)	70.0 (311)
Total axial turbine load, kips (kN)	486 (2160)

*From ACCIONA AW-109/3000, IEC class IIa

The self-weight of the tower also causes an axial compression that increases down the tower height. At the base of the tower, this is equal to 739 kips (3290 kN), assuming a unit weight of steel of 490 lb/ft^3 (77.0 kN/m^3). This weight corresponds to the final design of the 322 ft (98.2 m) steel tower described in Table 3-5.

The direct wind force on the steel tower was calculated using ASCE 7-05 (Structural Engineering Institute, 2005). It was assumed that this turbine was operating in an exposure category D in order to complete this calculation. This is a conservative assumption, and is reasonable as wind turbines are typically located in remote and wide-open areas. Since wind turbine towers typically have a first natural frequency less than 1 Hz, they are classified as flexible structures. Because of this, the natural frequency was needed to evaluate the wind load. Equation (2-95) was used to perform this calculation, and more detail is given later in this section.

Additionally, an input 3 second wind speed at 33 ft (10 m) elevation is required to calculate direct wind loading using the ASCE 7-05 (Structural Engineering Institute, 2005) method. Although the turbine loads listed in Table 3-1 were run at the speeds listed in Section 2.3.9, this speed should be justified. In this context, EWM50 and EOG50 wind speeds were calculated using the IEC 61400-1 (International Electrotechnical Comission, 2007) method. This yielded an EWM50, 3 second wind speed of 136.3 mph (60.9 m/s) and an EOG50 3 second speed of 60.5 mph (27.1 m/s) at a height of 33 ft (10 m). At the 328 ft (100 m) hub height, this translates to a EWM50 3 second wind speed of 175.5 mph (78.4 m/s) and an EOG50 3 second wind speed of 95.8 mph (42.8 m/s). The wind speeds used by LaNier (2005) were an EWM50 3 second gust of 133 mph (59.5 m/s) and an EOG50 3 second gust of 78 mph (35.0 m/s) at the hub height. While the calculated speeds do not agree with those

reported by LaNier, no details were given by that author as to how the speeds were calculated. Additionally, the calculated wind speeds in this study take into account the AW-109/3000, such as wind turbine cut-out speed and the specific wind operating environment that the turbine was intended for. Therefore, it was judged that the calculated wind speeds should be used in the computation of direct wind loads on the tower. The direct wind force and corresponding moments, calculated using the ASCE 7-05 (Structural Engineering Institute, 2005) method in conjunction with the calculated EWM50 and EOG50 wind speeds are given in Table 3-3. All direct wind shear forces in the table act in the x-direction, and the moments act in the y-direction.

Table 3-3: Estimated Direct Wind Force Loads at Midheight and Base of the 322 ft (98.2 m) Steel Tower at Service-Level

EWM50	V_{Mx} kips (kN)	M_{My} kip-ft (kN-m)	V_{Bx} kips (kN)	M_{By} kip-ft (kN-m)
	126.6 (563)	9930 (13,330)	252 (1121)	40,780 (55,300)
EOG50	V_{Mx} kips (kN)	M_{My} kip-ft (kN-m)	V_{Bx} kips (kN)	M_{By} kip-ft (kN-m)
	20.9 (93.0)	1623 (2200)	41.5 (184.6)	6730 (9120)

Note: The subscripts "M" and "B" represent tower midheight and base, respectively.

All turbine and direct wind moments and loads were determined using vector summation, in the following manner:

$$M_{applied}^2 = \left(M_y\right)^2 + (M_x)^2 \tag{3-1}$$

$$F_{applied}^2 = \left(F_y\right)^2 + (F_x)^2 \tag{3-2}$$

Additionally, a damage equivalent load (DEL) was given by LaNier (2005) for the 1.5, 3.6, and 5.0 MW turbine loading for the purpose of evaluating tower fatigue. As was done with the turbine loads, a curve was fit to these loads based on turbine rating, and a DEL for a 3.0 MW turbine was interpolated. These curves are provided in Figure 3.7 and Figure 3.8. LaNier (2005) states that industry practice is to consider fatigue loading independently of direct wind loading. This is justified as wind loading is calculated as a static load, and therefore would not contribute to the fatigue stress range.
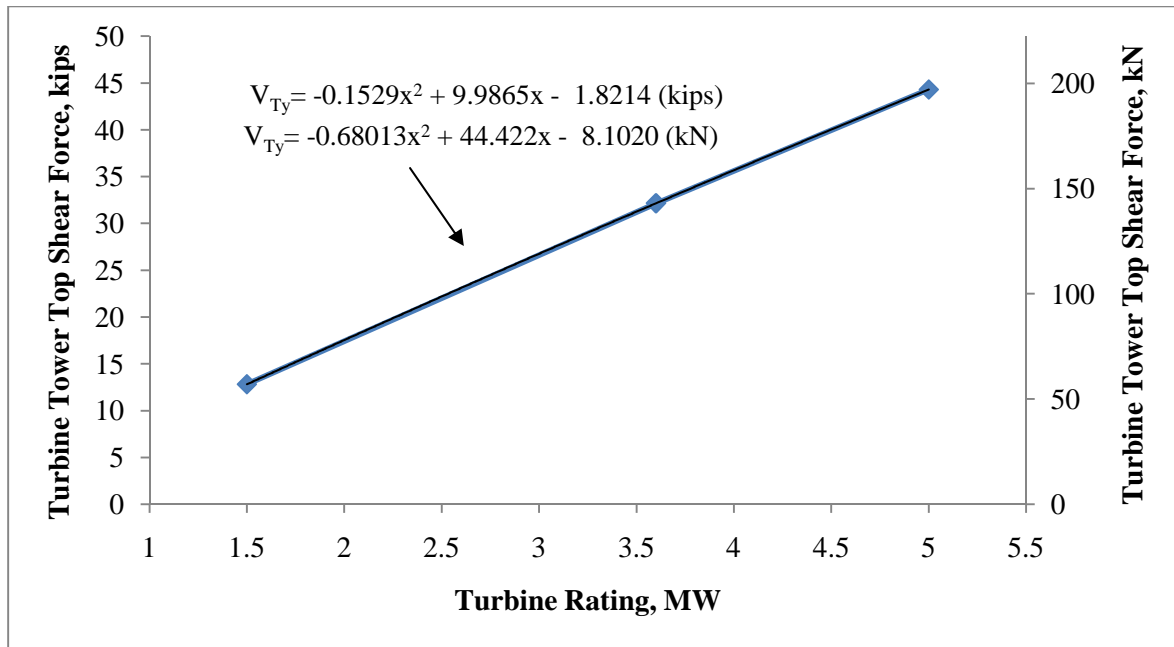
Figure 3.7: DEL Turbine Tower Top Shear Force

$V_{Ty}= -0.1529x^2 + 9.9865x - 1.8214$ (kips)
$V_{Ty}= -0.68013x^2 + 44.422x - 8.1020$ (kN)
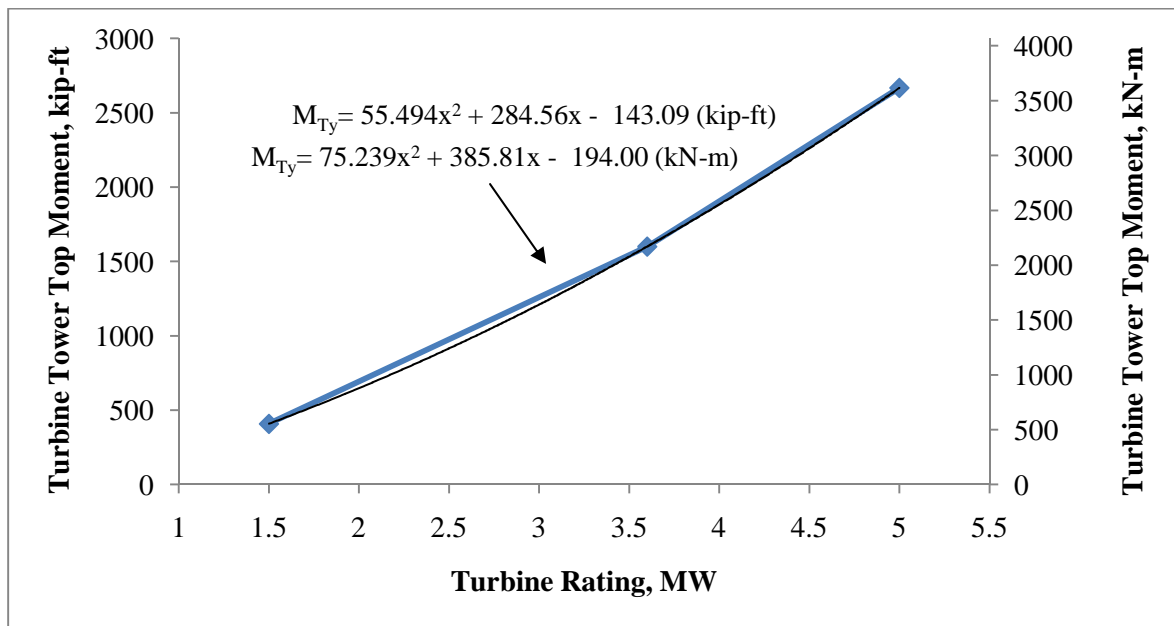
Figure 3.8: DEL Turbine Tower Top Moment

$M_{Ty}= 55.494x^2 + 284.56x - 143.09$ (kip-ft)
$M_{Ty}= 75.239x^2 + 385.81x - 194.00$ (kN-m)

The DEL loads estimated from Figure 3.7 and Figure 3.8 can be seen in Table 3-4. The Δ before each load implies that the reported values corresponding to the fatigue load cause a stress range, which subsequently causes fatigue damage. As the tower cross section is circular, and no direct wind forces are considered in the fatigue calculation, no vector summation was needed for the DEL calculation. The DEL thrust, $\Delta V_{Tx,fat}$, causes a moment in the same plane as the fatigue moment, $\Delta M_{Ty,fat}$.

Table 3-4: Estimated Damage Equivalent Loads at Tower Top

$\Delta V_{Tx,fat}$, kips (kN)	26.8 (119.2)
$\Delta M_{Ty,fat}$, ft-kip (kN-m)	1210 (1640)

Note: The subscript "fat" refers to fatigue.

3.2.2   Design

The design of the steel tower was performed using an iterative process, utilizing a spreadsheet to size the tower. The loads detailed above and the load cases discussed in Section 2.3.3 were used to complete the design of the tower. In order to optimize the design, the tower semi-vertex angle (i.e., taper angle) was varied three times along the height. The angle was kept constant between 0 and 110 ft (33.5 m), 110 ft (33.5 m) and 220 ft (67.1 m), 220 ft (67.1 m) and 322 ft (98.2 m). A summary of the design is presented in Table 3-5.

Table 3-5: Summary of the 322 ft (98.2 m) Tall Steel Tower for a 3 MW Turbine

Diameter at Base, in. (m)	216 (5.49)
Shell Thickness at Base, in. (mm)	1.5 (38.1)
Diameter at 110ft (33.5 m), in. (m)	198 (5.03)
Shell Thickness at 110ft (33.5 m), in. (mm)	1.25 (31.8)
Diameter at 220ft (67.1 m), in. (m)	168 (4.27)
Shell Thickness at 220ft (67.1 m), in. (mm)	1.25 (31.8)
Diameter at 322 ft (98.2 m), in. (m)	120 (3.05)
Shell Thickness at 322ft (98.2 m), in. (mm)	1.1 (27.9)
Steel Volume, ft^3 (m^3)	1507 (42.7)
Tower Weight, kips (kN)	739 (3290)
Fundamental Natural Frequency of Tower, Hz	0.338

The dimensions of the tower are linearly varied at any intermediate locations not shown in Table 3-5, and the tower limit states were checked at 5 ft (1.5 m) increments along the height. The overall design dimensions were primarily controlled by the fatigue resistance of the tower. However, at the tower base the interaction of flexural, axial, shear, and torsional capacities became critical. More details are given below.

Tower Ultimate Strength

For Load and Resistance Factor Design (LRFD), it is important to examine the interaction of limit states at the ultimate load level. This interaction is described by Equation (2-58). The governing ultimate load combination is given by Equation (2-9), which in turn was dominated by the EWM50 wind speed load case. Therefore, only the EWM50 loads are discussed below with regards to strength. Figure 3.9 depicts the criticality of strength along the height of the tower.
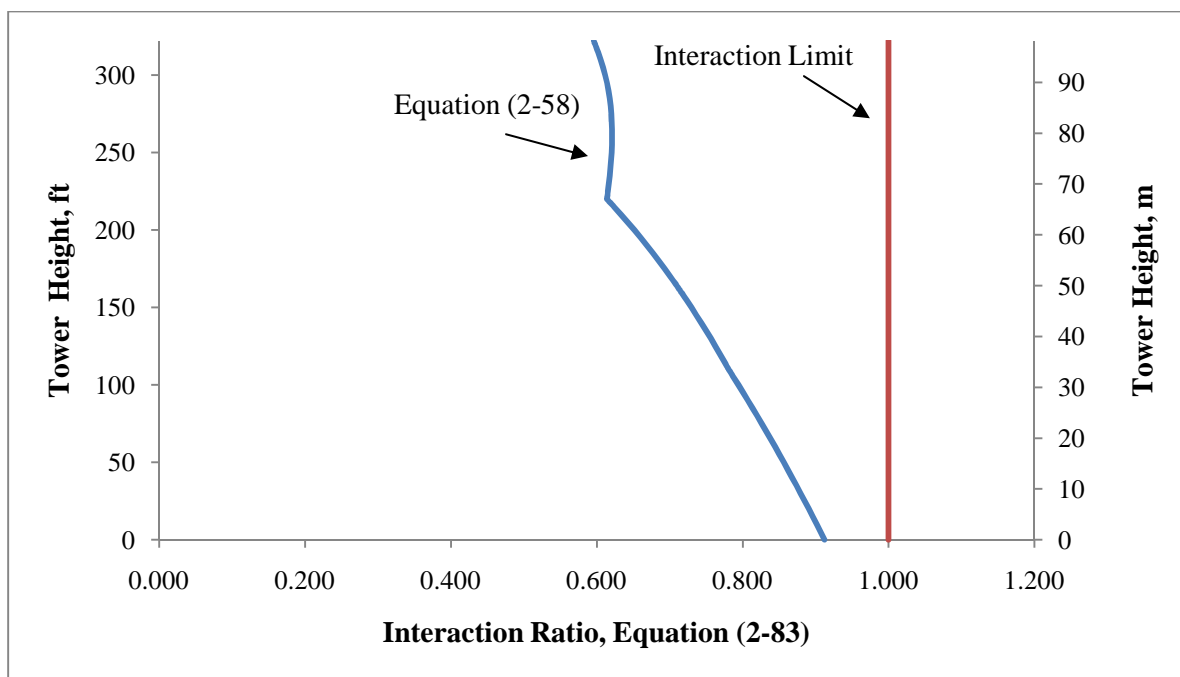
Figure 3.9: Strength Interaction Ratio for the 322 ft (98.2 m) Steel Tower Design as per Equation (2-58)

At the base of the tower, the ratio $M_u/\phi M_n$ is 0.811, and the total interaction ratio is 0.912. The axial compressive ratio $P_u/\phi P_n$ is 0.0963, and the combined shear and torsion term $(V_u/\phi V_n + T_u/\phi T_n)^2$ is 0.005. The individual components of the ultimate strength interaction ratio are discussed further below. The sharp discontinuities in Figure 3.9 at the height of 220 ft (67 m) correspond to the changing of the semi-vertex angle and variance of wall thickness. A discontinuity occurs at 110 ft (33.5 m) as well, but is less well-defined.

Ultimate Moment Capacity

The AISC (American Institute of Steel Construction, Inc., 2005) method, as detailed in Section 2.3.5, was used to calculate the flexural capacity of the steel tower. The tower falls into the category of a noncompact section, meaning that some local buckling is expected to occur before the full plastic moment capacity of the section is developed. Therefore, Equation (2-48) was used to calculate the moment capacity along the tower height. At the tower base, the factored-level moment demand was calculated as 177,500 ft-kip (241,000 kN-m). The capacity was determined to be 219,000 ft-kip (297,000 kN-m). At the tower top, the ultimate moment demand was 12,890 ft-kip (17,480 kN-m) with an ultimate moment capacity of 36,000 ft-kip (48,800 kN-m). All moment demand values took into consideration P-Δ effects caused by the sway of the tower. A B_2 factor was used to amplify the moment demand along the tower length. This factor was calculated from the following equation (after American Institute of Steel Construction, Inc., 2005):

$$B_2 = \frac{1}{1 - \frac{P_u}{P_e}}$$
(3-3)

where P_u = factored level axial demand;

P_e = elastic buckling capacity.

The elastic buckling capacity, P_e, for the steel tower was computed as 19,600 kips (87,200 kN) using the Rayleigh-Ritz method as described in Section 2.3.8. This resulted in a B_2 factor ranging from 1.08 at the tower base to 1.03 at the tower top.

Ultimate Compressive Strength

In order to calculate the compressive capacity of the tower, a modified version of the AISC method was used. As Equation (2-41) is intended for non-tapered sections, it was not utilized. Rather, the elastic buckling stress, F_e, was obtained by dividing the Rayleigh-Ritz elastic buckling load, P_e, by the tower cross sectional area. This resulted in an elastic buckling stress ranging from 19.37 ksi (133.6 MPa) at the tower base to 65.4 ksi (451 MPa) at the tower top. This stress was then used with Equations (2-42) and (2-43) in order to calculate the critical buckling load, P_{cr}. For all sections along the tower height, the tower was classified as slender for compression. Therefore, the reduction factor Q, as described in Equation (2-44), was used to account for local buckling. This factor ranged from 0.820 at the tower base to 0.806 at an elevation of 110 ft (33.5 m). This resulted in an ultimate compressive strength ranging from 15,400 kip (68,500 kN) to 8450 kip (37,600 kN) at the tower base and tower top, respectively. The factored-level compression demand ranged from 1480 kips (6580 kN) at the tower base to 594 kips (2640 kN) at the tower top.

Ultimate Shear Strength

The ultimate shear strength of the tower was calculated in accordance with the AISC specification (American Institute of Steel Construction, Inc., 2005) which was described in Section 2.3.5. The strength of the section is governed by the lesser of shear yielding and shear buckling stress. In all cases along the tower height the shear strength was governed by shear buckling. The critical buckling stress ranged from 21.99 ksi (151.6 MPa) at the tower base to 15.57 ksi (107.4 MPa) at the tower top. This resulted in an ultimate shear resistance ranging from 20,000 kips (89,000 kN) at the tower base to 4200 kips (18,680 kN) at the tower top. When this was compared to the maximum factored-level shear demand of 651 kips (2900 MPa), which occurred at the tower base, it was clear that tower shear strength was not a governing design factor.

Ultimate Torsional Strength

The ultimate torsional capacity was also checked using the AISC method (American Institute of Steel Construction, Inc., 2005). Similar to shear strength, the torsional capacity of the

tower is governed by the lesser of torsional buckling and torsional yielding strength. Shear buckling governed the design torsional strength along the entire tower height, resulting in an ultimate torsional capacity ranging from 137,400 kip-ft (186,300 kN-m) at the tower base to 16,030 kip-ft (21,700 kN-m) at the tower top. The factored-level torsional demand was constant along the tower height and was calculated as 5310 kip-ft (7200 kN-m). It was therefore concluded that torsional strength of the tower was not a governing design limit state.

Local Buckling

Although the occurrence of local buckling was accounted for by the LRFD design procedure, the ECCS method detailed in Section 2.3.5 was used as a second check. The calculated critical buckling stress ranged from 40.2 ksi (277 MPa) at the tower base to 39.9 ksi (275 MPa) at the tower top. This uniformity in buckling stress is due to the relatively constant ratio of tower diameter to thickness along the tower height. The maximum combined service-level stress level was 29.06 ksi at the tower base. This indicates that local buckling will not be of concern for service-level loading.

Fatigue

In general, the fatigue load combination given by Equation (2-12) governed the overall dimensions for the tower. Figure 3.10 shows stress range caused by the application of the DEL compared to the calculated allowable stress range along the tower height. The allowable stress range was calculated as 2.88 ksi (19.86 MPa) using Equation (2-102). The maximum calculated stress range caused by the DEL was 2.80 ksi (19.31 MPa) and occurred at 55 ft (16.76 m) along the tower height. The resulting demand-to-capacity ratio (DCR) was 0.974. The tower fatigue stress range shows a trend of a parabolic stress range versus height. Both the fatigue moment and cross-sectional dimensions of the tower decrease with height. However, the fatigue moment decreases following a linear variation, while elastic section modulus of the steel tower follows a cubic variation. This heterogeneity in variation is the cause of the parabolic shape. Although the DEL fatigue stress range diverges slightly from the allowable limit for the top third of the tower, it is estimated further optimization would

result in a material volume reduction of only 1.3%. However, this reduction would cause the top third of the tower to be classified as slender for buckling, resulting in a large decrease in flexural capacity.
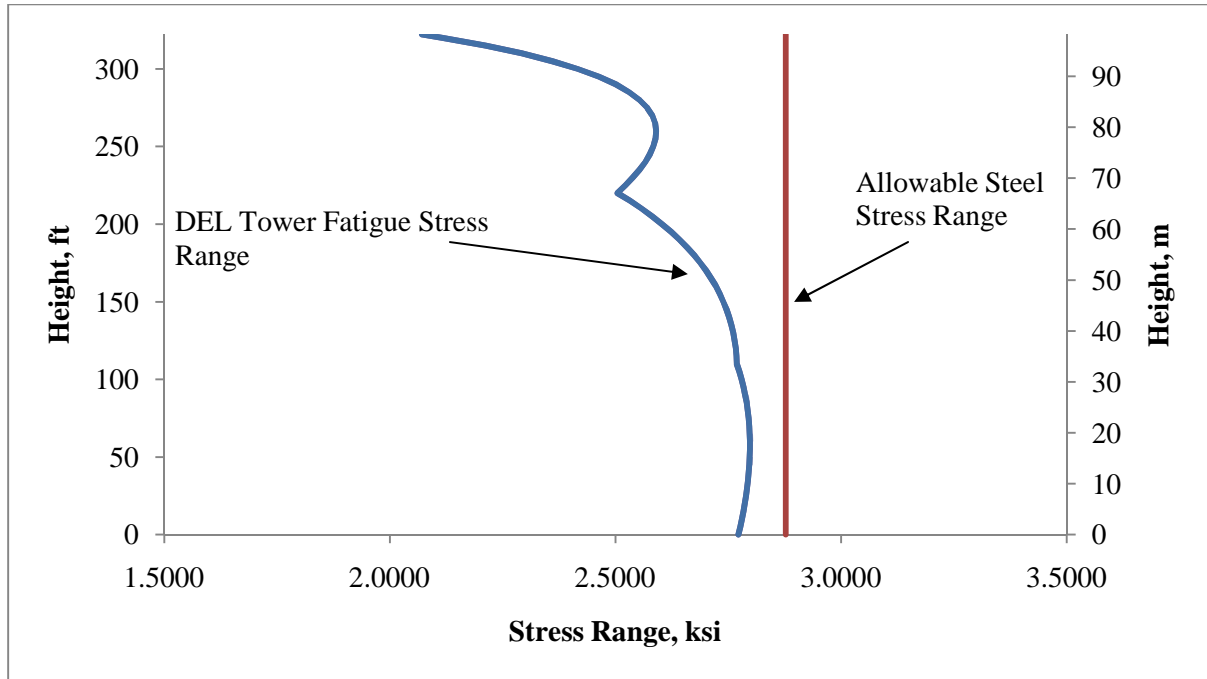
Figure 3.10: Damage Equivalent Load Fatigue Check for the 322 ft (98.2 m) Steel Tower Design

Dynamic Properties

The design resulted in a tower with a calculated fundamental natural frequency of 0.338 Hz, using the Rayleigh Method outlined in Section 2.3.8. This frequency lies within the 1.1P and 2.7P working frequency range (i.e., 0.242 Hz to 0.594 Hz), where P represents the rotational frequency of the turbine rotor, thereby avoiding any excessive dynamic excitation of the tower. Possible vortex shedding was also investigated for the steel tower. Based on the ACI 307 (1998) method, the critical vortex shedding wind speed for the steel tower is 11.10 mph (4.96 m/s). This wind speed is compared to the range of $0.5\overline{V}(z_{cr}) \leq V_{cr} \leq 1.30\overline{V}(z_{cr})$, where z_{cr} is taken as 5/6 times the tower height, as described in Section 2.3.6. In this instance, the EOG50 wind speed will govern over the EWM50. The EOG50 wind speed range is calculated 33.3-86.6 mph (14.89-38.72 m/s). Therefore, according to the ACI 307

(1998) specification, vortex shedding will not be a design criterion. However, it should be noted that at lower speeds (i.e., typical turbine operating speeds), it is possible that vortex shedding may occur, causing additional deflection of the tower, and therefore increased fatigue loading. Methods for investigation of vortex shedding have been developed by Chang (2007) for high-mast light poles, which could be extended to the towers that have been considered in this study. However, due to the lack of detailed turbine fatigue loading for a 328 ft (100 m) 3.0 MW turbine, it is not possible to determine how the occurrence of vortex shedding would affect the fatigue life of the tower. For a final design, it is expected that a detailed time history of fatigue loading would be available and that the contribution of vortex shedding to fatigue loading could be more rigorously investigated.

Deflection

Tower top deflection can be computed through Equation (2-11). The maximum displacement is given as:

$$\Delta_{max} = \int_{0}^{h} \frac{M(z)}{EI(z)}(h-z)dz$$

(3-4)

where $M(z)$ = moment demand along the tower height;

$EI(z)$ = tower flexural rigidity along the tower height;

h = tower height; and

z = elevation.

For the steel tower service-level EWM50 wind loading the tower top displacement was calculated as 63.6 in (1.617 m). This value corresponds to 1.646% tower drift.

3.2.3   Discussion of Results

The results of the steel tower design establish a baseline from which to compare the regular strength concrete and UHPC tower designs. The natural frequency of the steel tower is within the "working frequency range", allowing it to avoid excessive dynamic amplification. The total weight of the tower, 739 kip, falls between the Berger/ABAM 1.6MW and 3.6MW designs (516 kip and 899 kip, respectively). With a similar first natural frequency and

weight, this suggests that the ISU steel tower design has a similar stiffness to the BergerABAM towers.

As expected, the design of the steel tower yielded a necessary base diameter of 18 ft (5.49 m). As previously mentioned in Section 1.3.2, this exceeds the transportation limit of 14.1 ft (4.3 m), and could not be transported as complete sections without increasing the costs significantly. This further validates the need for alternative tower designs.

The deflection for the steel tower is very high, exceeding the criteria set out by ACI for concrete chimneys (ACI Committee 307, 1998). This suggests that deflection becomes a more critical issue at taller hub heights, as all other design limit states are satisfied for the steel tower design. It is likely the turbine manufacturers specify permissible towers deflections, and were these limits known the tower design could be revised. The most obvious solution for decreasing deflections is to increase the base diameter. However, this would also exacerbate the challenge of transporting large steel sections, as well as increase the volume of steel needed for the design. It should also be noted that these deflections correspond to the EWM50 wind speed, which is a nonoperating condition for the turbine. It is possible that turbine manufacturers have different deflection limits for operating and nonoperating states.

3.3 Concrete Towers

3.3.1 Loading

The prestressed concrete tower experiences the same loads as the steel tower except for the direct wind load and self-weight. The turbine loads and axial loads can be seen in Table 3-1 and

Table 3-2, respectively. In addition to the listed axial load, the total self-weight of the tower was 2220 kips (9880 kN) based on the concrete tower dimensions listed in Table 3-7. Again, the direct wind force on the tower was calculated using ASCE 7 (SEI, 2005) for flexible structures. Due to the variance in tower dimensions and natural frequency, this load is different from that calculated for the steel tower. The concrete tower has a significantly

larger natural frequency, 0.568 Hz, which results in a decreased wind pressure. However, the overall tower dimensions (discussed in Section 3.3.2) are nearly 1.5 times larger, resulting in a net increase in direct wind load on the tower. The results of the direct wind load for the EWM50 (3 sec. wind speed of 136.3 mph [60.9 m/s]) and an EOG50 (3 sec. speed of 60.5 mph [27.1 m/s]) are shown in Table 3-6.

Table 3-6: Estimated Direct Wind Force Loads at Midheight and Base of the 322 ft (98.2 m) Concrete Tower at Service-Level

EWM50	V_{Mx} kips (kN)	M_{My} ft-k (kN-m)	V_{Bx} kips (kN)	M_{By} ft-k (kN-m)
	137.6 (612)	10,260 (13,910)	300 (1334)	46,000 (62,400)
EOG50	V_{Mx} kips (kN)	M_{My} ft-k (kN-m)	V_{Bx} kips (kN)	M_{By} ft-k (kN-m)
	24.3 (108.1)	1805 (2450)	53.2 (237)	8120 (11,010)

Note: The subscripts "M" and "B" represent tower midheight and base, respectively.

Due to the lack of a detailed time history of fatigue loading for a 3.0 MW turbine at a 328 ft (100 m) hub height and as the MC90 (Comite Euro-International Du Beton, 1990) allows for the verification of fatigue strength through the application of a single load, the same Damage Equivalent Loads, shown Table 3-4, were used in checking the fatigue strength of the tower. For the concrete tower, it was assumed that the DEL caused as a stress range, $\Delta\sigma$, and a stress reversal of $\Delta\sigma/2$. Therefore, the total stress at a given point on a tower is $P + F/A \pm \Delta\sigma/2$, where P is the axial load on the tower, and F is the prestressing force at a given tower cross section.

3.3.2   *Design*

As with the steel tower design, the concrete tower was designed with an iterative process, as the design and loads were coupled through the tower geometry and dynamic properties. The results of the design are summarized in Table 3-7. In order to facilitate an easy comparison to previous designs, the concrete tower semi-vertex angle was also tapered three times. The tower was designed as a bonded post-tensioned structure assuming 10 ksi (68.9 MPa) high-strength grout was used. In order to further optimize the design, the area of post-tensioning steel was also varied three times, with cut-off points coinciding with the change in tower semi-vertex angle.

Table 3-7: Summary of the 322 ft (98.2 m) Tall Concrete Tower for a 3 MW Turbine

Compressive Strength, ksi (MPa)	7 (48)
Post-tensioning Effective Steel Stress, ksi (MPa)	180 (1241)
Diameter at Base, in (m)	360 (9.15)
Shell Thickness from 0-110 ft (0-33.5 m), in. (mm)	8.375(213)
Number of 0.6-in. (15 mm) diameters tendons along the center of the shell, 0-110 ft (0-33.5m)	94 (4-strand bundle)
Diameter at 110ft, in. (m)	312 (7.93)
Shell Thickness from 110-220ft (33.5-66.7 m), in. (mm)	7.875 (200)
Number of 0.6-in (15 mm) diameters tendons, 110-220 ft (33.5-66.7 m)	67 (4-strand bundle)
Diameter at 220ft (66.7 m), in. (m)	222 (5.64)
Shell Thickness from 220-322 ft (66.7-98.2 m), in. (mm)	9.4 (239)
Number of 0.6-in (15 mm) diameters tendons, 220-322 ft (66.7-98.2 m)	49 (4-strand bundle)
Diameter at 322 ft (98.2m), in. (m)	130.5 (3.31)
Concrete Volume, yd^3 (m^3)	574 (439)
Tower Weight, kips (kN)	2300 (10,230)
Fundamental Natural Frequency of Tower, Hz	0.568

Service-Level Moment Capacity

The tower was initially sized based on the criterion of allowing zero tension stress under service level load conditions. In addition, the allowable stress limits specified by ACI (Section 2.3.6) were considered. Since both the turbine and direct wind loads are dynamically amplified, they were again treated as an equivalent static load. Therefore, the lower and upper limits set by ACI for concrete compression, presented in Equation (2-82), were averaged, and a limit of $0.53f_c'$ was set for concrete compression under service loads. This yields the following design constraints,

$$M_a = \left(\frac{F+P}{A_{trans}}\right)\left(\frac{I_{trans}}{c_{tension}}\right) \tag{3-5}$$

$$\left(\frac{F+P}{A_{trans}}\right) + \left(\frac{M_r c_{compression}}{I_{trans}}\right) \leq 0.53f_c' \tag{3-6}$$

where F = prestressing force on the section;

P = service-level axial load;

A_{trans} = transformed section area;

I_{trans} = transformed section moment of inertia;

$c_{tension} = c_{compression}$ = distance from the neutral axis to the extreme compression or tension fiber; and

f_c' = 28-day concrete compressive strength.

As with the steel tower, the governing IEC load case was the EWM50 wind speed and the governing load combination was Equation (2-11). The governing limit states along the bottom two-thirds of the tower height were crushing of concrete and ensuring zero tension as per Equations (3-5) and (3-6), respectively. An ideal design should balance these conditions perfectly, so the tension side of the tower reaches zero stress as the compressive side reaches the imposed limit of $0.53 f_c'$. Presented below are plots of demand and capacity for these limit states. The sharp drops in capacity in Figure 3.11 correspond to the cut-off of post-tensioning tendons. Similarly, the drops in compressive stress (Figure 3.12) coincide with the elimination of unused post-tensioning ducts (and therefore an increase in net area).

At the tower base, the service level moment capacity was 125,000 ft-kip (169,500 kN-m) with a calculated demand of 124,700 ft-kip (169,100 kN-m). At the tower top, the service-level moment capacity was calculated as 19,130 kip-ft (25,940 kN-m) with a demand of 9,330 kip-ft (12,650 kN-m). This includes a B_2 factor, which was calculated from Equation (3-3) which and ranged from 1.007 to 1.042. In order to evaluate this factor, a global buckling load was necessary. This buckling load, calculated using the Rayleigh-Ritz method detailed in Section 2.3.8, was determined to be 82,300 kips (366,000 kN).
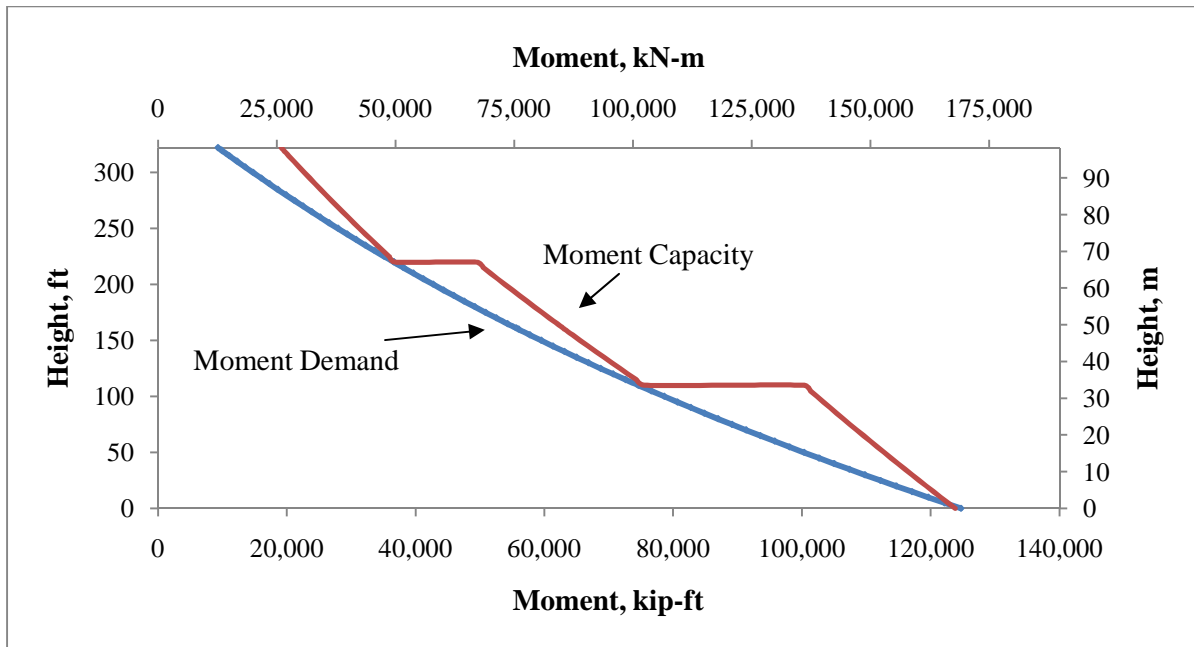
Figure 3.11: Comparison of Service-Level Moment Capacity and Demand for the 322 ft (98.2 m) Concrete Tower Design as per Equation (3-5)
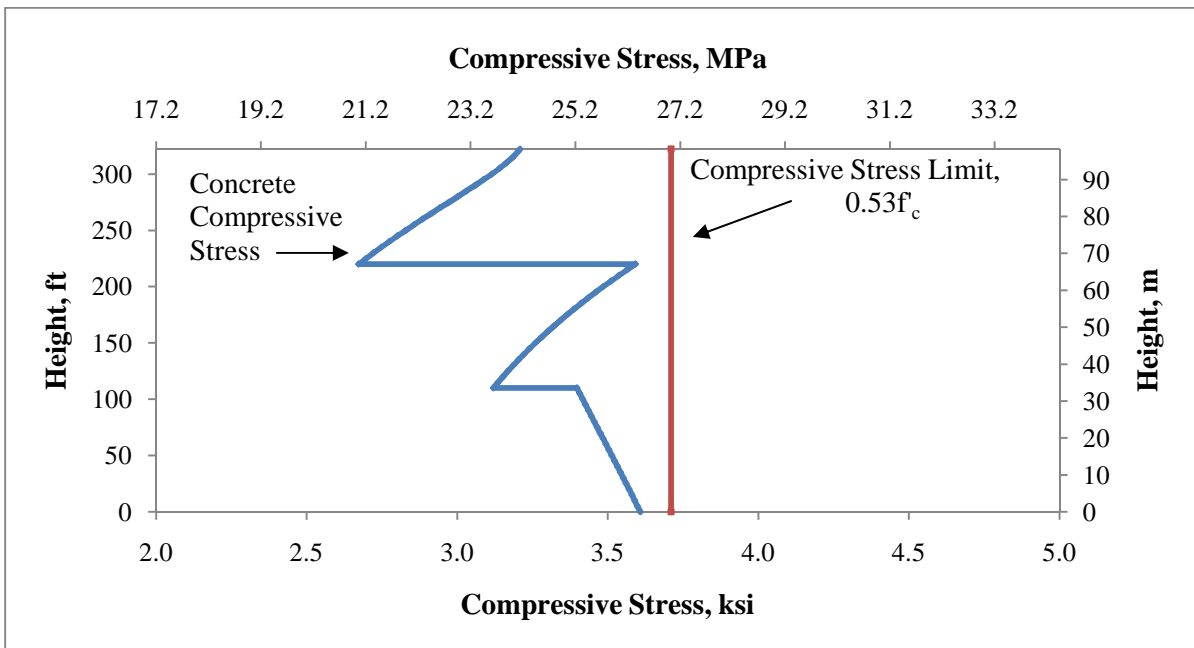
Figure 3.12: Comparison of Service-Level Compressive Stress Demand Against the Allowable Stress Limit for the 322 ft (98.2 m) Concrete Tower Design as per Equation (3-6)

Ultimate Moment Capacity

Although it is typical for service level moment capacity to govern over the ultimate moment limit state, an ultimate moment capacity was calculated at 6 points along the tower. In order to complete this calculation, the constraints of strain compatibility and force equilibrium were used. Rather than using a stress block approach, it was decided that the use of a characteristic concrete stress-strain curve would be more appropriate. For this method, the cross section was discretized into strips, and the values of stress/strain were assumed to be constant over each strip. The following steps detail the methodology used:

1) Choose a neutral axis depth, c_{NA}.

2) Assuming concrete crushing strain will govern the ultimate capacity, set the strain at the extreme compressive fiber to ε_{cu}; 0.004 was used for this design.

3) Calculate the strain at the centroid of all concrete strips, ignoring the contribution of concrete tension.

4) Calculate the stress, f_c, in each concrete strip using the model by Mander et al. (1988). This model is described in detail below.

5) Calculate the compressive force, c_i, in each concrete strip.

6) Calculate the incremental strain, $\Delta\varepsilon$, at the centroid of each steel tendon cluster.

7) Calculate the total strain, ε_{ps}, at the centroid of each steel tendon cluster (see further description of this calculation below). Ensure that no value of strain has exceeded the fracture strain; 0.05 was used in this study.

8) Calculate the tensile stress, f_t, in each tendon group (see PCI model below (PCI Industry Handbook Committee, 2004).

9) Calculate the tensile force, t_j, in each tendon group.

10) Sum the compressive forces, $C = \sum_1^n c_i$. Sum the tensile forces, $T = \sum_1^m t_j$. If $C + T = P$, move on to Step 11. Otherwise, revise the neutral axis depth and restart the process.

11) Sum the moments about the centroid to determine the ultimate nominal moment capacity, using the following equation:

$$M_n = \sum_1^n (c_i \times d_{ci}) + \sum_1^m (t_j \times d_{tj}) \tag{3-7}$$

where d_{ci} = the distance from the centroid of the concrete strip force, c_i, to the section centroid; and

d_{tj} = the distance from the centroid of the steel force, t_j, to the section centroid.

The flexural strength reduction factor was taken as $\phi_{bending} = 0.9$ (Post-Tensioning Institute, 2006). It should be noted that this method is not valid if tendon fracture governed the ultimate capacity. However, this was not observed for the design. Additionally, as this method is intrinsically iterative, it lends itself well to spreadsheet/solver methods.

ASTM A 416 tendons (270 ksi fracture stress) were used for this design. PCI (2004) provides an approximate stress-strain model for these tendons:

For $\varepsilon_{ps} \leq 0.0086$,

$$f_{ps} = \begin{cases} 28,500\varepsilon_{ps} \ (ksi) \\ 196,500\varepsilon_{ps} \ (MPa) \end{cases} \tag{3-8}$$

For $\varepsilon_{ps} > 0.0086$,

$$f_{ps} = \begin{cases} 270 - \dfrac{0.04}{\varepsilon_{ps} - 0.007} \ (ksi) \\ 1861.6 - \dfrac{0.27579}{\varepsilon_{ps} - 0.007} \ (MPa) \end{cases} \tag{3-9}$$

where ε_{ps} = the total strain in the post-tensioning strands; and

f_{ps} = the stress in the post-tensioning strands.

The concrete stress-strain model by Mander et al. (1988) was used to obtain stresses in the concrete for the ultimate capacity calculation. Although this model was designed for confined concrete stress-strain behavior, it can be used for unconfined concrete by setting the confinement stress equal to zero. The model (for unconfined concrete) is as follows:

$$f_c = \frac{f_c' x r}{r - 1 + x^r} \tag{3-10}$$

$$x = \frac{\varepsilon_c}{\varepsilon_{cc}} \tag{3-11}$$

$$r = \frac{E_c}{E_c - E_{sec}} \tag{3-12}$$

$$E_c = \begin{cases} 60{,}000\sqrt{f_c'} \ (psi) \\ 5000\sqrt{f_c'} \ (MPa) \end{cases} \tag{3-13}$$

$$E_{sec} = \frac{f_c'}{\varepsilon_{cc}} \tag{3-14}$$

where f_c = concrete stress for a given strain level;

f_c' = 28-day compressive strength of the concrete;

ε_c = concrete strain level; and

ε_{cc} = concrete crushing strain (0.002 was used for this report).

A stress-strain curve for this model, using 7 ksi (44 MPa) 28-day strength concrete, is presented in Figure 3.13.

The ultimate capacity of the tower was in all cases higher than the factored-level moment demand. At the tower base, the ultimate moment capacity was calculated as 235,000 ft-kip (319,000 kN-m) and demand was calculated as 178,200 ft-kip (241,600 kN-m) kip-ft. At the top of the tower, the capacity was determined to be 34,900 ft-kip (47,300 kN-m) with a calculated demand of 12,590 ft-k (17,070 kN-m).
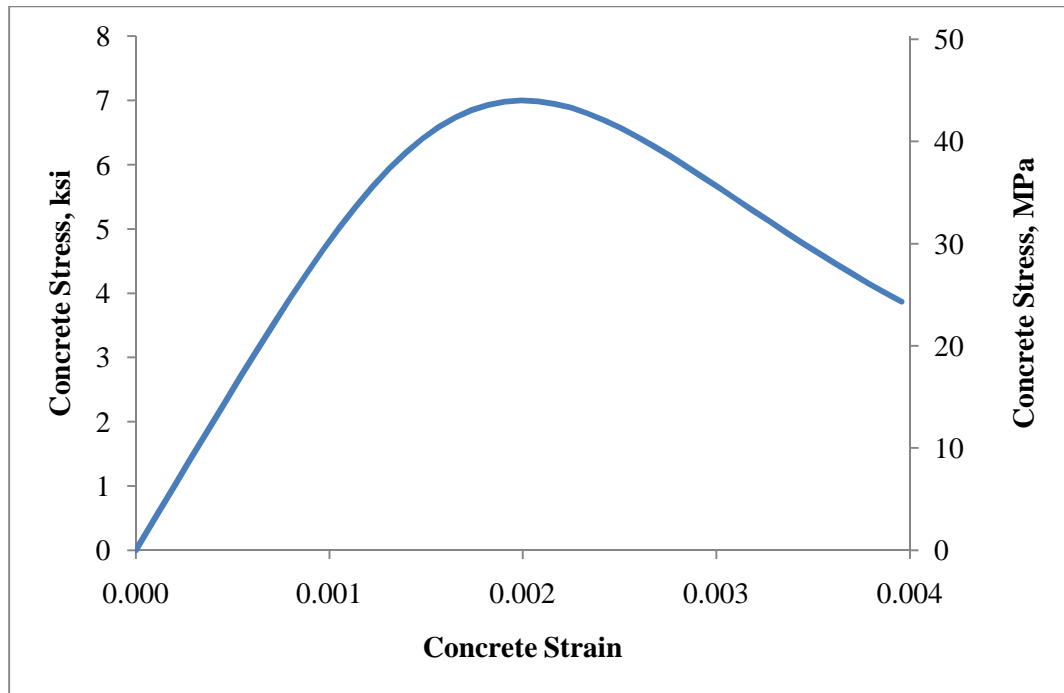
Figure 3.13: Stress-Strain Model for 7 ksi (44 MPa) Concrete as per Equations (3-10) to (3-14)

Service-Level and Ultimate Shear Capacity

In addition to the above limit states, shear was checked both as a service level limit state and ultimate limit state. At the service level, the tower was examined along the height for shear cracking due to the combination of shear and torsional stresses. Equation (2-94) was used to evaluate the possibility of cracking along the tower height. The maximum principal tensile stress developed through the combination of shear and torsional stresses was $p_t = 58.7$ psi (0.405 MPa). Compared to the tensile strength of concrete, estimated as 293 psi (2.02 MPa) by Equation (2-94), no shear cracking will occur under service level conditions. At the ultimate limit state, concrete shear strength is governed by the lesser of inclined shear cracking and flexure shear cracking. In all cases, flexure-shear cracking governed the ultimate shear strength of the concrete. At every point on the tower the design concrete strength, ΦV_n, was greater than the factored level shear demand, as seen in Figure 3.14.
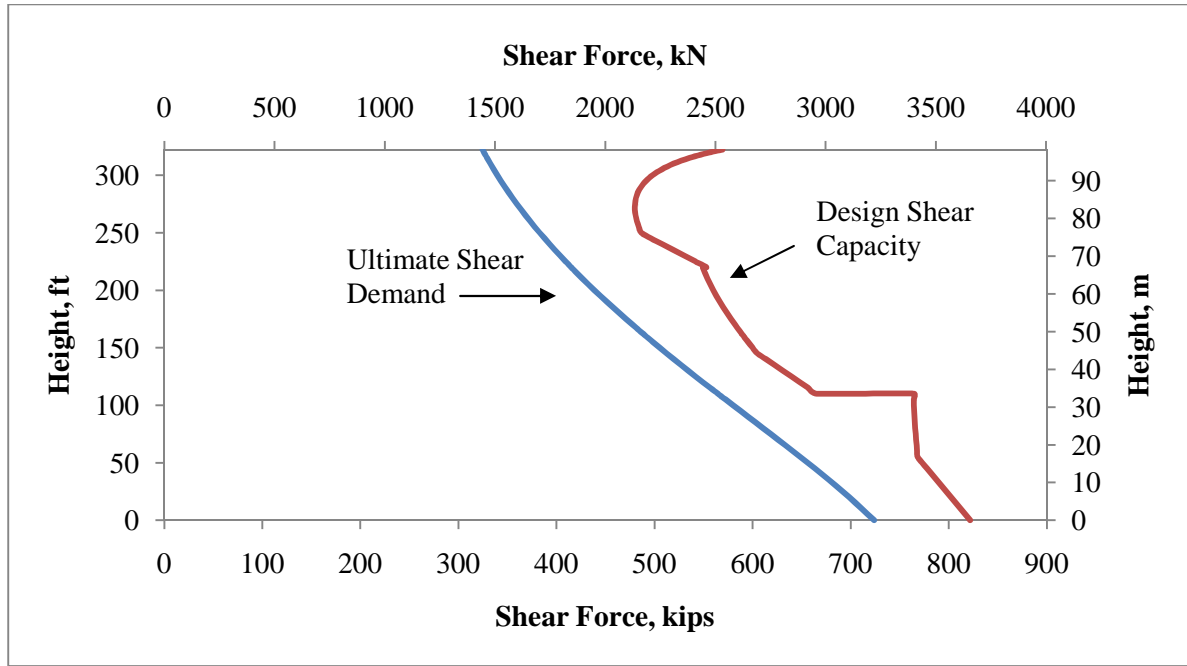
Figure 3.14: Comparison of Ultimate Concrete Shear Demand and Capacity for the 322 ft (98.2 m) Concrete Tower Design as per Equations (2-85) and (2-86)

As concrete shear strength is taken as the shear level when cracking occurs, and since a lateral force applied at the top of a cantilever column causes the largest moment at the bottom of the column, the applied shear at the bottom of the column is much nearer to the cracking shear than at the top. Therefore, the increasing shear strength at the top of the tower can be attributed to the widening gap between V_u and M_{cr}/M_u in Equation (2-84). However, the concrete shear strength is never twice demand, indicating the requirement for minimum shear reinforcement according to ACI recommendations (ACI Committee 318, 2008). It should also be noted that the shear area in Equations (2-84) and (2-86) was taken as $0.8A_{trans}$. Cheng et al. (2003) suggest a shear area given by Equation (3-15):

$$A_{shear} = \frac{\pi}{4}D(2t)$$

(3-15)

where D = shell outside diameter

t = shell thickness

This corresponds to approximately $0.5A_{gross}$. The use of this shear area for the 322 ft (100 m) concrete tower has been investigated further by Lewin and Sritharan (2010). Although the shear strength of the tower was reduced, it was found that through the use of minimal transverse shear reinforcing the total shear capacity was adequate.

Ultimate Torsional Capacity

The tower was checked for sufficient resistance to torsion at factored level loads. Equation (2-87) was used to check the adequacy of the tower cross sectional dimensions for the interaction of torsion and shear. The results of the equation indicate the tower has a high resistance to torsion. The most critical area of the tower for this limit state was the top, having a demand-to-capacity ratio (the left-hand side of Equation (2-87) divided by the right-hand side) of 0.311. Although this section is adequate for torsional resistance, it is important to note that a final design should specify transverse reinforcement to satisfy the torsion demand.

Fatigue

For concrete towers, the fatigue strength of both the steel post-tensioning tendons and concrete elements needed to be examined. For both cases, the approach described in Section 2.3.6 for the MC90 (Comite Euro-International Du Beton, 1990) was used. Although moment capacity governed the diameter of the entire tower, as well as wall thicknesses from 0-220 ft (0-67.1 m), concrete fatigue governed the wall thicknesses from 220-322.17 ft (98.2 m). In order to satisfy Equation (2-68), a wall thickness of 9.4 in. (239 mm) was required. The resulting fatigue life of the concrete is extremely high, ranging from 10.00×10^{26} cycles at the tower base to 6.27×10^{9} cycles at the tower top. Although the minimum fatigue life is far beyond the required 5.29×10^{8} cycles, this was achieved by a relatively modest increase in tower wall thickness. For example, were a wall thickness of 9.0 in. (229 mm) used in the top third of the tower, the fatigue life of the tower would be reduced to 1.333×10^{8} cycles. A small increase in concrete material allows for a large gain in fatigue life. For the prestressing steel, the allowable stress range was 10.05 ksi (69.3 MPa). At the largest, the steel fatigue stress range was 1.028 ksi (7.09 MPa), much lower than the allowable value. When

compared the number of cycles expected for a 20 year turbine life, 5.29×10^8, there is a potential for re-use of the tower after the turbine is decommissioned.

Dynamic Properties

The fundamental frequency of this tower was calculated as 0.568 Hz. Although this is towards the upper end of the working frequency range 1.1P and 2.7P (0.242 Hz to 0.594 Hz), it does not exceed it. Vortex shedding was also examined for this tower, as detailed in Section 2.3.6. The critical vortex shedding speed was calculated as 23.8 mph (10.63 m/s). This value is compared to the tower's design wind speed range, which for the EOG50 is calculated 33.3-86.6 mph (14.89-33.7 m/s). Therefore, vortex shedding will not occur for the 322 ft (98.2 m) concrete tower.

Deflection

The tower top deflection for the EWM50 wind speed was calculated for the concrete tower as 15.98 in (0.406 m), corresponding to 0.413% drift.

3.3.3   Discussion of Results

The design of the concrete tower satisfies, for the given loading, all necessary criteria. The tower natural frequency is approaching the upper end of the working frequency range, but does not exceed it. This design solution could be refined further through the calibration the turbine loads to include the specific dynamic amplification caused the concrete tower's natural frequency. It is also useful to note that the flexibility of the foundation will likely decrease the concrete tower's stiffness, and therefore its natural frequency (LaNier, 2005)

The tower weight, 2290 kips (10,190 kN), is significantly less than the BergerABAM 1.5 MW and 3.6 MW designs, 3254 kips (14,480 kN) and 4579 kip (20,370 kN), respectively (LaNier, 2005). This is likely due to Berger/ABAM's chosen base diameter of 25 ft (7.62 m). This dimension requires a wall thickness of around three times ISU's design. It is possible that BergerABAM tuned their tower dimensions in order to reach the target natural frequency range, as it is specified for their 1.5 MW tower that natural frequency controlled the design. Additionally, BergerABAM chose to use an effective post-tensioning stress of 160 ksi (1003

MPa), while the design here assumed an effective a post-tensioning stress after losses of 180 ksi (1241 MPa).

At first glance, Figure 3.10 suggests that the tower could be further optimized along its length. However, this would involve additional prestress staging. Feasibility of this would depend on the construction costs of post-tensioning at additional levels. This is a possibility, as the tower would likely be transported in more than three sections as is currently done with steel towers. Similar to the steel tower, the design could be refined by applying a history of simulated or field-collected load cycles in order to more accurately evaluate the fatigue life of the tower.

Although a limiting deflection for wind turbine towers has not been found, it judged that the 322 ft (98.2 m) concrete tower would require little revision for deflection were a limit specified.

3.4   Summary

Using the same loading criteria as Berger/ABAM towers, both 322 ft (98.2 m) steel and concrete towers designs were completed. A comparison of the design results, including controlling limit states for the towers is presented in Table 3-8. The 322 ft (98.2 m) steel tower resulted in a similar design to Berger/ABAM's solution, confirming the assumption that required section diameters would make highway transportation of conventional steel towers impossible. Both BergerABAM's (LaNier, 2005) 328 ft (100 m) steel tower and the steel tower designed in this study would likely require further refinement to meet deflection limits, with 0.919% and 1.646% respectively. This could include increasing of the 322 ft (98.2 m) steel tower's base diameter. However, this increases the challenges associated with transporting large diameter steel tubes using current methods. Additionally, the governing limit state for the 322 ft (98.2 m) tower designed in this study was fatigue, limiting the design life of the tower to 20 years.

The 322 ft (98.2 m) concrete tower design is significantly lighter tower than Berger/ABAM's design. This could be due to Berger/ABAM tuning their design to meet natural frequency requirements, as well as their choice of base dimension and steel post-tensioning stress.

Berger/ABAM's concrete towers' natural frequencies are closer to the center of this range, ranging from 0.377 to 0.384 (LaNier, 2005). The fundamental natural frequency of the ISU concrete tower design, 0.568 Hz, is just within the desired working frequency range. The ISU tower could be refined by tuning the dimensions to bring fundamental natural frequency closer to the center of the working range. Additionally, foundation flexibility would somewhat decrease the fundamental natural frequency of the ISU concrete tower. The deflection of the 322 ft (98.2 m) concrete tower is much lower than the steel tower, at 0.413% drift. The governing limit state for the concrete tower was the service-level moment capacity, rather than fatigue. This indicates that the 322 ft (98.2 m) concrete tower's design life would far exceed 20 years.

Table 3-8: Comparison of Design Results for 322 ft (98.2 m) Steel and Prestressed Concrete Tower Designs

	322 ft (98.2 m) Steel Tower	322 ft (98.2 m) Prestressed Concrete Tower
Weight, kips (kN)	739 (3290)	2290 (10,190)
Maximum Strength DCR	0.912, Equation (2-58)	0.997, Equation (2-82)
Maximum Shear DCR	0.0773	0.881
Maximum Fatigue DCR	0.972	0.0844
Deflection, % Drift	1.646	0.413
Fundamental Natural Frequency	0.338	0.568
Controlling Limit State	Strength at tower base, Fatigue along the tower height	Service-level tower flexural strength, concrete fatigue (wall thickness for 220-322 ft [67.1-98.2 m])

4   DESIGN OF UHPC TOWERS

4.1   Overview

As implied in Section 1.4, the use of UHPC was expected to provide innovative solutions to wind turbine towers. Additionally, it is important to look for innovative designs to make UHPC towers cost effective. Consequently, it was realized that there are multiple options that exist for the design of a UHPC wind turbine tower. The two that have been identified, and that will be subsequently investigated in this report, are the UHPC Shell Tower and the UHPC Lattice Tower, with several different variations for the latter concept. As baseline 322ft (98.2 m) tall concrete and steel designs have been developed, any UHPC tower design can then be compared directly to them. To facilitate this comparison, both UHPC tower alternatives have been designed for the same wind turbine, the ACCIONA Windpower AW-109/3000, as the concrete/steel alternatives. Additionally, they have been designed for the same surface roughness (class D) and wind speed load cases (EWM50 and EOG50, as discussed in Section 3.2.1).

4.2   UHPC Shell Tower

The UHPC Shell tower is an extension of the 322 ft (98.2 m) prestressed concrete tower design concept presented in Section 3.3. It does not represent a radical new design, but rather seeks to refine current designs using an innovative material. As was done with the prestressed concrete tower, the UHPC Shell concept was designed as a bonded, post-tensioned structure.

4.2.1   Loading

Since the UHPC shell tower does not represent a significant departure from the current wind turbine towers, the loading on the tower should be expected to remain similar. All tower top loads will remain the same as for the concrete and steel designs. Turbine loads can be seen in Table 3-1 and axial loads (excluding dead load) can be found in

Table 3-2. As direct wind loads are based on the tower dimensions and natural frequency, they will be unique for each tower. The direct wind loads for the UHPC Shell can be seen in Table 4-1.

Table 4-1: Estimated Direct Wind Force Loads at Midheight and Base of the 322 ft (98.2 m) UHPC Shell Tower at Service-Level

EWM50	V_{Mx} kips (kN)	M_{My} kip-ft (kN-m)	V_{Bx} kips (kN)	M_{By} kip-ft (kN-m)
	126.3 (562)	9890 (13,410)	261 (1161)	41,300 (56,000)
EOG50	V_{Mx} kips (kN)	M_{My} kip-ft (kN-m)	V_{Bx} kips (kN)	M_{By} kip-ft (kN-m)
	21.1 (93.9)	1650 (2240)	43.6 (193.9)	6900 (9360)

Note: The subscripts "M" and "B" represent tower midheight and base, respectively.

The self-weight of the UHPC tower (including steel post-tensioning tendons) is 866 kips (3850 kN). The fatigue loads on the tower remain the same as with previous designs, and are listed in Table 3-4.

4.2.2 Design

As with the steel and concrete designs, the design of the UHPC Shell tower was done using an iterative, spreadsheet driven process as detailed below. It is designed as a grouted post-tensioned tower, utilizing 0.6-in. (15 mm) diameter strands with 270 ksi (1860 MPa) ultimate tensile strength. The semi-vertex angle (wall slope) of the tower was varied at 110 ft (33.5 m) and 220 ft (67.1 m). As with the concrete tower design, post-tensioning was staged, and cut-off/anchor points coincide with the changes in semi-vertex angle. The results of the UHPC shell design are summarized in Table 4-2.

The design methodology for the UHPC Shell tower is similar to that used in the design of the regular strength concrete tower. To initially size the tower, zero tension stress was allowed to develop due to flexural action, while the compressive stress was limited to $0.53f_c'$, as was done with the 322 ft (98.2 m) concrete tower in Section 3.3.2. Equations (3-5) and (3-6) were modified, using the net area instead of the transformed area, and were used to evaluate this criteria. This approach was deemed necessary because of the mismatch in strength between UHPC strength (26 ksi [1860 MPa]) and typical grout (10 ksi [68.9 MPa]) that is used in

bonded post-tensioning. The governing load wind speed was EWM50, with Equation (2-11) as the governing load case.

Table 4-2: Summary of the 322 ft (98.2 m) Tall UHPC Shell Tower for a 3 MW Turbine

Compressive Strength, ksi (MPa)	26 (179.3)
Post-tensioning Effective Stress, ksi (MPa)	180 (1241)
Diameter at Base, in. (m)	270 (6.86)
Shell Thickness from 0-110 ft (0-33.5 m), in. (mm)	4.25 (108.0)
Number of 0.6-in. (15 mm) diameter tendons, 0-110 ft	121 (4-strand bundle)
Diameter at 110ft (33.5 m), in. (m)	213 (5.41)
Shell Thickness from 110-220 ft, in. (mm)	3.865 (98.2)
Number of 0.6-in (15 mm) diameter tendons, 110-220 ft (33.5-67.1 m)	93 (4-strand bundle)
Diameter at 220 ft (67.1 m), in. (m)	166.5 (4.23)
Shell Thickness from 220-322 ft (67.1-98.2 m), in. (mm)	3.25 (82.6)
Number of 0.6-in (15 mm) diameter tendons, 220-322 ft (67.1-98.2 m)	60 (4-strand bundle)
Diameter at 322 ft (98.2 m), in. (m)	132 (3.35)
UHPC Volume, yd^3 (m^3)	183 (139.9)
Tower Weight, kips (kN)	866 (3850)
Fundamental Natural Frequency of Tower, Hz	0.372

Service-Level Moment Capacity

The service level moment capacity at the base was 127,100 kip-ft (172,300 kN-m), with calculated demand of 124,200 kip-ft (168,400 kN-m). At the tower top, the moment capacity was determined to be 31,100 kip-ft (42,200 kN-m), with a calculated demand of 9,490 kip-ft (12,870 kN-m). As with the prestressed concrete design, a B_2 factor was calculated using Equation (3-3) to account for the P-Δ effects. Equation (2-101) was used to calculate a buckling strength for the UHPC Shell tower, resulting in $P_e = 24,200$ kips (107,700 kN). The B_2 ranged from 1.025 at the tower top to 1.071 at the tower base. This factor has already been included with the previously stated moment demand. Service-level moment capacity versus demand along the height of the tower, which was obtained through the evaluation of Equation (3-5), is presented in Figure 4.1. Stress limits along the height of the tower, described by Equation (3-6), can be seen in Figure 4.2. The sudden increase in capacity in

Figure 4.1 and sudden decrease in stress levels observed in Figure 4.2 are due to the decrease in post-tensioning force at the height of 110 ft (33.5 m) and 220 ft (67.1 m). Moment capacity is sharply reduced at these points due to reduction of prestressing force, while compressive stress drops due to the reduction of unnecessary post-tensioning ducts and an increase in net area. In general, these two limits govern the overall dimensions of the tower. However, it can be seen for the upper-third of the tower that the compressive stresses in the tower diverge from the limit, which is due to shear strength governing this portion of the tower. This is discussed further later in this section.
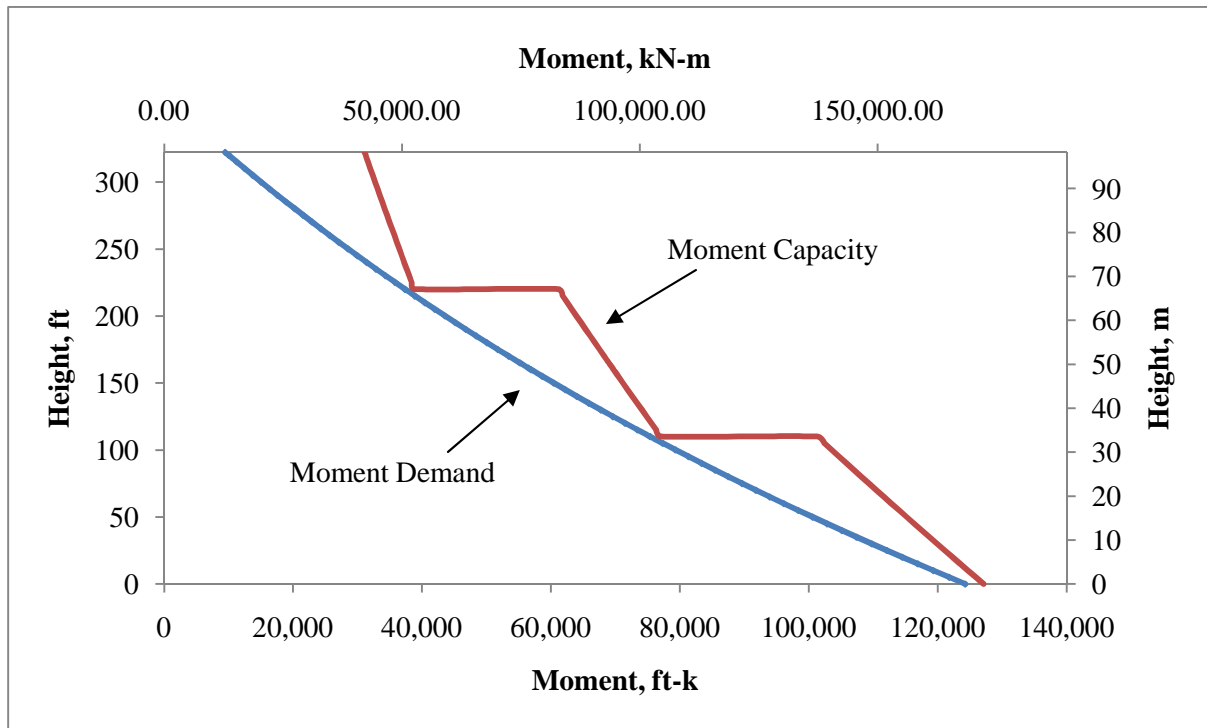
Figure 4.1: Comparison of Service-Level Moment Capacity and Demand for the 322 ft (98.2 m) UHPC Shell Tower Design as per Equation (3-5)
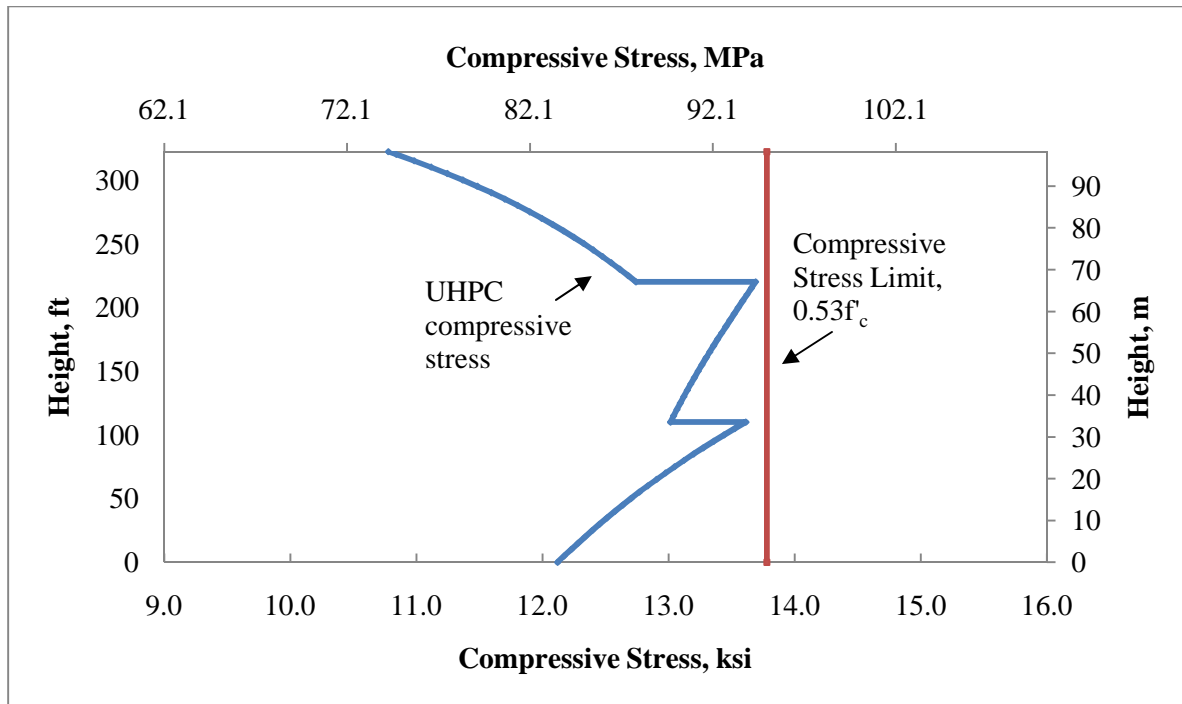
Figure 4.2: Comparison of Compressive Stress Demand against the Allowable Stress Limit for the 322 ft (98.2 m) UHPC Shell Tower Design as per Equation (3-6)

Ultimate Moment Capacity

The ultimate moment capacity of the tower was calculated at critical points along the tower height, in a similar manner as presented in Section 3.3.2 for the concrete shell design. The same stress-strain model was used for the post-tensioning tendons. The stress-strain behavior of the UHPC was modeled as shown in Figure 2.4. At the ultimate limit state, the tensile strength of the UHPC was conservatively ignored. In all cases, the ultimate moment capacity was shown to be higher than the factored-level moment demand including P-Δ effects. At the tower base, the ultimate moment capacity was 238,000 ft-kip (323,000 kN-m) while the demand was calculated as 176,700 ft-kip (240,000 kN-m). At the tower top, the ultimate moment capacity was determined to be 50,400 ft-kip (68,300 kN-m), a calculated demand of 12,800 ft-kip (17,350 kN-m).

Service-Level and Ultimate Shear Capacity

Shear capacity of the tower was checked at both serviceability and ultimate limit states along the tower height. At the service level state, the tower was checked for cracking caused by a combination of shear force and torsional moment. A modified version of Equation (2-94) was used to verify shear service level capacity as shown below:

$$\sqrt{\left(\frac{f_{pc}}{2}\right)^2 + (\tau)^2} - \frac{f_{pc}}{2} \leq f_{t,cracking}$$

(4-1)

where f_{pc} = axial stress at the centroid due to prestressing;

τ = service-level shear stress; and

$f_{t,cracking}$ = 1.3 ksi (8.96 MPa), and is the cracking tensile strength of UHPC (Bristow & Sritharan, To be published)

For the UHPC Shell design, the combination of shear and torsion at the service-level never overcome the cracking strength of UHPC. The most critical combination occurs at the tower top, with a principal stress value of only 0.0981 ksi (0.676 MPa). As this value is much lower than the capacity, shear cracking at service levels should not be of concern.

The ultimate shear capacity was checked based on the AFGC criteria (Association Française de Génie Civil/SETRA, 2002, Equations (2-88) and (2-89). Based on the recommendations from JGC No. 9 (2006), the crack width angle, β, was limited to a minimum of 30 degrees. The most critical location for shear demand versus capacity is at the tower top. However, the demand to capacity ratio (DCR) at this location is only 0.20, corresponding to a calculated capacity of 1657 kips (7370 kN) and a demand of 324 kips (1441 kN). It should be noted that the steel fiber shear resistance provides more than 6 times as much capacity as the pure concrete shear resistance. The shear area for Equations (2-88) and (2-89) was taken as $0.8A_{net}$.

Ultimate Torsional Moment Capacity

The torsion capacity at the ultimate limit state, as well as shear and torsion interaction was checked in accordance with Equation (2-91). The strength reduction factor for torsion, ϕ, was set to the value of 0.7 (Gowripalan & Gilbert, 2000). As with shear strength, the critical section for torsion is at the tower top. This should be expected, as the torsional moment is constant along the height of the tower. At the tower top, the DCR for torsion is 0.55, well below 1.0. This corresponds to a torsional moment capacity of 9,680 kip-ft (13,120 kN-m) and a demand of 5310 kip-ft (7200 kN-m).

Torsion and Shear Interaction

Although neither shear nor torsion govern the design individually, the interaction of the two becomes critical for the top-third of the tower. When Equation (2-92) is evaluated, it is critical at the tower top, reaching a value of 0.745 versus an allowed value of 0.75. The top-third tower diameter and wall thickness were governed by this limit state. Lewin and Sritharan (2010) evaluated the effect of using the shear area for hollow structural sections as suggested by Cheng et al. (2003) and described by Equation (3-15). This resulted in a shear area of approximately $0.51 A_{gross}$. However, when a more realistic value for UHPC tensile cracking strength was used in Equation (2-91), i.e., 1.3 ksi (8.96 MPa), the current UHPC Shell tower design satisfied the torsion and shear interaction limit state.

Fatigue

As with the concrete tower, both the UHPC and steel post-tensioning tendons were checked for fatigue loading. Recommendations from JGC No. 9 (2006) were followed to evaluate the UHPC fatigue resistance (Equation (2-93)). The allowable stress range for the concrete, given a design life of 5.29×10^8 cycles, was found to be 6.37 ksi (57.1 MPa). The largest calculated stress range in the tower was only 0.726 ksi (5.01 MPa), occurring at an elevation of 220 ft (67.1 m). The MC90 (Comite Euro-International Du Beton, 1990) was used to evaluate the fatigue resistance of the post-tensioning steel. Using Equation (2-65), the allowable stress range was determined to be 10.05 ksi (69.3 MPa). The largest stress range calculated in the steel was 2.78 ksi (19.17 MPa), also occurring at 220 ft (67.1 m).

<u>Dynamic Properties</u>

The calculated natural frequency of the tower was 0.372 Hz, well within the working range for a 3.0 MW turbine. Additionally, the critical wind speed for vortex shedding was calculated as 18.62 mph (5.67 m/s), falling below the EOG50 design wind speed range of 33.3-86.66 mph (14.89-38.7 m/s). Therefore, vortex shedding will not be of concern for the 322 ft (98.2 m) UHPC Shell tower.

<u>Deflection</u>

Lateral deflection was calculated for the UHPC Shell at service-level EWM50 wind speeds to be 55.18 in. (1.402 m) at the tower top corresponding to 1.427% drift.

4.2.3 *Discussion*

The results for the UHPC Shell Tower yielded a design that uses only 31.9 % of the material used in a regular strength concrete design. While this represents a more efficient use of resources, it also implies drastically reduced transportation and construction costs. The UHPC Shell tower's weight is very close to that of a steel tower: 866 kips (3850 kN) vs. 739 kips (3290 kN), respectively.

Fatigue is never the governing limit state for the design of the UHPC shell. The UHPC Shell tower's fatigue is 5.63×10^{13} cycles, much greater than that of the wind turbine itself, and is controlled by the fatigue of the steel tendons. This long fatigue life would allow the tower to outlast the typical turbine 20 year design life, implying the tower could be used with multiple turbines over its life cycle.

As noted previously, shear and torsion interaction governs the upper portion of the tower design. This is due to the material's excellent compressive strength, which allows for slender sections with high flexural resistance. However, as shear resistance is related to the square root of compressive strength, it was not unexpected that the shear becomes critical. This is not observed in the concrete tower, as larger wall thicknesses are necessary for moment resistance.

The natural frequency of the UHPC shell tower, 0.372 Hz, was well within the working frequency range for a 3 MW turbine, validating the assumed turbine loading.

The UHPC Shell deflection significantly exceeds the limits laid out by ACI 307 (1998), lying somewhere between the 322 ft (98.2 m) steel and concrete tower deflections. At 1.427% drift, its deflections are 1.53 and 2.78 times as large as BergerABAM's (LaNier, 2005) 3.6 MW steel and concrete towers, respectively. This would suggest that the UHPC Shell tower design would have to be refined if the turbine manufacturer required a small deflection for the tower, most likely increasing its base diameter and the volume of UHPC and prestressing steel.

4.3   UHPC Lattice Tower

The UHPC Lattice Tower is an investigation into a potentially more efficient use of UHPC while limiting lateral tower deflection and improving its constructability. While the UHPC Shell design represents a direct conversion of current steel and concrete designs, the Lattice Tower is a significant departure from standard practice. The value in examining this concept lies within the potential savings in materials, transportation, and erection costs.

The general concept of the Lattice Tower is to concentrate the UHPC into six columns. These columns utilize unbonded post-tensioning, and are tied together intermittently using bracing. If sufficiently braced, the columns will act compositely, and resist lateral loads as a whole. Depending on the direction of loading, half of the columns will generally be subjected only to tension, while the others experience compression. As long as these members do not act independently of each other, they can remain relatively slender. A conceptual rendering of the Lattice Tower concept is shown in Figure 4.3. While this rendering depcits the tower with only horizontal bracing members, multiple options exist for bracing the UHPC columns. An open-air concept would combine the horizontal bracing members shown in Figure 4.3 with diagonal cross bracing. The horizontal and cross bracing could consist of concrete, steel, or even UHPC members. For aesthetic reasons, the tower could then be wrappped in a structural fabric, giving it the appearance of typical wind turbine towers seen today. Alternatively, thin concrete or UHPC panels could span between the columns, connected intermittently through the use of pinned connections. A rendering of this concept can be seen in Figure 4.4.

Figure 4.3: A View of the Lattice Tower with Horizontal Bracing

Figure 4.4: A View of the Lattice Tower with Concrete Panel Bracing

4.3.1 Loading

Although multiple bracing options are available for the UHPC Lattice tower, this design focused on the use of horizontal bracing and diagonal cross bracing, rather than concrete panels. As such, the tower face is partially open, allowing some wind to pass though. This is one area where the loading on the tower significantly differs from the loading on the previously discussed designs. However, as this design is less common, the direct wind load on the tower is less well-defined. To determine this loading, the ASCE 7 (Structural Engineering Institute, 2005) was utilized in the following manner. The design has the same assumed environment as the steel, concrete, and UHPC Shell tower designs, and therefore the gust effect factor and velocity pressure were calculated as previously. However, the force coefficient, C_f, was significantly different for an open-air design versus a smooth shell. To calculate this coefficient for the Lattice design, it was judged that the provisions included for

"Trussed Towers" (Structural Engineering Institute, 2005) were the most appropriate, for which the following equations are provided by the standard:

$$C_f = 4.0\epsilon^2 - 5.9\epsilon + 4.0 \text{ for Square Tower Sections} \tag{4-2}$$

$$C_f = 3.4\epsilon^2 - 4.7\epsilon + 3.4 \text{ for Triangular Tower Sections} \tag{4-3}$$

where ϵ = ratio of solid area to gross area for the projected tower face.

If the members are rounded, the force coefficient can be multiplied by:

$$\psi_{round} = 0.51\epsilon^2 + 0.57 \le 1.0 \tag{4-4}$$

Since the tower Lattice tower cross section is roughly circular, the average of Equations (4-2) and (4-3) was used to calculate the force coefficients. A solidity ratio of 0.578 was calculated, yielding C_f = 1.926 and 1.819, for Equations (4-3) and (4-4), respectively. All members in the UHPC Lattice tower have a round cross section, and were multiplied by ψ_{round}, which was calculated as 0.740. Therefore, the resultant C_f was calculated as 1.386. This value is applicable for all portions of the tower. The details and design process of the UHPC Lattice tower column members are given later in this chapter and the details regarding the bracing and cross bracing members are given in Chapter 5. The direct wind forces resulting from this C_f on the UHPC Lattice Tower can be seen in Table 4-3.

Table 4-3: Estimated Direct Wind Force Loads at Midheight and Base of the 322 ft (98.2 m) UHPC Lattice Tower at Service-Level

	V_{Mx} kip (kN)	M_{My} ft-k (kN-m)	V_{Bx} kip (kN)	M_{By} ft-k (kN-m)
EWM50	158.2-198.0 (704-881)	12,630-15,730 (17,120-21,300)	310-389 (1379-1730)	51,100-64,000 (69,300-86,800)
	V_{Mx} kip (kN)	M_{My} ft-k (kN-m)	V_{Bx} kip (kN)	M_{By} ft-k (kN-m)
EOG50	27.4-34.3 (121.9-152.6)	2180-2720 (2960-3690)	53.8-67.6 (239-301)	8860-11,090 (12,010-15,040)

Note: The subscripts "M" and "B" represent tower midheight and base, respectively.

The range in Table 4-3 is present because the projected face of the tower changes with the orientation of loading. The two loading orientations considered are defined by Figure 4.5 and Figure 4.6. The larger load in Table 4-3 corresponds to the 0-Degree loading orientation.

The tower top loads for the Lattice design will be similar to the previously discussed designs, if it is assumed to have a similar natural frequency. Turbine lateral, axial, and fatigue loads can be found in Table 3-1, Table 3-2, and Table 3-3, respectively. The self-weight of the UHPC Lattice Tower 1227 was calculated as 1123 kips (5000 kN) based on the design presented in the following section, including the bracing.
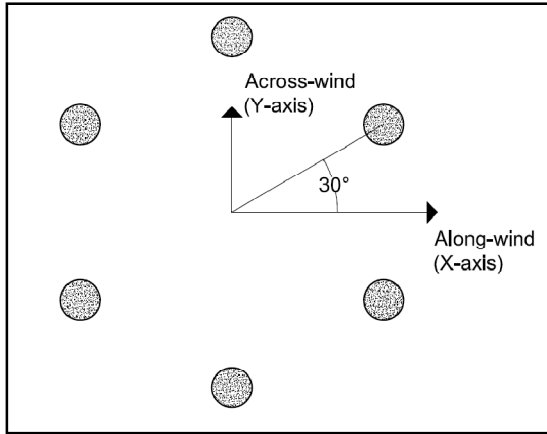
Figure 4.5: 0-Degree Loading Orientation
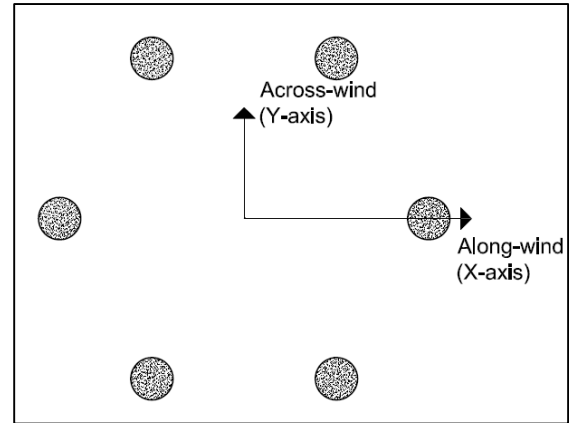
Figure 4.6: 30-Degree Loading Orientation

4.3.2   Design

As previously mentioned, the design of the UHPC Lattice tower was based on the assumption of composite section behavior. The underlying principle of this assumption is that linear strain variation exists across the entire tower cross section. Using this assumption, the columns were designed to handle the combined axial and bending stresses caused by the wind and dead loads. This resulted in a preliminary tower design, which was verified using finite element analysis, as described in Chapter 5. The resulting tower dimensions and properties can be seen in Table 4-4. For the Lattice tower design, the overall section diameter, D, and individual column diameters, d_{col}, are tapered, with their respective semi-vertex angle changing at 110 ft (33.5 m) and 220 ft (67.1 m). It should be noted that the overall section diameter refers to two times the distance from the centroid of the section to the centroid of the outermost column. Sketches of the tower cross section are presented in

Figure 4.7 through Figure 4.10. In order to take advantage of UHPC's high compressive strength, each column was designed with unbonded post-tensioning tendons running through embedded ducts along the entire tower length. A portion of these tendons are terminated at 110 ft (33.5 m) and 220 ft (67 m) in order to increase the economy of the tower. A detailed drawing of an individual column is shown in Figure 4.11. The use of unbonded reinforcement was chosen for the UHPC Lattice tower in order to allow the tower to be disassembled, moved, and reassembled at another location were the environmental conditions, i.e., wind speed, surrounding the tower to change over its design life. The UHPC Lattice tower is more suited to this concept than the concrete and UHPC Shell towers due to its small member sizes. Another advantage of unbonded post-tensioning is the elimination of concentrated steel stresses. Since the steel stress is distributed along the entire tower length, it is expected that even in an ultimate load condition, the post-tensioning steel will not yield. Since it remains elastic, the post-tensioning steel will then restore the tower to its original position when the ultimate load is removed. The numbers listed in Table 4-4 are for the entire tower and are split between the six UHPC columns.

Table 4-4: Dimensions and Properties for the 322 ft (98.2 m) UHPC Lattice Tower for a 3 MW Turbine

Compressive Strength, ksi (MPa)	26 (179.3)
Post-tensioning Effective Stress, ksi (MPa)	180 (1241)
Overall Diameter, D, at Base, in. (m)	354 (8.99)
Column Diameter, d_{col}, at Base, in. (mm)	26.625 (676)
Number of 0.6-in diameter strands, 0-110 ft (0-33.5 m)	486
Overall Diameter, D, at 110 ft (33.5 m), in. (m)	294 (7.47)
Column Diameter, d_{col}, at at 110 ft (33.5 m), in. (mm)	24.625 (625)
Number of 0.6-in diameters strands, 110-220 ft (33.5-67.1 m)	342
Overall Diameter, D, at 220 ft (67.1 m) , in. (m)	246 (6.25)
Column Diameter, d_{col}, at 220 ft (67.1 m), in. (mm)	19.75 (502)
Number of 0.6-in diameter strands, 220-322ft (67.1-98.2 m)	198
Overall Diameter, D, at 322 ft (98.2 m), in. (m)	120 (3.05)
Column Diameter, d_{col}, at 322ft (98.2 m), in. (m)	14.875 (378)
UHPC Volume, Columns Only, yd^3 (m^3)	173 (132.4)
Tower Weight, kips (kN)	1120 (4980)
Fundamental Tower Natural Frequency, Hz	0.495

Furthermore, the tendons are separated into groups, based on cut-off requirements. From 0-110 ft (0-33.5 m), each column has four 12-strand tendons, and a 33-strand tendon. From 110-220 ft (33.5–67 m), each column has two 12-strand tendons, and a 33-strand tendon. Finally, from 220-322 ft (67-98.2 m), each column has a single 33-strand tendon. For illustration, the tendon layout at the tower base can be seen in Figure 4.11.

The bracing used for this design consisted of rounded members, with the height of cross bracing equal to 13 in. (330.2 mm) and the height of the horizontal bracing equal to 9 in. (228.6 mm). The design of these members is presented in Chapter 5.

D = 354 in. (8.99 m)
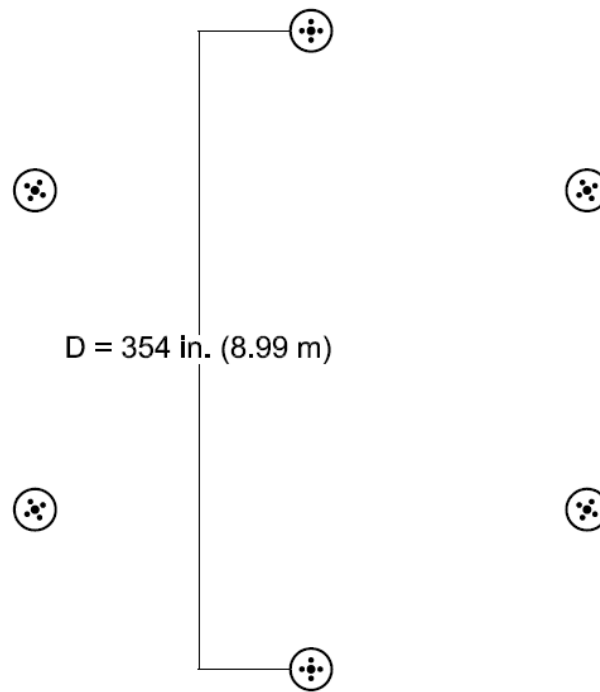
Figure 4.7: Cross Section of the UHPC Lattice Tower at the Base
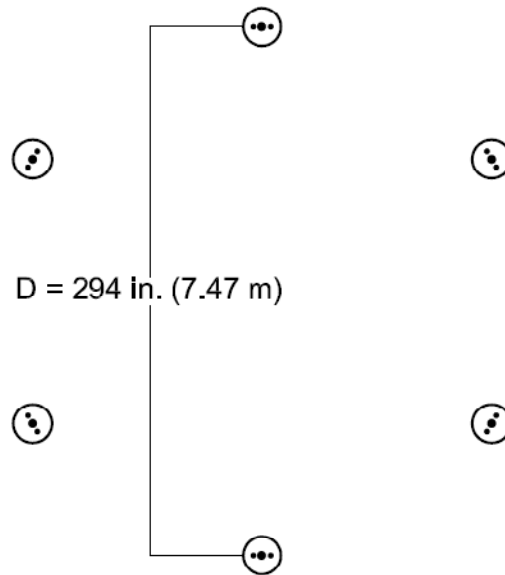
Figure 4.8: Cross Section of the UHPC Lattice Tower at 110 ft (33.5 m) after Post-tensioning Tendon Termination
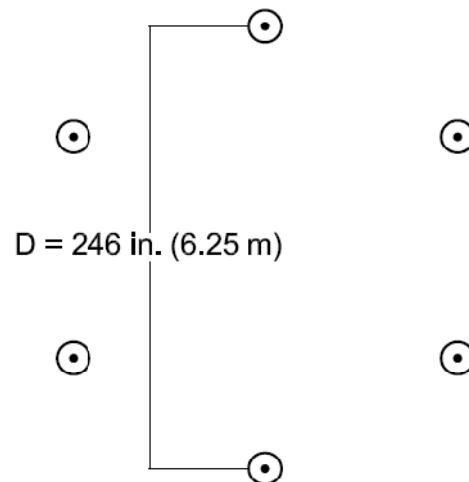
Figure 4.9: Cross Section of the UHPC Lattice Tower at 220 ft (67.1 m) after Post-tensioning Tendon Termination
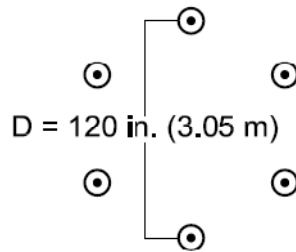
Figure 4.10: Cross Section of the UHPC Lattice Tower at Tower Top
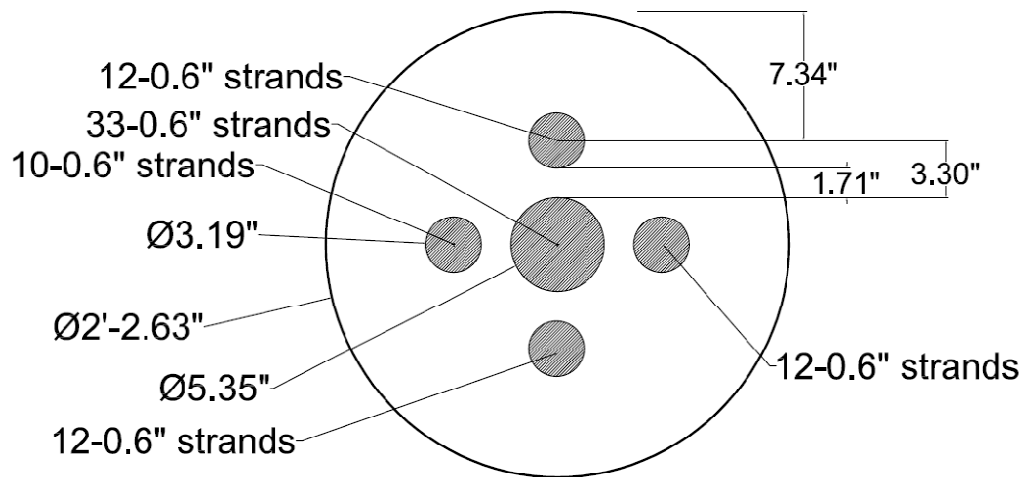
Figure 4.11: A Typical Column Cross Section/Tendon Layout at the Base of the UHPC Lattice Tower

Service-Level Moment Capacity

As with the concrete tower design, Equations (3-5) and (3-6) governed the UHPC Lattice column dimensions. However, depending on the wind loading direction, as illustrated in Figure 4.5 and Figure 4.6, the magnitude of the load as well as the elastic section modulus of the tower varied. In the preliminary design, the 0-degree loading orientation provided the most critical case. This is because the projected face of the tower is larger in this orientation, so it provided more area for the wind to act on. It should be noted that although the wind can be assumed to be blowing along a fixed-axis, either 0-degrees or 30-degrees, the axis of

bending actually depends on the combination of along-wind direct wind forces, along-wind turbine forces, and across-wind turbine forces. When the moments were combined as vectors, the tower bent about a rotated axis. The angle of that axis's rotation, as measured from the Y-axis is given in Equation (4-5):

$$\theta_B = \tan^{-1}\left(\frac{M_x}{M_y}\right)$$

(4-5)

where M_x = moment about the x-axis, caused by across-wind loading; and

M_y = moment about the y-axis, caused by along-wind loading.

This is only valid because the tower has the same moment of inertia in all directions, and therefore has a zero mixed moment for all orientations.

As with all previous designs, the EWM50 wind speed dominated the design. The moment capacity and demand is plotted in Figure 4.12 and Figure 4.9. The compressive stresses along the tower height are plotted in Figure 4.13 and Figure 4.10. The sharp discontinuities in moment capacity correspond to the location of post-tensioning cut-off. Likewise, the sharp discontinuities is compressive stress correspond to the location where post-tensioning ducts are removed, and net area is increased. In the 0-Degree loading orientation, using Equation (3-2), the base of the tower has a calculated service-level moment capacity of 141,700 kip-ft (192,100 kN-m) with a required demand of 134,600 kip-ft (182,500 kN-m). In the 30-Degree loading orientation, the tower has a base moment capacity of 155,900 kip-ft (211,400 kN-m) and a moment demand of 123,800 kip-ft (167,800 kN-m). It should be noted that a B_2 factor was not included in the preliminary analysis of the UHPC Lattice Tower. The reasoning behind this is that a large displacement finite element analysis would later be performed (detailed in Chapter 5) to validate the initial design assumptions. Since B_2 is an estimate, it was felt the finite element analysis would more accurately quantify the P-Δ effects of the loading.
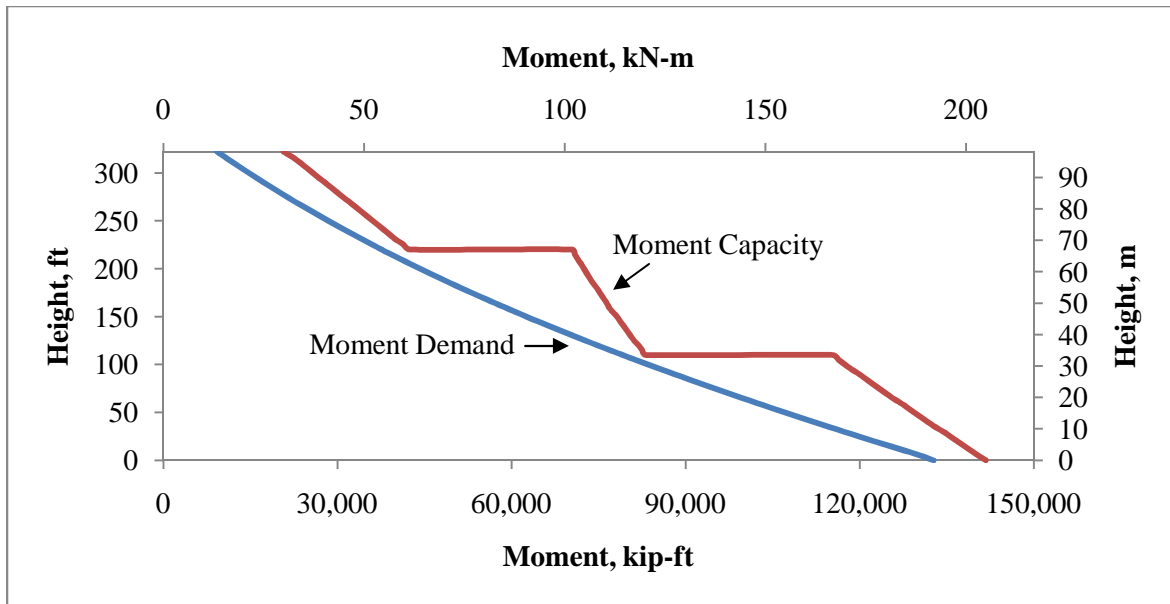
Figure 4.12: Comparison of Service-Level Moment Capacity and Demand for the 322 ft (98.2 m) UHPC Lattice Tower in the 0-Degree Loading as per Equation (3-5)
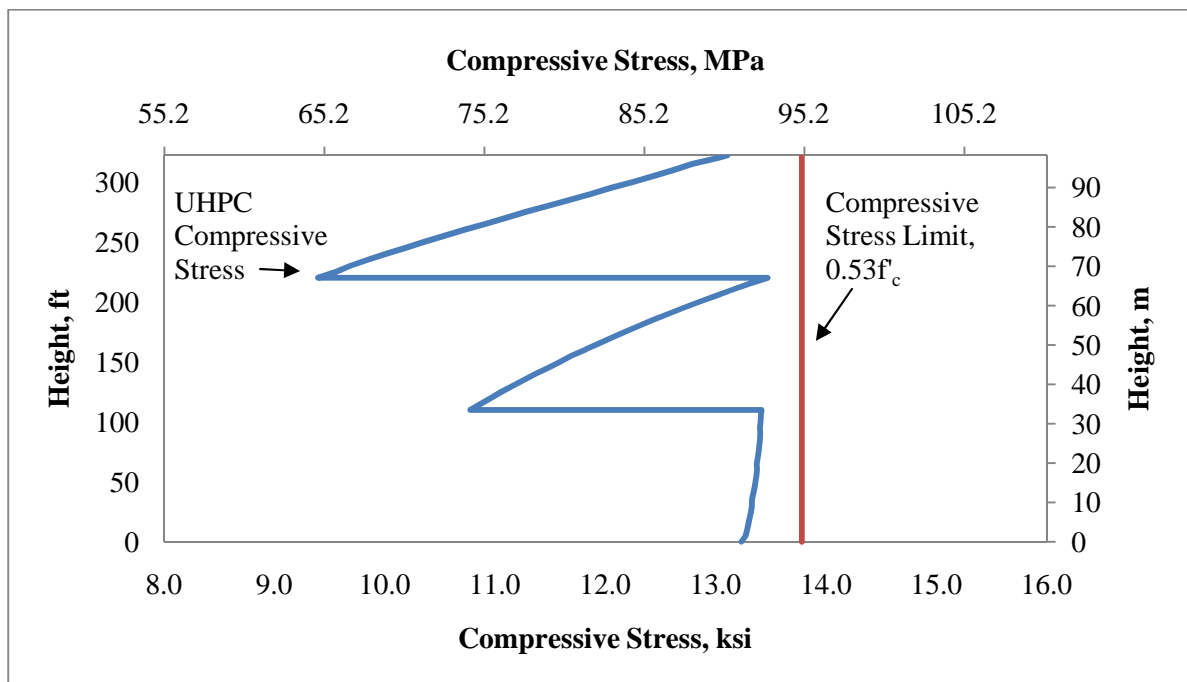
Figure 4.13: Comparison of Compressive Stress Demand Against the Allowable Stress Limit for the 322 ft (98.2 m) UHPC Lattice Tower in the 0-Degree Loading as per Equation (3-6)
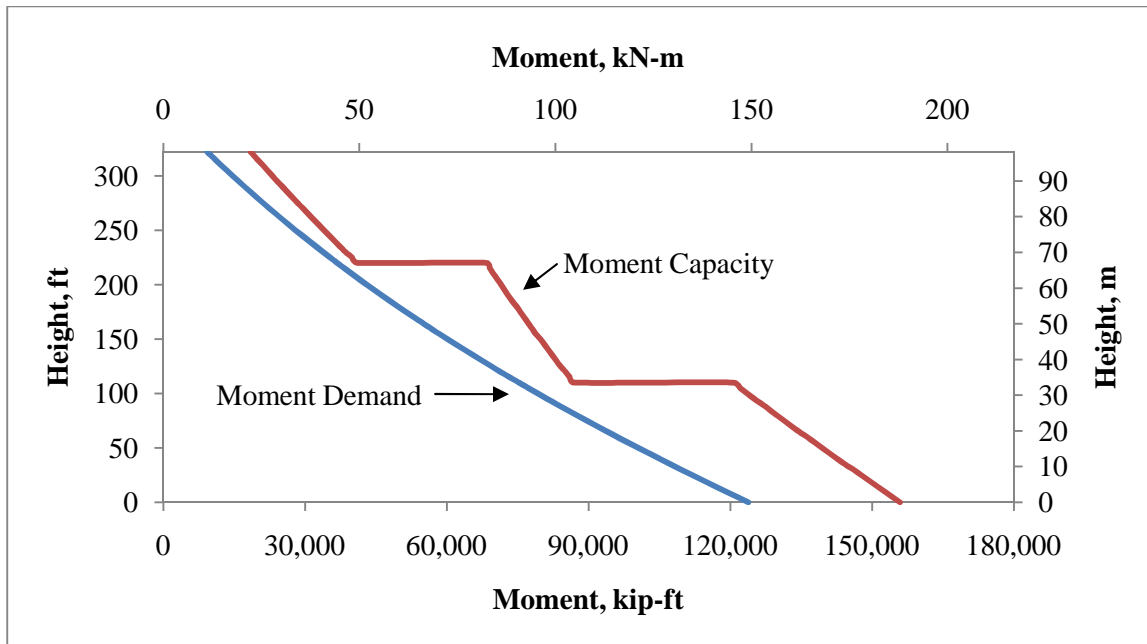
Figure 4.14: Comparison of Service-Level Moment Capacity and Demand for the 322 ft (98.2 m) UHPC Lattice Tower in the 30-Degree Loading as per Equation (3-5)
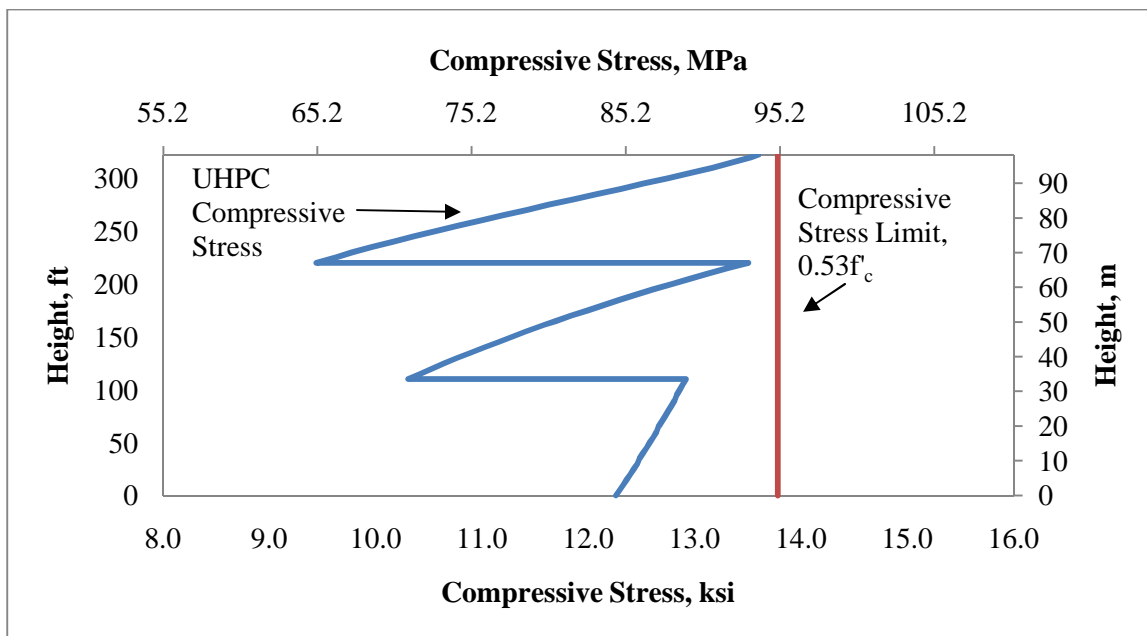

Figure 4.15: Comparison of Compressive Stress Demand Against the Allowable Stress Limit for the 322 ft (98.2 m) UHPC Lattice Tower in the 30-Degree Loading as per Equation (3-6)

Ultimate Moment Capacity

Estimating the ultimate moment capacity of the tower presented a unique challenge. Since the UHPC Lattice Tower does not use bonded post-tensioning, a strain compatibility approach could not be used. Without strain compatibility, it was not possible to calculate ultimate moment capacity using only section-level details, since unbonded post-tensioning allows steel strain to be averaged along the entire tower height. Consequently, it was necessary to consider the entire tower's behavior. If the tower's top displacement is known and the deformation along the tower height is assumed to be elastic, the total tendon elongation due to bending can be calculated. The assumption of elastic deformation is appropriate if the tension columns of the tower are allowed to uplift at the base (i.e., only the tendons at the base can sustain a tension force). By uplifting, the tower is able to concentrate the majority of its flexural cracking at the base, causing a concentrated rotation. Additionally, the tower has joints at 110 ft (33.5 m) and 220 ft (67.1 m) which are allowed to open when the tower is decompressed. However, this will only happen under an ultimate load condition. Therefore, the total tendon elongation is the sum of that due to bending and that due to rotation at the base, 110 ft (33.5 m), and 220 ft (67.1 m). This is elucidated in Figure 4.16, which shows a generic tower for illustration purposes. In the figure, a lateral force is applied to the tower. The total tower response is the combination of flexural action and rotation at the joints.

The procedure followed, which is detailed in the following pages, required iteration. The actual ultimate base moment can be defined several ways through this procedure. As with the ultimate strength calculations for the Concrete and UHPC Shell Towers, ultimate strength is reached when either concrete crushes or steel reinforcement fractures. However, a target maximum drift can also be used to define the ultimate limit state (if concrete crushing or steel fracture has not first occurred). It should also be noted that the post-tensioning in the UHPC Lattice tower was staged, with cut-offs points at 110 ft (33.5 m) and 220 ft (67.1 m). This is significant because the post-tensioning that is cut-off at 110 ft (33.5 m) will have a different average stress than the post-tensioning that runs from the base of the tower to the tower top.
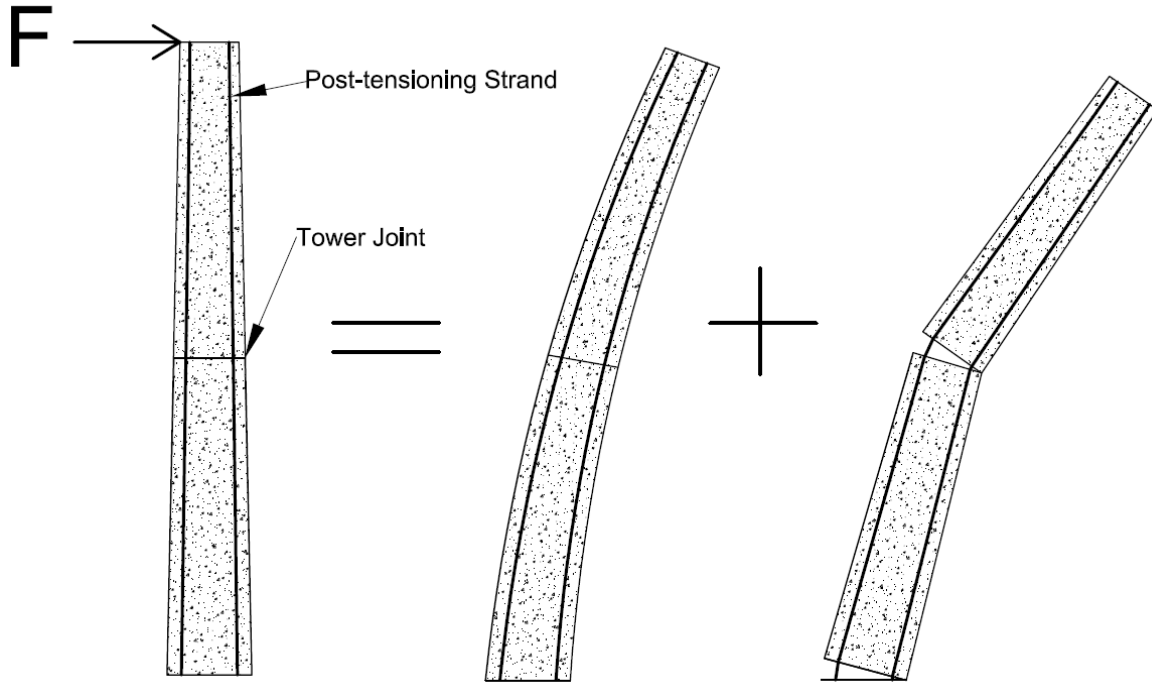
Figure 4.16: An Illustration of an Unbonded Post-tensioned Tower Subjected to a Lateral Load

The procedure to calculate the ultimate base moment capacity is as follows:

1) Choose a base rotation, θ.

2) Assume a base ultimate moment, M_{base}. This moment should be greater than the decompression moment for the tower base.

3) Assume the neutral axis depth at the base, c_{NA}. The neutral axis depth should be less than the tower base diameter.

4) Calculate the initial strain in the tendons due to prestressing:

$$\varepsilon_{pe} = \frac{f_{pe}}{E_{steel}}$$

(4-6)

where f_{pe} = effective post-tensioning stress; and

E_{steel} = elastic modulus of steel.

5) Using an assumed moment distribution along the tower height, calculate the lateral tower deflection due to flexure from Equation (4-7):

$$\Delta_{flex} = \int_0^{z_1} \frac{M(z)(z_1 - z)}{E_{UHPC}I_{tower}(z)} dz \tag{4-7}$$

where $M(z)$ = an assumed moment distribution corresponding to the base ultimate moment, M_{base};

   E_{UHPC} = elastic modulus of UHPC;

   $I_{tower}(z)$ = distributed tower moment of inertia;

   z_1 = elevation at which deflection is desired; and

   z = height.

6) Calculate the estimated additional elongation in each tendon to due elastic flexure:

$$\delta_{b,i} = \int_0^{L_{tendon,i}} \frac{M(z)}{E_{UHPC}I_{tower}(z)} d_{tendon,i} dz \tag{4-8}$$

where $d_{tendon,i}$ = distance from the tendon centroid to the tower centroid; and

   $L_{tendon,i}$ = total tendon length.

It should be noted that in any given column, each stage of post-tensioning will have a different length, and therefore a different elongation and stress. Additionally, Equation (4-8) will result in a positive elongation in the tension columns, and a negative elongation in compression columns, corresponding to an increase in length and a decrease in length, respectively.

7) Calculate the elongation in each tendon due to the base rotation:

$$\delta_{\theta,i} = \theta l_{tendon,i} \tag{4-9}$$

where $l_{tendon,i}$ = distance from the tendon centroid to the neutral axis depth at the base, c_{NA}.

8) Calculate the average tendon strain due to flexure and rotation:

$$\varepsilon_{\Delta,i} = \frac{\delta_{b,i} + \delta_{\theta,i}}{L_{tendon,i}} \tag{4-10}$$

9) Calculate the total strain in each tendon

$$\varepsilon_{ps,i} = \varepsilon_{pe} + \varepsilon_{\Delta,i} \tag{4-11}$$

10) Calculate the stress in each tendon, $f_{t,i}$, according to Equations (3-8) and (3-9).

11) Calculate the force in each tendon, t_i.

12) Calculate the concrete strain at the outermost compression fiber using a modified version of monolithic beam analogy (Thomas & Sritharan, 2004; Pampanin, Priestly, & Sritharan, 2001):

$$\varepsilon_{max} = c_{NA}\left(\frac{\theta}{L_p} + \frac{\psi_{decomp}M_{base}}{E_{UHPC}I_{tower,base}}\right) \tag{4-12}$$

where

$$L_p = 0.06h \tag{4-13}$$

and $I_{tower,base}$ = tower moment of inertia at the base;

h = total tower height; and

ψ_{decomp} = factor accounting for decompression, which is described in the discussion following this process description.

13) Calculate the compression strain at the center of each column location, $\varepsilon_{c,j}$, assuming a linear strain profile at the tower base.

14) Calculate the average compressive stress in each column, $f_{c,j}$, using the stress-strain model in Figure 2.4.

15) Calculate the compressive force, c_j, in each column.

16) Evaluate the equilibrium condition from Equation (4-14):

$$\sum_{1}^{6} c_j - \sum_{1}^{n} t_i = P_u \tag{4-14}$$

where P_u = factored-level axial load in the tower at the base;

n = total number of tendons; and

17) Calculate the base moment by summing the moment about the section centroid, using Equation (4-15):

$$M_n = \sum_1^n (c_i \times d_{ci}) + \sum_1^m (t_j \times d_{tj})$$

<div align="right">(4-15)</div>

18) If Equation (4-14) results in a negative value, c_{NA} should be increased. If $M_{base} \neq M_n$, M_{base} should be revised to more closely match M_n. If either condition does not hold, revise c_{NA} and/or M_{base}, and restart the procedure.

For step 5), it was necessary to use an assumed moment distribution along the tower. It can be seen from Figure 4.1 that the required moment distribution on the tower is approximately linear. However, it was judged that is was more accurate to approximate the moment demand with a tri-linear relationship. Therefore, the assumed moment profile for the 0-degree load orientation was:

$$M(z) = \begin{cases} M_{base,guess} - \dfrac{(M_{base} - 0.577M_{base})}{h_1} \cdot z \text{ if } 0 \leq z < h_1 \\[2mm] 0.577M_{base,guess} - \dfrac{(0.577M_{base} - 0.265M_{base})}{h_2 - h_1} \cdot z \text{ if } h_1 \leq z < h_2 \\[2mm] 0.265M_{base,guess} - \dfrac{(0.269M_{base} - 0.0639M_{base})}{h_3 - h_2} \cdot z \text{ if } h_2 \leq z < h_3 \end{cases}$$

<div align="right">(4-16)</div>

The assumed moment profile for the 30-degree loading orientation was:

<div align="right">(4-17)</div>

$$M(z) = \begin{cases} M_{base,guess} - \dfrac{(M_{base} - 0.595M_{base})}{h_1} \cdot z \text{ if } 0 \leq z < h_1 \\[2mm] 0.595M_{base,guess} - \dfrac{(0.595M_{base} - 0.284M_{base})}{h_2 - h_1} \cdot z \text{ if } h_1 \leq z < h_2 \\[2mm] 0.284M_{base,guess} - \dfrac{(0.284M_{base} - 0.0703M_{base})}{h_3 - h_2} \cdot z \text{ if } h_2 \leq z < h_3 \end{cases}$$

where $h_1 = 110$ ft (33.5 m);

$h_2 = 220$ ft (67.1 m); and

$h_3 = 322.2$ ft (98.2 m).

ψ_{decomp} in Equation (4-12) was calculated so that equilibrium was achieved at the point of tower base decompression. This was done by setting c_{NA} equal to the base diameter, and iterating on M_{base} and ψ_{decomp} until equilibrium was achieved in Equation (4-14) and the

calculated moment in Equation (4-15) was equal to M_{base}. This resulted in $\psi_{decomp} = 0.951$ and 0.943 for the 0 and 30-degree loading orientations, as per Figure 4.5 and Figure 4.6.

In addition to rotation at the base, the tower can experience rotation at the anchor locations of 110 ft (33.5 m) and 220 ft (67.1 m). These rotations introduced additional lateral displacement into the tower, thereby causing an increase in post-tensioning force. The same procedure, as described in steps 1-18 above, was applied at the tower at an elevation of 110 ft (33.5 m) and 220 ft (67.1 m). The increases in post-tensioning due to these rotations were then added to Equation (4-10) in the tower base ultimate capacity calculation, and the neutral axis at the tower base and base moment were revised to achieve the equilibrium conditions presented in Steps 16 and 18.

Additionally, as the tower experiences significant lateral deformation due to bending, the true ultimate moment at the base will be due to a combination of lateral loading and P-Δ effects. Since the aim of this calculation was to determine the ultimate moment that can be applied from lateral loading, the P-Δ caused moment must be subtracted. The P-Δ caused moment can be calculated at follows:

$$M_{P-\Delta} = P_u \Delta_{top} + \int_0^h \Delta(z)W(z)dz \tag{4-18}$$

with $\Delta(z)$ defined by Equation (4-19):

$$\Delta(z) = \begin{cases} \int_0^{z_1} \dfrac{M(z)(z_1 - z)}{E_{UHPC}I_{tower}(z)}dz + z\theta_{base} & \text{if } h_1 < z \leq h_2 \\ \int_0^{z_1} \dfrac{M(z)(z_1 - z)}{E_{UHPC}I_{tower}(z)}dz + z\theta_{base} + (z - h_1)\theta_1 & \text{if } h_2 < z \leq h \\ \int_0^{z_1} \dfrac{M(z)(z_1 - z)}{E_{UHPC}I_{tower}(z)}dz + z\theta_{base} + (z - h_1)\theta_1 + (z - h_2)\theta_1 & \text{if } h_2 < z \leq h \end{cases} \tag{4-19}$$

where Δ_{top} = total lateral displacement at the tower top;

$\quad$ $W(z)$ = distributed tower weight;

$\quad$ P_u = total factored-level axial load at the base due to dead load;

$\quad$ h = tower height;

$\quad$ z_1 = the height along the tower at which deflection is calculated;

θ = tower base rotation, rad;

θ_1 = tower rotation at 110 ft (33.5 m), rad; and

θ_1 = tower rotation at 220 ft (67.1 m), rad.

The final ultimate moment strength due to lateral load is then calculated as:

$$\phi M_{n,lat} = \phi(M_n - M_{P-\Delta}) \tag{4-20}$$

ϕ is taken as 0.9 for this calculation, as suggested by the Post-Tensioning Manual (Post-Tensioning Institute, 2006).

The ultimate capacity for the UHPC Lattice tower has been defined as the minimum top displacement needed to achieve the required ultimate moment demand, while ensuring that no crushing of concrete or fracture of steel occurs. The ultimate moment demand for the tower was calculated as 195,600 kip-ft (265,200 kN-m) at the tower base for the zero degree loading orientation, and 177,800 kip-ft (241,000 kN-m) for the thirty degree loading orientation. Using the above described procedure, the tower base moment capacity was calculated as 199,800 kip-ft (271,000 kN-m) in the zero degree orientation and 197,700 kip-ft (268,000 kN-m) in the thirty degree orientation, using Equation (4-20). At the tower top, the design capacities are 13,250 kip-ft (17,960 kN-m) for the zero degree orientation and 14,400 kip-ft (19,520 kN-m) thirty degree, with a calculated demand of 12,500 kip-ft (16,950 kN-m). These design capacities correspond to 1.361% and 1.319% tower drift for the zero and thirty degree orientations, respectively. Although the above values have been defined as ultimate capacity, for all calculations the tower post-tensioning remained elastic, and the UHPC strain remained below the compressive yield strain, 0.002966. This indicates that the tower has a significant reserve capacity beyond the calculated ultimate capacities.

Service-Level and Ultimate Shear Capacity

Under the assumption of composite action in the UHPC Lattice tower, very little of the lateral load applied to the tower should be transferred to base as column shear. Rather, it will be transferred through the horizontal and cross bracing. However, without a more detailed analysis, the actual shear demand in the columns in not well-defined. This was further

investigated through the use of finite element analysis, and is discussed in Chapter 5. However, it was still considered useful to determine the ultimate shear strength of a single column. This was determined with Equations (2-88) and (2-89), assuming 80% of the net column area resists shear, and is presented in Figure 4.17.
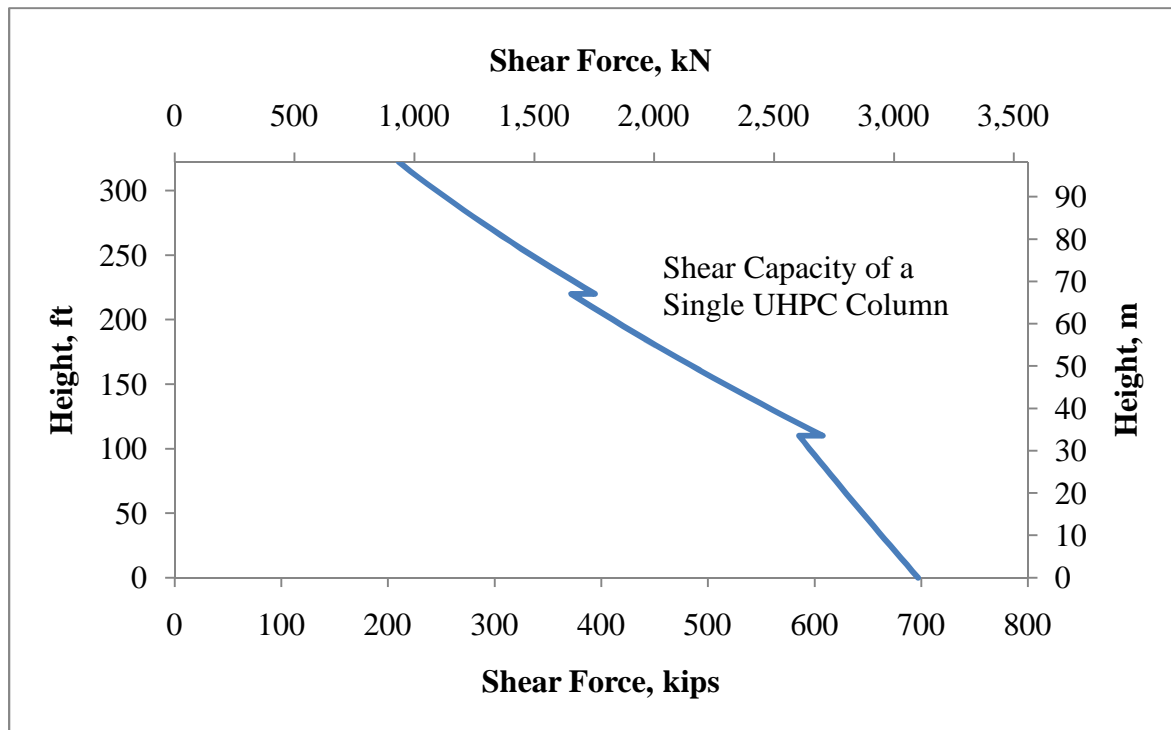
Figure 4.17: Shear Capacity of a Single Column in the UHPC Lattice Tower as per Equations (2-88) and (2-89)

Ultimate Torsional Capacity

In the preliminary design the torsional moment on the tower was neglected. Due to the high degree of indeterminacy of the structure, further analysis is needed to understand how the torsional moment will distribute through the system. This was investigated through finite element analysis and detailed in Chapter 5.

Fatigue

Fatigue of the tendons and UHPC was checked in the same manner as for the UHPC Shell design (Section 1.4.4). The fatigue strength of the UHPC was always sufficiently high, with

a maximum stress DCR of 0.1052 occurring at an elevation of 300 ft (91.4 m). As with the UHPC Shell Tower, the steel fatigue strength was relatively more critical. Conservatively, the steel fatigue was checked as if it were bonded. Realistically, the steel stresses would be distributed over the height of the tower, avoiding any large stress concentrations. Using this approach, the maximum stress DCR for the steel tendons was 0.255, occurring at 300 ft (91.4 m). While higher than the UHPC's fatigue DCR, this value is still very low, indicating a long fatigue life for the UHPC tower.

Dynamic Properties

In order to obtain a more accurate natural frequency, the stiffness of the UHPC Lattice Tower was increased 25.7% to account for the presence of the bracing in the structure, based on results from the finite element model, as discussed in Chapter 5. The natural frequency of the UHPC Lattice was calculated as 0.495 Hz, well within the working frequency range for a 3 MW turbine. The ACI 307 approach (1998) vortex shedding recommendations has limited applicability to the UHPC Lattice tower, as it is an open section. However, an option exists with the UHPC Lattice tower to cover it with it a structural fabric. If this were the case, the tower could be analyzed for vortex shedding as if it were a closed section. Assuming that this covering has a negligible effect on natural frequency of the tower due to its insignificant weight, the critical vortex shedding wind speed was calculated as 24.1 mph (10.76 m/s), as compared to the EOG50 wind speed range of 33.3-86.6 mph (14.89-38.7 m/s). If no covering were used on the exterior of the tower, an alternative method would need to be employed to investigate the possibility of vortex shedding on individual columns or bracing members. Were concrete or UHPC panels used as bracing, the stiffness and mass of the tower would be significantly affected, and a separate analysis would need to be completed to evaluate vortex shedding for this case.

Deflection

Lateral deflections for the UHPC Lattice Tower were calculated as 28.7 in. (0.729 m) and 27.2 in. (0.691 m) for the 0-deg and 30-deg load orientations, respectively. This represented

0.741% and 0.703% drift. These corresponded to the EWM50 wind speed at service-level loading and included the 25.7% increased tower stiffness.

Preliminary Bracing Design

For preliminary design, brace spacing was chosen to prevent buckling of the individual columns at the ultimate load condition. In the most extreme case, the entire outermost compression column would entirely in the plastic portion of its stress-strain curve (Figure 2.4). However, a portion of this stress is caused by prestressing, which will not contribute to buckling. Therefore, the maximum buckling load of the column at its ultimate limit state is:

$$P_u = (0.85f_c' - F/A_{net})A_{net} \tag{4-21}$$

where f_c' = compressive strength of UHPC;

$\quad F$ = the prestressing force in the column; and

$\quad A_{net}$ = the net area of the column.

As an initial estimate for the prestressing force, F was set equal to initial force due to prestressing. Results from the ultimate capacity analysis suggest that this approach is conservative, as the largest compressive stress developed at the ultimate limit state in a column is 16.88 ksi (116.4 MPa), developed in the thirty degree loading orientation.

In turn, the buckling strength of the column is defined as:

$$P_{cr} = \frac{\pi^2 E I_{net}}{(kL)^2} \tag{4-22}$$

where E = elastic modulus of UHPC;

$\quad I_{net}$ = net moment of inertia of the column;

$\quad k$ = effective length factor; and

$\quad L$ = length between brace points.

Since each column has some level of fixity between brace points, the value of k was taken to equal 0.825. This is the averaged value of a k for a pinned-pinned connection, taken as 1.0, and k for a fixed-fixed connection, taken as 0.65 (American Institute of Steel Construction,

Inc., 2005). Although the columns are tapered, their taper is not that large over their unbraced length. Therefore, the smallest critical buckling value was conservatively compared to the highest axial load in the column, over the unbraced length. Additionally, the critical buckling strength was multiplied by a ϕ factor of 0.769, as recommended for UHPC compression members (Japan Society of Civil Engineers, 2006). The bracing layout can be seen in Table 4-5. An example of the bracing layout can be seen in Figure 4.18. This illustration depicts the lower 90 ft (2734 m) off the tower, with bracing and cross bracing members.

Table 4-5: UHPC Lattice Tower Bracing Layout

Bracing Level	Elevation, ft (m)
1	30 (9.15)
2	60 (18.3)
3	90 (27.4)
4	120 (36.6)
5	150 (45.7)
6	180 (54.9)
7	205 (62.5)
8	220 (67.1)
9	245 (74.7)
10	270 (82.3)
11	290 (88.4)
12	310 (94.5)

Level 2:
60 ft (18.3 m)

Level 1:
30 ft (9.15 m)
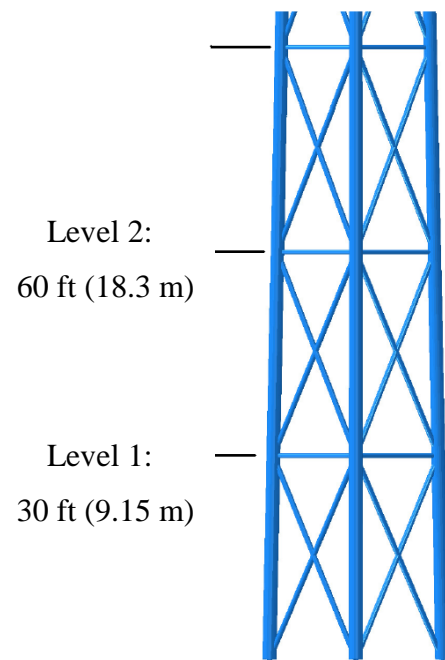
Figure 4.18: An Illustration of the Bracing Layout at the UHPC Lattice Tower Base

4.3.3 Discussion

While the UHPC Lattice tower was intended as a preliminary design, it is still useful to compare it to the UHPC Shell, concrete, and steel designs. An interesting aspect of the UHPC Lattice tower is the increased wind load on the tower, as compared to the UHPC Shell Design. While the Lattice Tower has a truss-like layout, its overall width is larger than the UHPC Shell Tower. Additionally, the UHPC shell tower enjoys a lower force coefficient (C_f). Since the shell tower is a smooth cylinder, its C_f ranges from 0.64-0.72. Although the

UHPC Lattice tower has less surface area, its components attract higher wind forces with a C_f of 1.39. As C_f is directly proportional to the direct wind force, this makes a significant difference. However, as previously stated, the wind load on the Lattice Tower is less well-defined as compared to the cylindrical towers. Wind tunnel or computer simulations would be useful in accurately quantifying the direct wind load on the Lattice Tower.

Without considering the volume of material required for bracing, the Lattice tower uses less UHPC than the UHPC Shell: 173 yd^3 (132 m^3) versus 183 yd^3 (140 m^3). It is important to note however that the Lattice Tower will require bracing, which will add increased cost and labor to the design. The choice of bracing material, as well as connections could significantly affect the overall price of the UHPC Lattice Tower. The bracing members used for this study added 76 yd^3 (58.1 m^3) of UHPC to the UHPC Lattice tower. This brought the total required volume of UHPC for the Lattice tower to 249 yd^3 (190 m^3)

As with the UHPC Shell Tower, fatigue is never a governing limit state for design. This implies the tower could be used with multiple turbines over the course of its design. Additionally, due to its use of unbonded post-tensioning, it could be dismantled and re-assembled at another site. Long fatigue life makes both of these options a possibility.

The Lattice Tower design has an estimated natural frequency of 0.495 Hz, within the working range of 0.242 Hz to 0.594 Hz for a 3.0MW turbine. This indicates that the turbine top loads, and more specifically the assumed dynamic amplification, are valid for the structure.

Deflection of the UHPC Lattice Tower does not meet the ACI 307 (1998) recommendations for concrete chimneys, but is significantly lower the UHPC Shell tower. This is due to the increased base diameter and therefore the increased lateral stiffness of the UHPC Lattice tower, as compared to the UHPC Shell tower. The generalized stiffness of the UHPC Lattice tower, determined during the evaluation of the tower's natural frequency, was calculated as 15.03 kip/in (2630 kN/m) while the UHPC Shell's was only 7.63 kip/in (1336 kN/m). The UHPC Lattice tower deflection falls between the BergerABAM (LaNier, 2005) concrete and steel towers. This was expected, because when used effectively stiffness of a UHPC structure

should lie somewhere between that of a comparable steel and concrete structure, as its compressive strength is much higher than concrete's, and weighs only 3.3% more than concrete.

4.4   Summary

Using the same loading criteria as BergerABAM (LaNier, 2005), the UHPC Shell and UHPC Lattice Tower designs were completed. A summary of the controlling design limit states can be seen in Table 4-6. Additionally, the controlling limit states for the steel and concrete towers are repeated for ease of comparison. The UHPC Shell and UHPC Lattice tower, with bracing, require 32% and 43% of the volume of material of the regular strength concrete design, respectively. As compared to the steel tower, they are approximately 17% and 52% heavier, for the UHPC Shell and UHPC Lattice Towers, respectively. Both UHPC Tower designs are significantly lighter than the regular strength concrete tower, which is 200% heavier than the steel tower. However, the UHPC Shell tower experiences a 92.6% higher tower top deflection than the UHPC Lattice. It is expected that the UHPC Shell design would need to be revised to meet turbine manufacturers' permissible deflections, and therefore would move closer to the UHPC Lattice tower in required material. Despite the differences in material, the UHPC Lattice tower has much smaller member sizes than the UHPC Shell tower. Therefore, it would require reduced transportation, site development, and erection costs as compared to the UHPC Shell. The governing factor between which tower is a better option depends on transportation savings, as well as how much more volume of UHPC the UHPC Shell tower would require to limit deflection.

Both UHPC towers are able to meet the natural frequency requirements necessary to remain in the working frequency range during turbine operation. This was expected, as the UHPC designs lie between the regular strength concrete tower and steel tower in terms of required material and weight. Additionally, it can be seen in Table 4-6 that the towers with the lowest natural frequencies experienced the highest deflection. It is expected then that were the UHPC Shell tower base diameter increased to reduce deflections, its natural frequency would increase, putting it closer to the upper end of the working frequency range. Neither UHPC

tower was governed by fatigue concerns, allowing them to have service lives much higher than the typical 20 year operational life of a wind turbine.

Table 4-6: Comparison of Design Results for 322 ft (98.2 m) UHPC Shell , UHPC Lattice, Steel, and Concrete Towers

	322 ft (98.2 m) UHPC Shell Tower	322 ft (98.2 m) UHPC Lattice Tower	322 ft (98.2 m) Steel Tower	322 ft (98.2 m) Prestressed Concrete Tower
Weight, kips (kN)	866 (3850)	1123 (5000)	739 (3290)	2290 (10,190)
Maximum Strength DCR	0.978, Equations (3-5) and (3-6)	0.949, Equations (3-5) and (3-6)	0.912, Equation (2-58)	0.997, Equation (2-82)
Maximum Shear DCR	0.745 (Torsion and Shear Interaction)	Discussed in Chapter 5	0.0773	0.881
Maximum Fatigue DCR	0.277 (steel tendon)	0.255 (steel tendon)	0.972	0.0844
Deflection, % Drift	1.427	0.741 (0-deg. loading)	1.646	0.413
Fundamental Natural Frequency	0.372	0.495	0.338	0.568
Controlling Limit State	Service-level moment capacity, shear and torsion interaction at tower top	Service-level moment capacity	Strength at tower base, Fatigue along the tower height	Service-level tower flexural strength, concrete fatigue (wall thickness for 220-322 ft [67.1-98.2 m])

In order to make a true comparison, further investigation into the UHPC Lattice Tower is needed. This analysis would include verification of the assumed section behavior, as well as determination of the bracing member forces. In order to obtain this information, a finite element analysis was completed, and is described in Chapter 5.

5   DETAILED ANALYSIS AND DESIGN OF THE UHPC LATTICE TOWER

5.1   Overview

Although multiple bracing options exist for the UHPC Lattice tower, the focus of this chapter is the use of horiztonal and cross bracing members, rather than panel bracing as mentioned in Chapter 4. Since the Lattice tower is a highly indeterminate structure, a more detailed analysis was performed to determine the structural response and individual member forces. In particular, the forces in the bracing were needed to complete their design. In order to obtain this information, a centerline finite element model was created. Additionally, the preliminary design of the lattice tower considered axial forces in the UHPC columns, caused by bending of the structure, as the main design criterion. The finite element model was also needed to validate those axial forces and the assumption that plane sections will remain plane (i.e., composite behavior exists between the columns) when bending occurs. Furthermore, the model enabled the quantification of critical values of any localized moments, shears, and torsion in the columns caused by the interaction between the columns and the bracing.

5.2   Model Design

5.2.1   Model Overview

The commercial finite element program Abaqus (Dassault Systèmes, 2009) was utilized to complete the finite element model. A centerline model using 3D beam and truss elements was created to analyze the service-level response of the structure, including displacements and member forces. This approach was chosen over solid modeling due to its versatility and processing efficiency. Although it does not provide information about stress concentrations or allow the modeling of actual connections, it was decided that this information could be obtained by analyzing individual columns with appropriate boundary conditions at this stage of development.

5.2.2   Elements

For all column and bracing members, 3D, three node quadratic beam elements were used. These elements were chosen to allow for a more accurate displaced shape while using fewer elements, as compared to a linear beam. Abaqus designates this element as B32. B32 elements are Timoshenko beams and can be used for "thick ("stout") as well as slender beams" (Dassault Systèmes Simulia Corp, 2009) and can be subjected to "large axial strains". Additionally, these beams are shear flexible, allowing for transverse shear deformation. Abaqus automatically calculates the shear stiffness in most cases based on user inputs.

For the post-tensioning tendons, 2-node truss elements were used. Abaqus designates these elements as T3D2, and they have linear displacement functions. As post-tensioning is assumed to carry only an axial force, it was judged that truss elements were the most appropriate choice.

5.2.3   Material Models

As was discussed in Chapter 4, the service-level moment demand governs the design of the UHPC Lattice tower. Therefore, the goal of the finite element model was to determine service-level displacements and forces, and a linear material-model was used for the UHPC. This is valid as long as stresses in UHPC members are limited to 22.1 ksi in compression, and 1.3 ksi in tension (see Chapter 4). As the tower was designed to experience no tension under service-level loading, this approach was deemed adequate. The idealized stress-strain relationship can be seen in Figure 2.4 and Figure 2.5, and the material values were used in the analysis are given in Table 5-1.

Table 5-1: UHPC Material Properties

f'_c	26 ksi (179.3 MPa)
E_c	7450 ksi (51400 MPa)
γ_c	155 pcf (24.3 kN/m^3)

An elastic material model was also used with the post-tensioning, as it was expected to remain in the elastic region during service level conditions. According to the PCI Handbook (PCI Industry Handbook Committee, 2004), 270 ksi (1860 MPa) ASTM A 416 prestressing strands have a yield strength of 243 ksi (1675 MPa) and an elastic modulus of 28,500 ksi (196,500 MPa). Since this limit will not be reached according to this theoretical steel stress-strain model, it is only necessary to input the elastic modulus of the steel into the finite element model.

5.2.4   Model Construction

Since a centerline modeling approach was used, several simplifications were necessary to complete the model. In order to accurately model the cross sectional properties of the columns, a generalized cross section was used within Abaqus. Using this approach, the principal moments of inertia, as well as the mixed moments of inertia and torsional properties were specified for each column section. While the columns themselves had a round cross section, the generalized section was needed to account for the voided areas caused by the post-tensioning ducts. One downside of using this cross sectional definition was that it did not explicitly allow for the use of tapered sections. To overcome this challenge, each column was partitioned at 5 ft (1.524 m) intervals, and the average cross sectional dimensions were used over that height. This was found to be sufficiently accurate, as the interval chosen provided less than 2% error in deflection for the shortest column span. This was verified by modeling a cantilever beam in Abaqus with the same length as the portion of the UHPC spanning from 220 ft (67.1 m) to 322 ft (98.2 m) elevation. A uniform load was applied to this beam, and the maximum deflection was calculated. This value was then compared to a hand calculation of the displacement for the same beam and applied loads. Additionally, column member areas were linearly interpolated between 0-110 ft (0-33.5 m), 110-220 ft (33.5-67.1 m), and 220-322.2 ft (67.1-98.2 m) for simplicity. As the change in column was spread over these long distances, this assumption estimated the column areas within 97.8% accuracy.

Since the post-tensioning is unbonded, it only applies axial loads on the columns at anchor locations and horizontal loads on the columns at harping locations (i.e., where the taper of the

UHPC columns is changed). However, it must also follow the displaced shape of the columns along the height. To enforce these conditions, the post-tensioning had all three of its displacement degrees of freedom coupled to the column at anchor points. To force the tendons to follow the displaced shape of the columns, they were partially coupled to the columns at 25 ft (7.62 m) intervals. Accordingly, the tendons were allowed to slide along the columns' length, but had their transverse displacements coupled to the columns'. This was done by creating local coordinate systems for each column, with their z-axes parallel to the column axes.

All braces and columns in the model are connected to each other through the use of Abaqus's coupling connectors. It was assumed that the brace-to-column connections would be designed to have moment resistance. To account for this, the bracing and cross bracing had all 6 degrees of freedom coupled at column interfaces. This assumption is appropriate so long because no large moments are developed at these connections (see Table 5-3 for further details on member forces). In order to reduce unbraced length for buckling, the x-type cross bracing members were coupled at their cross-points (denoted by red circles in Figure 5.1). However, it is unlikely that significant moment resistance could be developed by such a connection, so only translational degrees of freedom were coupled at these locations. This fixed-pinned support condition gives each cross-bracing member a theoretical effective length of 0.8 (American Institute of Steel Construction, Inc., 2005). As a result, each cross-brace's effective length is 40% of its total length.

Figure 5.1: A View Showing UHPC Lattice Tower Cross Bracing Connections in the Finite Element Model

The boundary conditions at the base of the tower were modeled as pin supports. Since unbonded post-tensioning is used, and the tension columns would be allowed to uplift

under extreme loading conditions, no moment resistance is provided at these column bases. The post-tensioning tendons were also pinned at the base of the tower.

In order to tie the columns together at the top of the tower, a generic platform was put in place, using rigid elements. An image of this platform is presented in Figure 5.2. Since the design of such a platform is beyond the scope of this research but required for mounting the turbine, the use of rigid elements eliminated the variable of platform deformation from the analysis. A final design for such a tower would need to include the actual platform dimension, and quantify the effects of platform flexibility on the rest of the tower. Since this platform will have to be rigid, the expected flexibility effects will be small.

The completed model is presented in Figure 5.3. Figure 5.4 displays the model using realistic dimensions for the elements. This is useful because it provided a sense of scale between the various tower members and gave a visual verification that the member sizes input into the program are realistic. Figure 5.3 is the centerline representation of the model. All of the actual geometry, forces, and displacements are based off of this representation.

An important difference to note between the conceptual image of the lattice tower, shown in Figure 4.3, and Figure 5.3 and Figure 5.4 is the addition of the cross bracing. The cross bracing is necessary to tie the columns together, as well as transfer shear to the base using the braced system compositely.
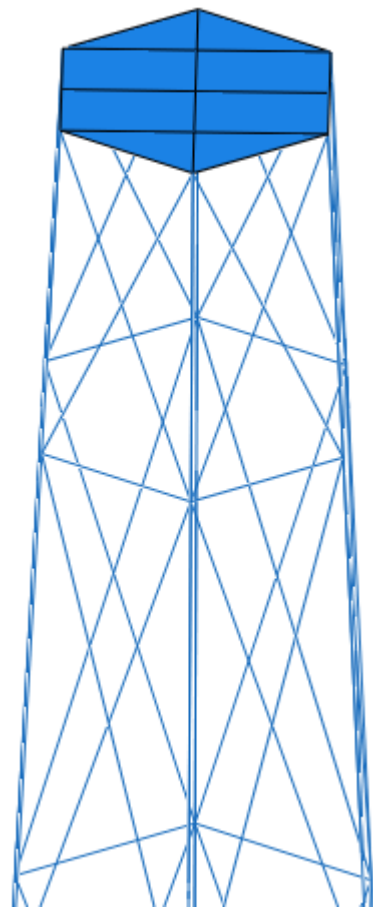
Figure 5.2: A View of the Rigid Platform in the UHPC Lattice Tower Finite Element Model

Figure 5.3: A View of the Wireframe UHPC Lattice Tower Model Developed for Service-Level Loading
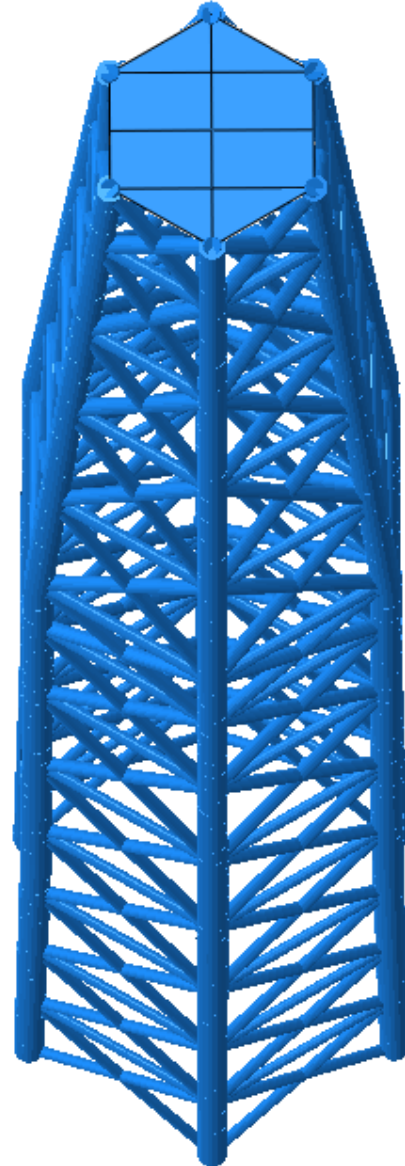
Figure 5.4: A View of the Rendered UHPC Lattice Tower Model Developed for Service-Level Loading

5.2.5   Loading

The loading on the tower was applied in five separate steps. These steps are listed in Table 5-2. All loading applied to the model corresponds to the EWM50 wind condition and the load combination described by Equation (2-9), which was found to govern the design of the UHPC Lattice tower in Chapter 4.

Table 5-2: Model Loading Steps

Step	Description
1	Initial (Required by Abaqus)
2	Prestress Release
3	0-Degree Loading
4	0-Degree Loading – Reverse Torsion
5	30-Degree Loading
6	30-Degree Loading – Reverse Torsion

The "Initial" step is when the geometry of the structure was defined and connections/boundary conditions are created. No loads were applied in this step.

The second load step applied the prestressing forces to the tower, and was termed "Prestress Release". This had to be done in a special manner, since the Abaqus interface does not support the use of prestressing. To apply the prestressing to the columns, additional pinned boundary conditions were added to the post-tensioning at all anchor points during the "Initial" step. A velocity with a unit magnitude was then applied to the tendons, in the form of a "predefined field". This predefined field was then changed to a stress in the Abaqus keyword editor. The value of the stress was then changed to the desired jacking stress to maintain the right amount of prestressing in the columns. During the "Prestress Release" step, the additional pin supports were released, transferring the prestress force to the columns through the anchor connection points.

The remaining load steps correspond to different loading orientations, which are defined in Figure 4.5 and Figure 4.6. The "Reverse Torsion" label in Table 5-2 refers to the torsional moment applied at the tower top to represent wind turbine operation reversing in direction. In

steps 3-6, the prestressing load from the "Prestress Release" is always present on the tower. However, loads applied during all subsequent steps were active only during their respective step.

In Steps 3-6, the turbine loads were applied to a reference point in the center of the platform at the tower top shown in Figure 5.2. The direct wind loads were applied to the tower directly, but only to the portion of the tower facing the wind. This was consistent with how direct wind loading was calculated with the ASCE 7 (SEI, 2005). Since the wind pressure varied with height, the wind load on the tower varied as well. For the columns, an average wind pressure was calculated at 5 ft (1.524 m) intervals, and applied to the respective column segment as a constant line load. The cross bracing loads were based on the wind pressure at each cross brace's average elevation, and applied as a constant line load. Each level of horizontal braces experienced a wind constant pressure, which was applied as a line load. Additionally the self-weight of the tower and the turbine weight were applied in Steps 3-6.

To capture the P-Δ effects of the tower loading, Steps 3-6 were run as large-displacement analyses. This allowed Abaqus to account for the geometrical nonlinearities of the system.

5.3   Bracing Design

The purpose of the bracing on the tower is to provide composite action between the six main UHPC columns. If this is not present, the columns will bend individually and not in a composite manner. Since each of the columns was not designed as an independent flexural member, they cannot develop the necessary moment resistance when acting individually. If composite action is present, the columns will bend as one section, and each column will experience primarily axial tension or compression. If the entire tower is considered to act as a beam, the bracing and cross bracing act as the web of the beam, while the columns represent the flanges. This also significantly increases the effective moment of inertia of the tower section, reducing lateral displacements.

5.3.1   Bracing Analysis

In order to start the analysis, a preliminary member was needed. Since the forces in the bracing were initially unknown, a WT member was used. Using the results of the initial

analysis, new members were then selected. However, as the tower is a highly indeterminate and the axial stiffness of the members greatly influenced the amount of force distribution throughout the tower, further iteration was necessary.

Although the members in the tower experience a diverse array of forces, a design methodology was chosen that limited the number of unique bracing members in the tower. This simplified the design, as well as increased the economy of the tower design by reducing the need for a wide range of member sizes. In that context, bracing and cross bracing were split into three different groups for analysis and design purposes. The cross bracing was grouped along the tower height as follows: CB1, 0-120 ft (0-36.6 m); CB2, 120-270 ft (36.6-82.3 m); and CB3, 270-322.2 ft (82.3-98.2 m). These groups were based on giving the cross bracing members comparable unbraced lengths for buckling. Similarly, the horizontal bracing was grouped as follows: HB1, 30-120 ft (9.15-36.6 m); HB2, 150-220 ft (45.7-67.1 m); and HB3, 245-310 ft (74.7-94.5 m). The bracing groups roughly correspond to the cross bracing groups along the tower height.

To further simplify the analysis of these members, the envelope forces from the above described groups were used for sizing members. Rather than analyzing the force combination in every member within each group, the maximum axial, shear, and moments from any members were obtained. A single member was then designed for the combination of these forces. While this was a conservative approach, the bracing members experienced primarily axial force. For example, CB1 experienced an envelope that included an axial compression of 663 kips (2950 kN), a shear force of 2.71 kips (12.05 kN), a resultant bending moment of 20.0 kip-ft (27.2 kN-m), and a torsional moment of 5.47 kip-ft (7.42 kN-m). Since the axial force was dominant, the range of moments, shears, and torsions in the rest of the members marginally affected the required member size. This range was also limited because the cross bracing and bracing were already split into three groups. This method resulted in members that were designed for a worst case loading condition. A further optimization of the tower bracing is possible by specifically investigating individual members. However, since wind loading can come from any direction, there is likely little more to be gained from this optimization.

Multiple member shapes and materials were used as trial sections during the bracing analysis. The three main trials included steel WT-shapes, concrete-filled round steel HSS sections, and finally round, hollow prestressed UHPC members. Although highly feasible, the option of using thin UHPC panels or high-strength prestressed concrete panels was not pursued in this study as it would change the wind loading on the tower. The trials involving the WT-shapes and concrete-filled HSS members resulted in the braces attracting very large forces, requiring excessively large members for cross and horizontal bracing. The primary variable that governed how much force was in each brace was the brace's cross sectional area, multiplied by its modulus of elasticity (AE). This is intuitive, as axial stiffness is defined as AE/L. While the WT-shapes have smaller areas, the modulus of elasticity of steel is very high compared to concrete. The concrete-filled HSS sections had a smaller modulus of elasticity, and thus required a large cross sectional area. UHPC has roughly 5 times the compressive strength of regular concrete, but the modulus of elasticity is only 1.6 times as large (for a regular strength concrete with a 7 ksi (48.3 MPa) 28-day compressive strength). This put its AE term somewhere between that of the WT-sections and the concrete-filled HSS, allowing it to pick up only a moderate amount of force. Therefore, due to ease and economy of designing UHPC hollow prestressed members, they were chosen both for cross and horizontal bracing. The design of the hollow prestressed UHPC members is detailed in Section 5.3.

The final iteration of member forces can be seen in Table 5-3. From left to right, the columns represent the required, service-level compressive forces, tensile forces (shown as positive values), shear force, bending moment, and torsional moments. CB denotes the cross bracing and HB refers to the horizontal bracing, which are separated into the groups as detailed previously. It should be noted that as the geometry of the bracing changes, the loads on the tower will correspondingly be altered. After each step it was necessary to update the tower loading to reflect the new dimensions of the bracing. In the last iteration, the loading applied to the finite element model was within 2% of the calculated tower loading, with all members meeting the strength requirements (as described in Section 4.3.2). Therefore, it was judged that the loading and required member sizes had converged.

An important characteristic of the loads in Table 5-3 is that horizontal bracing always experienced a tensile force, while the cross bracing was subjected to either a large compressive load or moderately-sized tensile force, depending on its location in the structure with respect to the tower's axis of bending.

Table 5-3: Service-Level Horizontal Bracing and Cross Bracing Force Envelope Values Obtained from the Finite Element Analysis

	C_r , kips (kN)	T_r , kips (kN)	V_r , kips (kN)	M_r, kip-ft (kN-m)	Mz_r, kip-ft (kN-m)
CB1	663 (2950)	-65.3 (290)	2.71 (12.05)	20.0 (27.2)	5.52 (7.48)
CB2	641 (2850)	-85.2 (-379)	4.31 (19.17)	28.6 (38.8)	7.35 (9.97)
CB3	660 (2940)	-78.6 (-350)	8.78 (39.1)	38.9 (52.7)	10.93 (14.82)
HB1	-	-421 (-1873)	3.85 (17.13)	19.42 (26.3)	0.828 (1.123)
HB2	-	-366 (-1628)	4.27 (18.99)	20.8 (28.2)	0.971 (1.316)
HB3	-	-282 (-1254)	8.63 (38.4)	25.5 (34.6)	3.12 (4.23)

5.3.2   *Design of UHPC Bracing*

As previously noted, the final choice for cross bracing and horizontal bracing was UHPC hollow circular members due to their high strength and economy of design. All bracing and cross bracing members utilized prestressing, with the option of using either pre-tensioning or post-tensioning. From the finite element model results, the horizontal braces were found to be tension members. To counter this tensile force, they were highly pre-stressed. The cross bracing members see both large compression forces and moderate tensile forces, and thus utilize a lower level of prestressing. A bracing and cross bracing schedule can be seen in Table 5-4 and Table 5-5, respectively. Detailed cross sectional illustrations are presented in Figure 5.5 to Figure 5.7.

Table 5-4: Horizontal Bracing Schedule

UHPC Horizontal Bracing: 30-120 ft (9.15-36.6 m)
Outside Diameter: 9 in. (229 mm)
Wall Thickness: 2 in. (50.8 mm)
Number of Prestressing Strands: 18-0.6 in (15 mm)
UHPC Horizontal Bracing: 150-310 ft (45.7-94.5 m)
Outside Diameter: 9 in. (229 mm)
Wall Thickness: 2 in. (50.8 mm)
Number of Prestressing Strands: 16-0.6 in (15 mm)

Table 5-5: Cross Bracing Schedule

UHPC Cross Bracing: 0-322 ft (0-98.2 m)
Outside Diameter: 13 in. (330 mm)
Wall Thickness: 2 in. (50.8 mm)
Number of Prestressing Strands: 6-0.6 in (15 mm)
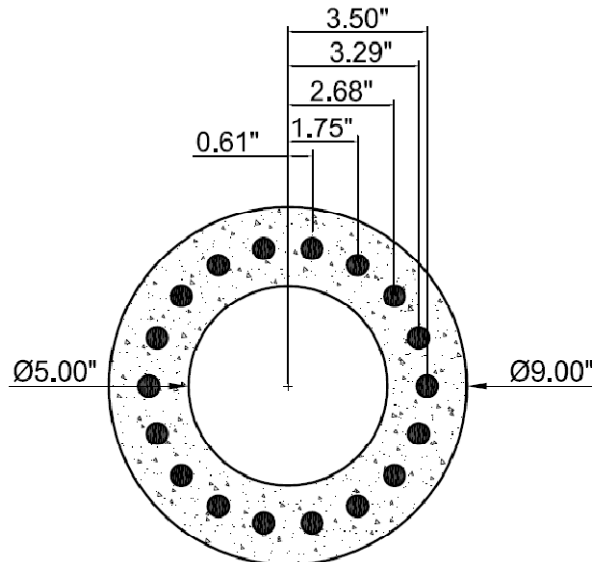
Figure 5.5: An Illustration Showing the Cross Section of the UHPC Horizontal Brace 9x2 in. (229x50.8 mm) with 18-0.6 in. (15mm) Strands
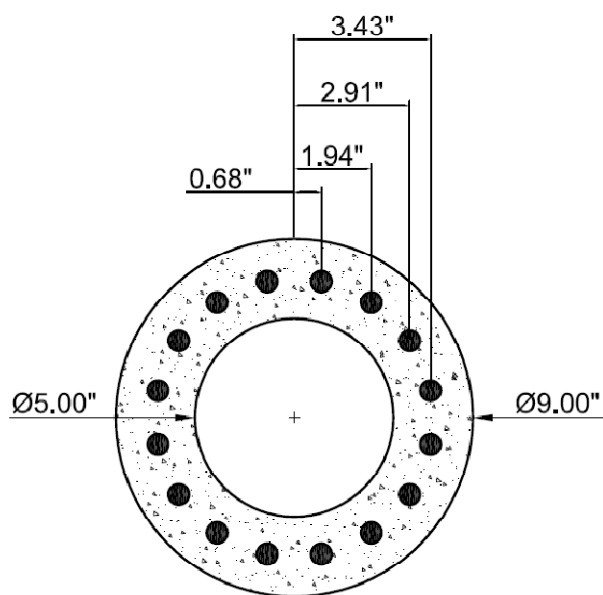
Figure 5.6: An Illustration Showing the Cross Section of the UHPC Horizontal Brace 9x2 in. (229x50.8 mm) with 16-0.6 in. (15mm) Strands
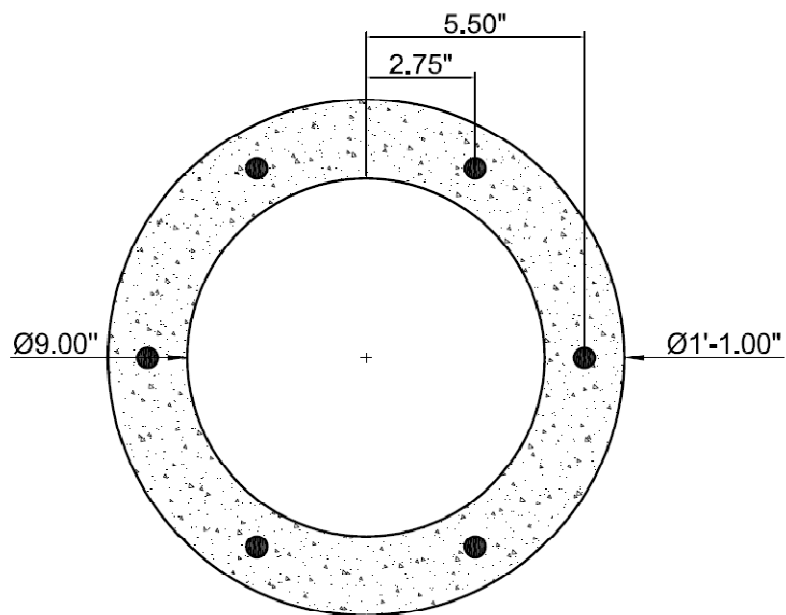

Figure 5.7 An Illustration Showing the Cross Section of the UHPC Horizontal Brace 13x2 in. (330x50.8 mm) with 6-0.6 in. (15mm) Strands

Although the horizontal and cross bracing were initially split into three groups each, the majority of these groups were eliminated, and the same member was able to be repeated. In a general sense, the horizontal bracing and cross bracing transfer the shear force applied to the tower to the foundation. This action is analogous to a web in a wide-flange beam. Although the level of shear resisted by the tower increases inversely with respect to height, the required local bending and torsional moments are higher in the braces and cross bracing located at higher elevations. This keeps the required member size for bracing and cross bracing constant along the tower height. The only exception to this is the bottom group of horizontal bracing, which require two additional prestressing strands. The design of both the cross bracing and bracing were completed as pretensioned members. As previously mentioned, bonded or unbonded post-tensioning could be used as well. The use of unbonded post-tensioning would allow for the damage-free removal of the horizontal and cross bracing, if the ability to move the tower in the future was desired. One downside of this approach is that the bracing and cross bracing would see a small decrease in ultimate capacity. This difference in ultimate capacity is discussed later in this section.

<u>Horizontal Bracing</u>

As the horizontal bracing are tension members, the design criterion governing their geometry and area of steel was the prevention of cracking under service level conditions. The maximum longitudinal tensile stress under these conditions is given as,

$$\sigma_{tension} = \frac{F}{A_{trans}} - \frac{T_r}{A_{trans}} - \frac{M_r(d_{out}/2)}{I_{trans}} \tag{5-1}$$

where F = prestressing force in the brace;

T_r = required service level tensile force;

M_r = required service level bending moment;

A_{trans} = transformed area;

I_{trans} = transformed moment of inertia; and

d_{out} = outside diameter of the brace.

Note that the transformed area was used in this calculation since the member is pretensioned. Were the members designed using post-tensioning, the net area is more appropriate.

While the initial design of the UHPC Lattice Tower used zero tension as a design condition, it was felt that a small amount of tension could be allowed in the bracing members. This methodology was justified because the brace forces were more well-defined from the finite element analysis. In contrast, the initial design of the UHPC Lattice Tower columns inherently included more assumptions regarding structural behavior. Therefore, the tensile stresses in the bracing have been limited to the tensile cracking strength of UHPC, which is given as 1.3 ksi (Bristow & Sritharan, To be published). However, in no cases did tensile cracking occur in the bracing under design service-level loads. The most critical longitudinal stress was $\sigma = 2.19$ ksi (15.10 MPa) in compression. This stress level occurred in the bracing group in the 150-220 ft (45.7-67.1 m) range. This implies that the horizontal bracing is not decompressed under service level loading.

Since the tower is not always fully-loaded, the bracing will not always experience this load combination. When no external load exists on the braces, a compressive force is present from the prestressing. Therefore, the compression stresses due to prestresssing must be limited to prevent crushing. This limit set out according to ACI 318 (ACI Committee 318, 2008):

$$\frac{F}{A_{trans}} \leq 0.6 f_c' \tag{5-2}$$

As with the limiting tensile stress, the compression limit is slightly less conservative than that used for the preliminary design of the UHPC Lattice Tower columns in Section 4.3.2. The rationale behind this decrease in conservatism is the same as before: the loading is more well-defined in the bracing due to the finite element analysis results. The most critical case for this limit state occurred in the bracing group in the 30-120 ft (9.15-36.6 m) range, where a compressive stress of 13.42 ksi (92.5 MPa) was reached, versus a limit of 15.60 ksi (107.6 MPa).

The horizontal bracing was also checked to ensure that no cracking occurred at the service level due to the combination of torsion and shear force. This limit state was checked using

Equation (4-1). The largest principal stress developed occurred in the bracing group 245-310 ft (74.7-94.5 m), where a principal tensile stress of -0.096 ksi (-0.662 MPa) was observed. This is significantly below the cracking strength of UHPC, indicating shear cracking will not occur from torsion and shear force.

The ultimate strength of the horizontal bracing was calculated using strain compatibility and the numerical approach of strips. The same approach was used for the UHPC Shell Tower ultimate capacity calculation, in Section 4.2.2. One modification to this approach was that the tensile strength of UHPC was included, as per Figure 2.5. As with the UHPC Shell Tower, crushing of the UHPC governed the ultimate capacity of the horizontal bracing members. In order to carry out this calculation, it was necessary to know the axial load on the bracing members. However, this load was not defined because the finite element model was elastic, and could only be accurately used for service level loading. As a conservative estimate, the axial load at service level was multiplied by a factor of 1.6, the largest load factor in the load combination in Section 2.3.3. This was considered to give a worst case scenario. Additionally, to investigate the effect of using unbonded post-tensioning, a modified version of this calculation was carried out. As unbonded post-tensioning distributes the increase in steel strain along its entire length, the increase at any given section will be smaller than in a member utilizing bonded post-tensioning. The 0.5 factor estimates the effect of the steel strain being distributed over the entire member. In order to estimate the capacity of the members using unbonded reinforcement, the method as used in Section 4.2.2 was modified. Accordingly, in step 6, the incremental steel strain was calculated using strain compatibility. This strain was then halved, to approximate the steel strain increase due to bending being averaged over the entire member length. The results of the analysis are presented in Table 5-6.

Table 5-6: Estimated Ultimate Capacity of the UHPC Horizontal Bracing

Member Designation	Axial Load, kip (kN)	Ultimate Moment Capacity*, ft-kip (kN-m)	Ultimate Moment Requirement, kip-ft (kN-m)
UHPC 9x2	-586 (2610)	86.5 (117.3)	40.7 (55.2)
UHPC 9x2 Unbonded	-586 (2610)	55.4 (75.1)	40.7 (55.2)
UHPC 9x2X**	-674 (3000)	90.5 (122.7)	32.0 (43.4)
UHPC 9x2X Unbonded	-674 (3000)	58.2 (78.9)	32.0 (43.4)

*Includes strength reduction factor
** UHPC 9x2X represents the level of bracing containing 2 extra strands

A strength reduction, or "phi", factor was used in accordance with ACI 318 Chapter 9 (2008). It can be seen that for all members the ultimate capacity was satisfied. Based on this estimate, the use of unbonded post-tensioning the members, as opposed to pre-tensioning, would serve to reduce the ultimate capacity in the range of 55.5-56.1%. A portion of this decrease is due to the unbonded tendons having much smaller incremental steel strains, resulting in a strength reduction very close to 0.65. The use of unbonded post-tensioning would allow the bracing members to be directly anchored to the columns, serving as the connection. Were pre-tensioning used, a welded or bolted connection would need to be devised.

Cross Bracing

Based on the finite element analysis results, the diagonal cross bracing were subjected to a much larger range of forces, as compared to the horizontal bracing. Depending on the location of the cross bracing with respect to the axis of bending, members experienced either tension or compression. Members nearest to the compression columns saw the largest compression forces, while members closer to the tension columns saw tension forces as well. Because of these load reversals, cross bracing must be designed for both the compression and tension load combinations.

For the condition when the cross bracing is subjected to tensile forces, the limit state is identical to that used for longitudinal stress in the horizontal bracing. This limit state was

checked using Equation (5-1). The largest tensile stress developed was -0.369 ksi (-2.54 MPa), occurring in the cross bracing group CB3. This value is well under the cracking strength of UHPC, 1.3 ksi (8.96 MPa).

For the case when the cross bracing was subjected to a large compression force, the following equation was used to calculate the maximum compressive stress:

$$\sigma_{compression} = \frac{F}{A_{trans}} + \frac{C_r}{A_{trans}} + \frac{M_r(d_{out}/2)}{I_{trans}} \tag{5-3}$$

where F = prestressing force in the brace;

C_r = required service level compressive force;

M_r = required service level bending moment;

A_{trans} = transformed area;

I_{trans} = transformed moment of inertia; and

d_{out} = outside diameter of the brace.

The stress calculated in Equation (5-3) was then compared to the compression stress limit set out in Equation (5-2): $0.6f_c'$, or 15.6 ksi (107.6 MPa) (ACI Committee 318, 2008). The largest compressive stress developed in the cross bracing group CB3, with a value 15.12 ksi (104.2 MPa).

Due to the long length of the cross bracing, as well as their reduced area and moment of inertia (as a result of UHPC's high compressive strength), buckling becomes was also consideration. Euler's buckling strength was utilized to calculate the theoretical buckling load for the cross bracing members. This equation is given as follows:

$$P_{cr} = \frac{\pi^2 E_{UHPC} I_{trans}}{(kL)^2} \tag{5-4}$$

where E_{UHPC} = modulus of elasticity for UHPC;

I_{trans} = transformed moment of inertia;

k = effective length factor; and

L = unbraced length.

In order to reduce the unbraced length of the cross bracing, it was decided that the members would be connected to each other at their crossing point. This connection was assumed to constrain translation, but not rotation. Since there is some assumed fixity at the connection point between the cross bracing and the columns, the value of k was taken as 0.80, as recommended by AISC (2005) for fixed-pinned columns. This factor should be revised when connection details are developed.

One potential concern with connecting the cross bracing members at their midpoints is that if both cross braces simultaneously buckle, they will not provide the lateral restraint necessary to reduce the unbraced length. This would be valid if any given connected set of cross bracing had the same axial force demand. However, due to the tower loading, the axial forces in a set of cross bracing are not equal. Therefore, one will always buckle before the other. This is illustrated in Figure 5.8, which displays the axial forces in the bracing members. In this figure, SF1 represents the axial force, with a negative value corresponding to compression. For this loading condition, the upper left section of the tower was in compression. It can be seen that for each pair of cross bracing members, one member had a significantly higher compression force than the other. When the member with higher compression force attempts to buckle, the member with the lower force will still be able to provide lateral restraint. Therefore, connecting cross bracing members at their midpoints will indeed reduce the unbraced length for buckling.

The highest DCR for buckling, 0.405, was experienced in CB. This cross bracing group had a calculated buckling load of 1640 kips (7300 kN) based on the maximum member length and a required compressive axial load of 663 kips (2950 kN).
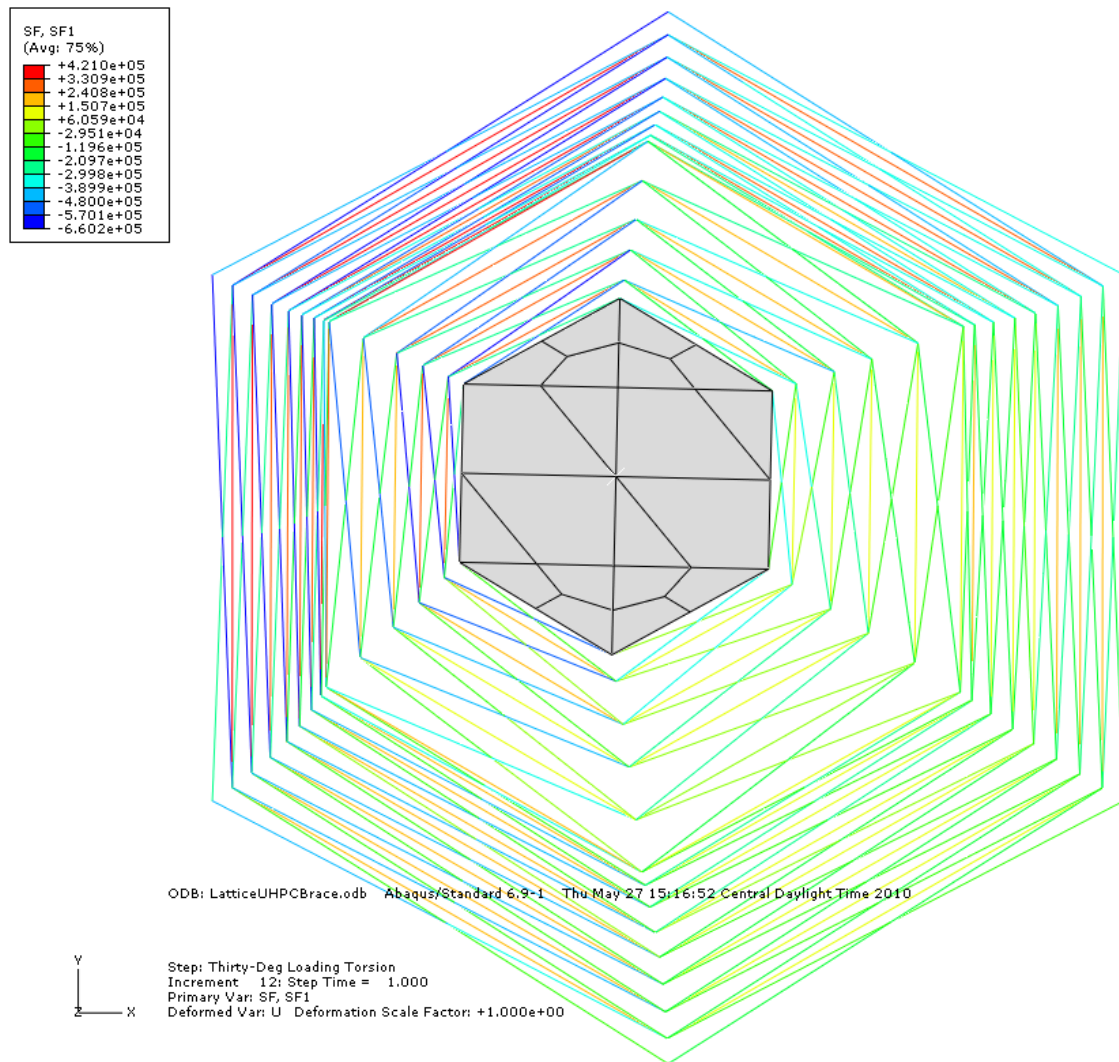
Figure 5.8: Top View of the UHPC Lattice Tower Depicting Axial Forces in the Bracing Members

The cross-bracing was also checked for cracking at the service level due to torsion and shear, using Equation (4-1). The largest principal stress was developed in the cross-bracing group 270-322.2 ft (82.3-98.2 m), reaching a value of -0.824 ksi (5.68 MPa) in tension. This is larger than any tensile stress created in the horizontal bracing, but still under the UHPC's cracking strength of 1.3 ksi (8.96 MPa).

The ultimate capacity of the cross-bracing was calculated in the same manner as for the horizontal bracing. However, for the cross-bracing, there are additional load cases, as the

cross-bracing is sometimes in compression, and sometimes in tension. In all cases the ultimate capacity for the cross-bracing under compressive loading had a reduced capacity. This was a result of the high compressive loading, which caused the prestressing to shorten. As this is defined as a compression controlled failure by ACI 318 (ACI Committee 318, 2008), a strength reduction factor of 0.65 was applied to these sections. The results of the analysis are listed in Table 5-7.

Table 5-7: Estimated Ultimate Capacity of the UHPC Cross Bracing

Member Designation	Axial Load, kip (kN)	Ultimate Moment Capacity*, kip-ft (kN-m)	Ultimate Moment Requirement, kip-ft (kN-m)
UHPC 13x2*	-136.3 (606)	103.4 (140.2)	62.2 (84.3)
UHPC 13x2* Unbonded	-136.3 (606)	95.6 (129.6)	62.2 (84.3)
UHPC 13x2*	1061 (4720)	72.7 (98.6)	62.2 (84.3)
UHPC 13x2* Unbonded	1061 (4720)	74.1 (100.5)	62.2 (84.3)

*Including strength reduction factor

For both the bonded and unbonded cases, the estimated ultimate capacity is larger than the demand, which was estimated based applying a load factor of 1.6 to the service-level loads. The use of unbonded post-tensioning was estimated to reduce the ultimate capacity of the members by approximately 8.2% in the tensile loading cases. In the compressive loading cases the use of unbonded tendons had little effect, as all tendons in the section shortened due to the high compressive ultimate load.

5.3.3   Discussion

While the design of the bracing satisfies the requirements established in this chapter, a refined design would need to more accurately account for the ultimate loads applied to the bracing. This could be accomplished through the completion of a 3D, solid finite model that included the material nonlinearities present at the ultimate loading condition. This would account for any force re-distribution due to differential yielding of tower members. Additionally, the variable amplification of loading (i.e., the different load factors for direct

wind vs. turbine wind loads) would affect to load distribution. When a final decision is made on the use of bonded or unbonded tendons in the bracing, adequate cover and spacing distances should be ensured.

As mentioned above, other options do exist for bracing. One such option is a WT-section. WT's would be suitable for cross bracing because they are able to pass flange-flange with minimal member offset. However, any change in bracing would require additional analysis using the centerline finite element model, as force distribution would be expected to occur. Additionally, the use of rounded sections reduces the wind load on the bracing and cross bracing. For WT sections of the same height, the loading on each member would be approximately 35% higher. In general, the use of a WT would attract larger forces and would increase the size of bracing members.

With the use of UHPC bracing and cross bracing, an additional volume of 76 yd^3 (58.1 m^3) is necessary to complete the tower construction. This brings the total volume of UHPC needed for the Lattice Tower to 249 yd^3 (190 m^3).

If unbonded tendons were selected for use with the UHPC bracing and cross bracing, the design would need to be refined slightly for the reduction of area and altered moment of inertia due to the presence of the ducts. Additionally, a more refined procedure would be necessary to determine the ultimate capacity of the bracing and cross bracing.

5.4   Verification of the UHPC Column Design

5.4.1   Column Analysis

One of the main purposes of the finite element model was to verify that the columns would act in composite manner with bracing, and that the stress levels in the columns are within acceptable levels under service level loading conditions. In this context, the most critical columns to be investigated are those farthest from the neutral axis when the tower is subjected to flexural action. The critical columns will either have the largest compressive axial force, or largest tensile axial force. For the 0-degree and 30-degree loading conditions, the northwest and southeast columns were the most critical. These columns are identified in Figure 5.9, which shows the tower in plan view. Although member forces were available

from the model at 2.5 ft (0.76 m) increments, examining each of these locations would have been extremely time-consuming. An alternative approach was followed, wherein only the vital locations were identified and examined in the northwest and southeast columns. The locations that were examined include the base, the top, and points directly before and after post-tensioning cut-off locations. Recall that post-tensioning cut-offs were chosen at 110 ft (33.5 m) and 220 ft (67.1 m). In addition to the above locations, the points of maximum moment (M_x, M_y, and M_z) of all six columns were examined in ranges of 0-110 ft (0-33.5 m), 110-220 ft (33.5-67.1 m), and 220-322.2 ft (67.1-98.2 m).
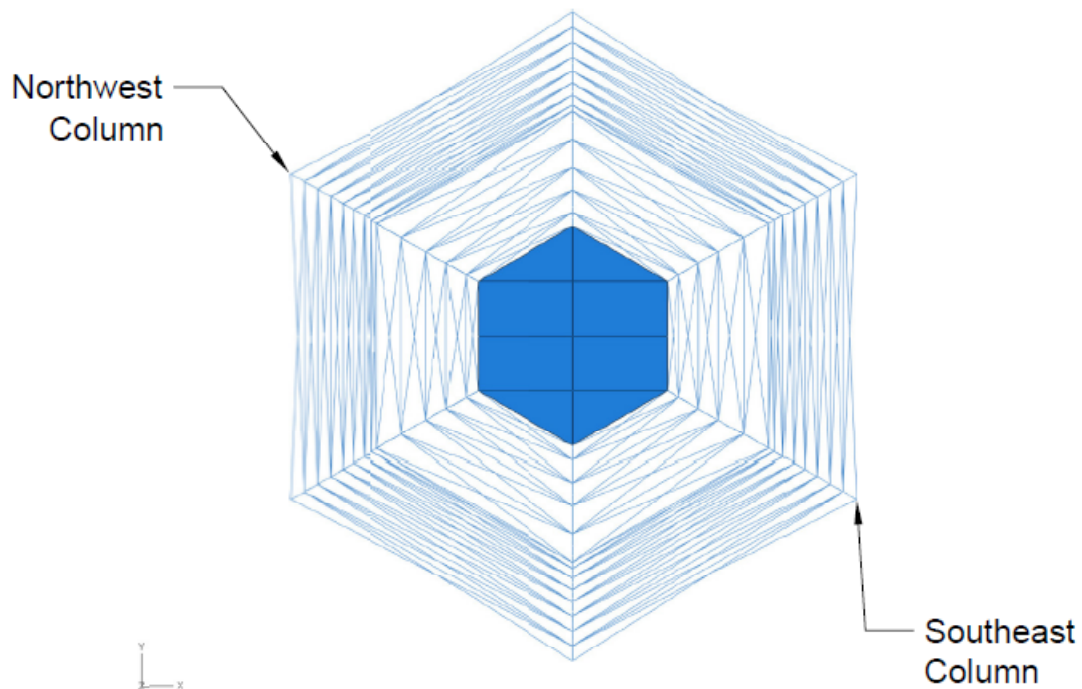
Figure 5.9: Locations of Critical Columns Caused by Service-Level Wind Loading

For the column members the finite element analysis provided member end forces. These forces were then combined, and the appropriate stresses were calculated. For every location that was checked an axial compression force was present. This indicated no locations were decompressed under service level conditions. Since this was the case, the maximum compression/tension stress could be calculated elastically at any location along the columns:

$$\sigma = \frac{C_r}{A_{net}} \pm \frac{M_r(D_{col}/2)}{I_{trans}}$$

<div align="right">(5-5)</div>

where C_r = compressive axial force in the column, due to loading and prestressing;

A_{net} = net section area of the column;

M_r = required, local bending moment in the column;

D_{col} = column diameter; and

I_{net} = transformed moment of inertia of the column.

The results of this analysis at the transition sections are listed in Table 5-8. In Equation (5-5), M_r is the vector summation of the required local column bending moments. For the columns ranging from 0–110 ft (0-33.5 m) and 220-322 ft (67.1-68.2 m) along the tower height, the individual column moment of inertia is the same for all orientations. Therefore, the mixed moment of inertia of the section is zero for any orientation. For columns in the range of 110-220 ft (33.5-67.1 m) along the tower height, the columns' major and minor principle moments of inertia were not the same. Therefore, Equation (5-5) does not provide the exact stress when M_r was applied about a non-principle axis. However, the major and minor moments of inertia for columns in this range differed by only 3.3-8.3%, resulting in a very small mixed moment of inerta. For simplicity, the moment M_r for columns in this range was considered to act about the minor axis. This was a conservative assumption, and was estimated to the cause the calculated values reported in Table 5-8 to vary from the true stress by 0.01-0.03 ksi (0.07-0.2 MPa). This was judged to be a negligible variance, as no columns were found to exceed the allowable stress limits.

In all column locations examined, in only one were tensile stresses developed due to the combination of axial load and local column bending moments. This occurred at an elevation of 110 ft (33.5 m) immediately after a post-tensioning cut-off, and was calculated as -0.313 ksi (-2.16 MPa). It is important to note that this location represents a column joint and the column-to-column connection would be provided exclusively by prestressing force. Therefore, in reality this tensile stress would not be developed. Rather, a joint opening would occur. However, as the average stress level in the column was found to be 0.259 ksi (1.786 MPa) in compression, only the outer edge of the column joint would open. Since the

corresponding joint opening would be very small, and in a concentrated area, it was judged that the overall effect on the model was minimal. If such an opening were considered undesirable, it could be prevented through use of positive connections at column joint locations.

Table 5-8: Column Longitudinal Stresses at Selected Locations

Elevation	Tension/Compression Side of Neutral Axis	Longitudinal Stress, ksi (MPa) (+ve compression)
0 ft (0 m)	Tension	0.881 (6.07)
	Compression	10.31 (71.1)
110 ft (33.5 m) (Before PT cut-off)	Tension	2.11 (14.55)
	Compression	11.14 (76.8)
110 ft (33.5 m) (After PT cut-off)	Tension	-0.313 (-2.16)
	Compression	8.82 (60.8)
220 ft (67.1 m) (Before PT cut-off)	Tension	3.28 (22.6)
	Compression	11.14 (76.8)
220 ft (67.1 m) (After PT cut-off)	Tension	0.1783 (1.229)
	Compression	6.75 (46.5)
322.2 ft (98.2 m)	Tension	1.826 (12.59)
	Compression	9.57 (66.0)

The largest compressive stress developed in the model was 11.14 ksi (76.8 MPa), which occurred at the 110 ft (33.5 m) immediately before a post-tensioning cut-off, and at 220 ft (67.1 m), immediately after a post-tensioning cut-off. In the remaining locations that were checked (i.e., locations where maximum moments occurred), all stresses were within the envelope presented in Table 5-9 and therefore, they are not listed.

The columns were also investigated with regards to cracking under service level shear conditions, due to the combination of torsion and shear. In general, the columns with the smallest axial compressive force had the largest principal stresses. Therefore, only the

columns on the tension side of the overall tower neutral axis location have their shear and principal stresses listed. These stresses are summarized in Table 5-9.

Table 5-9: Tension Column Shear and Principal Stresses at Selected Locations

Elevation	Total Shear Stress, ksi (MPa)	Principal Stress, ksi (MPa) (-ve tension)
0 ft (0 m)	0.271 (1.868)	-0.000829 (-0.00572)
110 ft (33.5 m) (Before PT cut-off)	0.1417 (0.977)	-0.00943 (0.0650)
110 ft (33.5 m) (After PT cut-off)	0.1478 (1.019)	-0.371 (-2.56)
220 ft (67.1 m) (Before PT cut-off)	0.1742 (1.201)	-0.00903 (-0.0622)
220 ft (67.1 m) (After PT cut-off)	0.1909 (1.316)	-0.1212 (-0.836)
322.2 ft (98.2 m)	0.469 (3.23)	-0.1121 (0.773)

In no locations checked did the principal stress exceed the cracking strength of UHPC, 1.3 ksi (8.96 MPa). Therefore, the tower should experience no shear cracking in the columns under service level forces. The principal stresses in the other locations examined were within the envelope created by Table 5-9. The relatively low level of shear stresses suggests that the bracing effectively transfers the lateral load from turbine operation and wind force to the foundation and prevents it from entering into the columns as a shear force. Rather, it contributes to the axial load in the columns.

In addition to verifying column behavior, the model was also used to refine the moment of inertia that was calculated in the preliminary design of the UHPC Lattice tower. Since the moment of inertia was previously calculated by only considering the columns, the finite element model was used to capture the additional stiffness of the system caused by the presence of bracing. This was done in the following manner. A 100 kip (444 kN) force was applied at the tower top in the finite element model. The displacement from the model was then recorded, and compared to the calculated displacement considering only the UHPC

Lattice tower columns' moment of inertia. The finite element result showed a lateral displacement of 7.36 in. (0.1869 m), while the calculated displacement was 25.7% larger at 9.25 in. (0.235 m). As the tower's lateral displacement is inversely proportional to its stiffness, it was concluded that the bracing contributed an additional 25.7% lateral stiffness to the tower. Therefore, the moment of inertia of the UHPC Lattice tower was multiplied by a factor of 1.257 for the deflection and natural frequency calculations in Chapter 4.

At service-level loading, the maximum tower displacement in the finite element model was 28.6 in. (0.726 m) for the 0-degree loading orientation, and 27.1 in. (0.688 m) for the 30-degree loading orientation. These displacements corresponded within 0.4% of the displacements calculated in Chapter 4 using the modified moment of inertia. This indicates that the model is correctly loaded and provided reasonable results.

5.4.2 *Discussion*

In almost all locations the tower remains decompressed under service-level loading. However, it should be noted that the maximum compressive stresses seen in the tower were significantly lower than the initial design stresses. This is due to the assumption that all compression and tension due to bending would be carried through the columns. However, it is observed from the analysis that indeed a portion of the longitudinal bending forces are transferred through the bracing system.

Another effect of this is a reduction in the transfer of post-tensioning stresses into the columns, ranging from 60% effective at the tower top to 84% effective for at the tower base. In the finite element model, the bracing was considered attached to the tower before prestressing occurs. The actual construction sequence would need to consider whether bracing was needed to support the columns as they were erected, or if the post-tensioning would be applied before any bracing is attached. As the tower is currently modeled, nearly all sections remain in compression under service-level loading (except for one localized point).

5.5   Summary

The centerline finite element model analyzed the behavior of the UHPC Lattice tower as an entire system. It was observed that the bracing and cross bracing act in concert with the

UHPC columns and assist in taking a portion of the longitudinal compressive and tensile forces caused by bending. Additionally, a portion of the prestressing force is transferred through the bracing and cross bracing. A final design summary of the UHPC Lattice tower is presented in Table 5-10.

The results of the centerline finite element analysis led to design of the bracing and cross bracing as hollow UHPC, pre-tensioned members. Only three unique member sizes are needed for the entire tower. Other options are possible for the bracing, although changing bracing and cross bracing sizes would require re-analysis of the finite element model with updated sizing. In general, the initial design of the UHPC Lattice Tower overestimated the forces in the columns. The result was a design that carries some conservatism. This conservatism could be limited through the reduction of column sizes (therefore increasing the stress in the columns and further utilizing the higher compressive strength of UHPC). Another option would be to prestress the columns before the bracing is attached, but utilize a smaller amount of PT steel. However, the design in its current iteration meets all design criteria.

While the centerline finite element model was able to more accurately determine the service-level response of the lattice tower, as well as provide the information necessary to complete the bracing design, a refined design of the Lattice tower could include the investigation of the tower response at factored-level loads. This would include the completion of a 3D, solid finite element model. This model should incorporate the material nonlinearities of UHPC and steel in order to truly estimate the tower ultimate capacity. This would provide insight into any possible stress concentrations, as well as provide the true factored-level loading in the bracing members. However, it was judged that this would most likely not govern the design, as calculations from Section 4.3 have shown that service-level loading is more critical.

Table 5-10: Final Design Summary of the 322 ft (98.2 m) UHPC Lattice Tower

Compressive Strength, ksi (MPa)	26 (179.3)
Post-tensioning Effective Stress, ksi (MPa)	180 (1241)
Overall Diameter, D, at Base, in. (m)	354 (8.99)
Column Diameter, d_{col}, at Base, in. (mm)	26.625 (676)
Number of 0.6-in diameter strands, 0-110 ft (0-33.5 m)	486
Overall Diameter, D, at 110 ft (33.5 m), in. (m)	294 (7.47)
Column Diameter, d_{col}, at at 110 ft (33.5 m), in. (mm)	24.625 (625)
Number of 0.6-in diameters strands, 110-220 ft (33.5-67.1 m)	342
Overall Diameter, D, at 220 ft (67.1 m) , in. (m)	246 (6.25)
Column Diameter, d_{col}, at 220 ft (67.1 m), in. (mm)	19.75 (502)
Number of 0.6-in diameter strands, 220-322ft (67.1-98.2 m)	198
Overall Diameter, D, at 322 ft (98.2 m), in. (m)	120 (3.05)
Column Diameter, d_{col}, at 322ft (98.2 m), in. (m)	14.875 (378)
Horizontal Bracing, 30-120 ft (9.15-36.6 m)	UHPC 9x2 in. (229x50.8 mm), 18-0.6 in. (15 mm) tendons
Horizontal Bracing, 150-310 ft (45.7-94.5 m).	UHPC 9x2 in. (229x50.8 mm), 16-0.6 in. (15 mm) tendons
Cross Bracing, 0-322.2 ft (0-98.2 m)	UHPC 13x2 in. (330x50.8 mm), 6-0.6 in. (15 mm) tendons
UHPC Volume, yd^3 (m^3)	249 (190.4)
Tower Weight, kips (kN)	1123 (4980)
Fundamental Tower Natural Frequency, Hz	0.495

6   SUMMARY AND CONCLUSIONS

6.1   Summary of Research

In Chapter 1, the need for the advancement of tower wind turbine towers in order to achieve the Department of Energy's "20% by 2030" wind energy goal was discussed, as well as the challenges associated with extending the current technology of tubular steel towers to higher elevations. The benefits of taller hub heights were detailed, including the increased quantity and reliability of power production as a result of higher wind speeds. The suitability of concrete and UHPC for taller wind turbine towers was examined, including two potential UHPC tower concepts. In Chapter 2, a review of the material properties and behavior of UHPC was completed. The loads experienced by wind turbine towers were described, and literature and standards where tower loading can be obtained were identified. The limit states associated with steel and prestressed concrete/UHPC were identified, and specifications and other methods suitable for evaluating those limit states were discussed. Additionally, a design study that completed designs for 328 ft (100 m) towers with steel and prestressed concrete was reviewed. Chapter 3 presented designs for both a 322 ft (98.2 m) steel and prestressed concrete tower. Chapter 4 presented a design for the 322 ft (98.2 m) UHPC Shell tower and a preliminary design for the UHPC Lattice tower. The results of these designs were then compared to the concrete and steel towers that were developed in Chapter 3, as well as the results of the design study that was introduced at the end of Chapter 2. Chapter 5 presented a detailed design for the UHPC Lattice tower. The design was completed through the use of finite element analysis, which verified the design assumptions and behavior used in Chapter 4 with regards to the UHPC Lattice Tower. The bracing for the UHPC Lattice Tower was also designed using the results of the finite element analysis.

6.2   Conclusions

6.2.1   Steel Towers for 328 ft (100 m) Hub Heights

The 322 ft (98.2 m) steel tower design completed in this study has shown that the necessary base diameter for tubular steel towers will be too large to transport using traditional shipping

methods. This base diameter was calculated as 18 ft (5.49 m), which exceeds the limit of 14.1 ft (4.3 m) set for highway clearance. The overall tower dimensions were governed by a combination of strength and fatigue. As such, the tower's operational design life is approximately 20 years. Under service-level loading, the steel tower design experiences very large deflections, with a maximum tower drift of 1.65%. The base diameter of the tower would likely need to be increased to reduce deflections, further exacerbating the transportation concerns associated with this design. In general, it is concluded that the above discussed challenges associated with tubular steel shells indicate that there is much room for innovation for towers at hub heights of 328 ft (100 m) and higher.

6.2.2   *Prestressed Concrete Towers for 328 ft (100 m) Hub Heights*

A 322 ft (98.2 m), prestressed concrete tower design was completed in this study in order to provide a comparison for the UHPC Shell and UHPC Lattice Towers. The diameter of the tower was governed by service-level moment demand. For the bottom two-thirds of the tower, the wall thickness was dictated by service-level stress limitations recommended by ACI (ACI Committee 318, 2008). The wall thickness in the top-third of the tower was governed by fatigue limitations. However, with a small increase in wall thickness the tower's fatigue life was increased to 12 times greater than that of the turbine. This would allow for the tower to be re-used after the expiration of the turbine's design life. The concrete tower was better able to handle deflections than the steel tower, with a maximum drift of only 0.413% at the ultimate limit state. Although there are no currently known deflection limits for wind turbine towers, this limit comes the closest to the 0.333% drift recommended by ACI (ACI Committee 307, 1998) for concrete chimneys. Based on the design results, it is concluded that prestressed concrete provides a possible solution for 328 ft (100 m) hub height wind turbine towers. Concrete's fatigue resistance allows for the possible re-use of the tower with multiple towers, which would dramatically increase the value of the tower over its life-cycle. However, the concrete tower was more than three times as heavy the steel tower, potentially increasing foundation costs.

6.2.3   Prestressed UHPC Shell Towers for 328 ft (100 m) Hub Heights

The completed design of the 322 ft (98.2 m) UHPC Shell tower represents an extension of current turbine tower designs with an advanced material. The tower dimensions were governed by moment demand for the bottom two-thirds of the tower height and shear and torsion interaction for the top-third of the tower. This is notable, as the top-third of the tower was governed by a different limit state than the regular strength concrete tower. This suggests that replicating current designs with more advanced materials may not be the most efficient solution. However, the UHPC Shell tower used only 31.9% of the material required for the regular strength (i.e., 7 ksi [48.3 MPa]) concrete tower. This would greatly reduce the transportation costs associated with bringing this material to the project site, as compared with the regular strength concrete tower. The fatigue life of the tower is very high, with a minimum of 5.63×10^{13} allowable load cycles. As with the concrete tower, the UHPC Shell tower has the potential to be re-used with multiple turbines, spreading its initial cost over a longer design life. The UHPC Shell experienced large deflections, with a drift of 1.43% at the service-level limit state. While not as high as the steel tower drift, this represents a very large deflection under service-level loading. Were manufacturer deflection limits known, it is likely that the design would need to be refined to reduce deflections. The most effective option for this refinement would be an increased base diameter. In general, it is concluded that UHPC Shell tower provides a good solution for wind turbine towers at 328 ft (100 m) or taller hub heights. Its reduction in required materials not only mitigates transportation costs, but makes it a more sustainable design. The following is a summary of the primary conclusions obtained from the 322 ft (98.2 m) UHPC Shell tower design:

- Practicable solution to the transportation challenges associated with taller steel towers, owing to the UHPC Shell's modular design and thin required wall thickness, which ranged from 4.25-3.25 in. (108-82.6 mm);
- More efficient use of material as compared to the concrete tower, with a 68% reduction in volume; and
- Strong suitability for use with multiple turbines over the tower's life-cycle due to its excellent fatigue resistance, increasing the value of the tower as compared to current steel towers.

In general, it is concluded that the UHPC Shell tower provides a good solution for wind turbine towers at 328 ft (100 m) or high hub heights.

6.2.4   *Prestressed UHPC Lattice Tower for 328 ft (100 m) Hub Heights*

The UHPC Lattice tower is a completely new design concept, attempting to more efficiently utilize UHPC as compared to the UHPC Shell tower while improving transportability and constructability. The UHPC Lattice tower design was governed only by moment demand, never by fatigue because of UHPC's high fatigue resistance and the tower's high stiffness, leading to a reduced applied fatigue stress range. This indicates, as with the UHPC Shell and regular strength concrete shell, the possibility for re-use of the UHPC Lattice Tower, dramatically increasing the value of the tower as compared to steel designs. This long fatigue life, coupled with the use of unbonded tendons and small member sizes, would also allow the tower to be disassembled and moved to another location if required. The preliminary design of the UHPC Lattice tower columns resulted in 94.5% of the volume of UHPC required for the UHPC Shell tower. The total volume of UHPC for the Lattice tower is strongly influenced by the choice of bracing material. If UHPC is used for bracing and cross-bracing members, as designed in Chapter 5, the UHPC Lattice tower would require 36.1% more material than the UHPC Shell Tower. However, this amounts to only 43.4% of the material required by the regular strength concrete tower. Additionally, as the deflection of the UHPC Lattice tower is only 51.7% of the UHPC Shell Tower's, the UHPC Lattice tower will likely require much less refinement to meet deflection limits. Therefore, it is probable that the volume of UHPC required for the Shell will increase, bridging the gap between the two designs. The results of the finite element model suggested that the bracing effectively enables composite action between the columns of the UHPC Lattice tower, verifying the primary design assumption behind the Lattice concept. The following is a summary of the primary conclusions were drawn regarding the 322 ft (98.2 m) UHPC Lattice Tower:

- Viable solution to the transportation challenges associated with taller steel towers, with column diameters ranging from 26.625-14.875 in. (676-378 mm) and bracing member diameters ranging from 9-13 in. (229-330 mm);

- Increased value as compared to steel towers due to long tower fatigue life and potential for re-use and re-deployment;

- Excellent deflection control as compared to the steel and UHPC shell towers; and

- More efficient use of material than the regular strength concrete tower, with approximately 57% reduction in volume.

It is concluded that the UHPC Lattice tower has strong potential as a design alternative for 328 ft (100 m) hub height towers because of its relatively small deflections, small required member sizes, and high fatigue resistance. As compared to the regular strength concrete tower, both UHPC designs make more efficient use of material, increasing their sustainability. The advantage of using the UHPC Lattice versus UHPC shell will ultimately depend on manufacturer deflection requirements and the choice of bracing elements for the UHPC Lattice tower.

6.3 Future Research

One of the main tasks of future research for the UHPC tower designs would to be to obtain turbine loads from a manufacturer. While it is believed the loads used in this study were appropriate for general conditions, loading for a specific turbine would help to refine the designs presented in this report, as well as allow for a direct comparison to current steel and concrete tower alternatives for 328 ft (100 m) hub heights. Additionally, the determination of a deflection limit would allow for a more direct comparison between the UHPC Shell and UHPC Lattice towers. Both of these goals could be accomplished through input from a turbine manufacturer.

The UHPC Lattice tower concept could be refined through further investigation of other bracing types. This could include regular strength concrete panels that span between the UHPC columns. Additionally, wind tunnel testing could be used to more accurately quantify the loading requirements for the bracing members. While the ASCE 7 (Structural Engineering Institute, 2005) is an accepted American design standard, it is believed that it does not take into account the intricacies of the loading on the UHPC Lattice tower. However, as the ASCE 7 is commonly used on a wide range of buildings today, it is likely a conservative estimate of the direct wind loading on the UHPC Lattice tower.

While main member sizes have been presented here, a detailed connection and foundation design should be completed to further evaluate the total material requirements for each design, and therefore the costs differences between tubular steel tower designs and the UHPC towers designs presented in this study. These connection designs should then be tested to ensure their assumed behavior.

With the UHPC Lattice or UHPC Shell design refined for specific turbine loading, large-scale testing should then be undertaken to further verify the theoretical behavior of the towers, as considered in this study.

REFERENCES

ACCIONA Windpower. (n.d.). AW-3000. West Branch, Iowa: ACCIONA Windpower.

ACI Committee 307. (1998). *ACI 307-98: Design and Construction of Reinforced Concrete Chimneys.* Farmington Hills: American Concrete Institute.

ACI Committee 318. (2008). *Building Code Requirements for Structural Concrete (ACI-318) and Commentary.* Farmington Hills: American Concrete Insititution .

American Institute of Steel Construction, Inc. (2005). *Specifications for Structural Steel Buildings.* Chicago: American Institute of Steel Construction, Inc.

American Wind Energy Association. (2010). *AWEA U.S. Wind Industry Annual Market Report Year Ending 2009.* AWEA.

American Wind Energy Association. (2010). *AWEA Year End 2009 Market Report.* AWEA.

American Wind Energy Association. (1999, November 24). *Wind Energy Tax Credit Extended*. Retrieved July 6, 2010, from AWEA News Releases: http://www.awea.org/news/News991123ptc.html

Association Française de Génie Civil/SETRA. (2002). *Ultra High Performance Fibre-Reinforced Concretes, Interim Recommendations.* Paris: AFGC.

Berg, O. (2010). *Performance Evaluation and Finite Element Verification of an Ultra-High Performance Concrete Pi-Girder Bridge.* Ames: Iowa State University.

Bierwagen, D. (2009). *UHPC Pi-Girder in Iowa.* Retrieved July 20, 2010, from http://www.iowadot.gov/operationsresearch/lunchandlearn/2009/sept/Research%20Office%209-21-09.pdf

Blais, P., & Couture, M. (1999). Precast, Prestressed Pedestrian Bridge - World's First Reactive Powder Concrete Strcuture. *PCI Journal* , 60-71.

Bristow, B., & Sritharan, S. (To be submitted). Uniaxial and Cyclic Behavior of Ultra-High Performance Concrete. *ACI Materials Journal* .

Brughuis, F. (2004). *Improved Return On Investment due tolarger wind turbines.* Retrieved June 12, 2009, from MECAL Wind Energy: http://www.mecal.nl/files/algemeen/ewec2004-ATS_paper.pdf

Burton, T., Sharpe, D., Jenkins, N., & Bossanyi, E. (2001). *Wind Energy Handbook.* West Sussex: John Wiley & Sons, Ltd.

Caithness Windfarm Information Forum. (2008, December 31). *Summary of Wind Turbine Accident data to March 31st 2009*. Retrieved June 24, 2009, from Caithness Windfarm Information Forum: http://www.caithnesswindfarms.co.uk/fullaccidents.pdf

Chang, B. (2007). *A Time-Domain Model for Predicting Aerodynamic Loads on a Slender Support Structure for Fatigue Design.* Ames: Iowa State University.

Cheng, C.-T., Yang, J.-C., Yeh, Y.-k., & Chen, S.-E. (2003). Seismic Performance of Repaired Hollow-Bridge Piers. *Construction and Building Materials* , 339-351.

Cheyrezy, M., & Behloul, M. (2001). Creep and Shrinkage of Ultra-High Performance Concrete. *Creep, Shrinkage and Durability Mechanisms of COncrete and other Quasi-Brittle Materials - Proceedings of of the Sixth INternational Conference CONCREEP-^@MIT*, (pp. 527-538). Cambridge.

Cheyrezy, M., & Richard, P. (1995). Composition of Reactive Powder Concretes. *Cement and Concrete Research , 25* (7), 1501-1511.

Chopra, A. K. (2007). *Dynamics of Structures, Theory and Applications to Earthquake Engineering* (3rd Edition ed.). Upper Saddle River, NJ: Pearson Education, Inc.

Chryssanthopoulos, M. K., Poggi, C., & Spagnoli, A. (1998). Buckling Design of Conical Shells Based on Validated Numerical Models. *Thin-Walled Structures* , 254-270.

Comite Euro-International Du Beton. (1990). *CEB-FIP Model Code 1990.* Lausanne: Thomas Telford.

Comite Euro-International Du Beton. (1993). *CEB-FIP Model Code 1990.* Lausanne: Thomas Telford.

Dassault Systèmes. (2009). Abaqus/CAE 6.9-1. Providence, RI.

Dassault Systèmes Simulia Corp. (2009). Abaqus Analysis User's Manual. Providence, RI, USA: Dassault Système.

Degen, B. (2006). *Shea Design and Behavior of Ultra-High Performance Concrete.* Ames: Iowa State University.

DNV/Risø. (2002). *Guidelines for Design of Wind Turbines 2nd Ed.* Copenhagen: Det Norske Veritas.

Dodge, D. M. (2006). *Illustrated History of Wind Power Development*. Retrieved June 12, 2009, from Telosnet: http://www.telosnet.com/wind/index.html

Electrotechnical Commission. (n.d.). *IEC History*. Retrieved June 30, 2009, from IEC: http://www.iec.ch/about/history/

European Committee for Standardisation. (1992). *Eurocode 3 : Design of steel structures — Part 1.1: General rules and rules for buildings.* London: BSI.

European Convention for Constructional Steelwork. (1988). *Recommendations on Buckling of Shells.*

Evolve Green. (2010). *How to calculate wind speed in your area*. Retrieved July 7, 2010, from Evolve Green: http://www.evolvegreen.ca/howto.html

Fanella, D. A., & Rabbat, B. G. (1997). *Design of Concrete Beams for Torsion.* Skokie: Portland Cement Association.

Fehling, E., Bunje, K., & Leutbecher, T. (2004). Design Relevant Properties of Hardened Ultra High Performance Concrete. *International Symposium on Ultra High Performance Concrete*, (pp. 327-338). Kassel.

Gelsi, S. (2008, July 22). *U.S. blows by Germany in wind-energy output*. Retrieved June 16, 2009, from Market Watch: http://www.marketwatch.com/story/us-blows-by-germany-in-wind-energy-pickens-speaks-to-senate

Global Energy Concepts. (2002). *WindPACT Turbine Rotor Design Study, NREL/SR-500-32495.* Golden: National Renewable Energy Laboratory.

Gowripalan, N., & Gilbert, R. I. (2000). *Design Guidelines for RPC Prestressed Concrete Beams.* Sydney: VSL Pty Ltd.

Graybeal, B. A. (2009, January/February). *UHPC Making Strides*. Retrieved July 7, 2009, from U.S. Department of Transportation: Public Roads: http://www.tfhrc.gov/pubrds/09janfeb/03.htm

Graybeal, B. (2006). *Material Property Charactertization of Ultra-High Performance Concrete.* MacLean: Office of Infrastructure Research and Development.

Grupo Inneo. (2008). *Assembly Process*. Retrieved July 7, 2010, from Precast Concrete Wind Towers: http://www.inneotorres.es/web/index.php/en/installation-process.html

Hajar Ziad, L. D., Simon, A., & Petitjean, J. (2004). Design and Construction of the World First Ultra-High Performance Concrete Road Bridges. *2004 UHPC Symposium Proceedings*, (pp. 39-68). Kassel.

International Electrotechnical Comission. (2007). *IEC 61400-1 :Wind Turbines - Part 1: Design Requirements.* International Electrotechnical Commission.

International Electrotechnical Commission. (2007). *IEC 61400-1 {Ed. 3}.* IHS.

Japan Society of Civil Engineers. (2006). *Recommendations for Design and Construction of Ultra High Strength Fiber Reinforced Concrete Structures (Draft).* Tokyo: Subcommittee on Research of Ultra High Strength Fiber Reinforced Concrete.

Keierleber, B., Phares, B., Bierwagen, D., Courture, I., & Fanous, F. (2007). Design of Buchanan County, Iowa, Bridge Using Ultra High Performance Concrete and PI Girders. *2007 Mid-Continent Transportation Research Symposium.* Ames: Iowa State University.

Lafarge. (2009). *Concrete Reborn.* Lafarge.

LaNier, M. P. (2005). *LWST Phase I Project Conceptual Design Study: Evaluation of Design and Construction Approaches for Economical Hybrid Steel/Concrete Wind Turbine Towers.* Golden: National Renewable Energy Laboratory.

Lewin, T., & Sritharan, S. (2010). *Design of 328-ft (100-m) Tall Wind Turbine Towers Using UHPC.* Department of Civil, Construction, and Environmental Engineering. Ames: Iowa State University.

Lewin, T., & Sritharan, S. (2010). Mesasures for Reducing Energy Costs by Improving Design and Construction of Wind Turbine Towers. *WINDPOWER 2010.* Dallas.

Ma, J., & Schneider, H. (2002). Properties of Ultra-High-Performance Concrete. *LACER* .

Malcolm, D., & Hansen, A. (2002). *WindPACT Turbine Rotor Design Study.* Golden: National Renewable Energy Laboratory.

Mander, J., Priestly, M., & Park, R. (1988). Theoretical Stress-Strain Model for Confined Concrete. *Journal of the Structural Division, ASCE , 114* (8), 1804-1826.

Morin, V., Cohen Tenoudji, F., Feylessoufi, A., & Richard, P. (2001). Superplasticizer Effect on Setting and Structuration Mechanisms of Ultrahigh-Performance Concrete. *Cement and Concrete Research , 31* (1), 63-71.

Naaman, A. E. (2004). *Prestressed Concrete Analysis and Design.* Ann Arbor: Techno Press.

Orgass, M., & Klug, Y. (2004). Fibre Reinforced Ultra-High Perforamce Concretes. *International Symposium on Ultra High Performance Concrete*, (pp. 637-647). Kassel.

Pampanin, S., Priestly, M., & Sritharan, S. (2001). Analytical Modeling of the Seismic Behavior of Precast Concrete Frames Designed with Ductile Connections. *Journal of Eathquake Engineering , 5* (3).

Paulay, T., & Priestly, M. (1992). *Seismic Design of Reinforced Concrete and Masonry Buildings.* John Wiley & Son, Inc.

PCI Industry Handbook Committee. (2004). *PCI Design Handbook.* Chicago: Precast/Prestress Concrete Institute.

Post-Tensioning Institute. (2006). *Post-Tensioning Manual, Sixth Edition.* Phoenix: Post-Tensioning Institute.

Priestly, M., Seible, F., & Calvi, G. (1996). *Seismic Design and Retrofit of Bridges.* New York: John Wiley & Sons.

Reda, M., Shrive, N., & Gillot, J. (1999). Microstructural Investigation of Innovative UHPC. *Cement and Concrete Research , 29* (3), 323-329.

Renewable Energy Policy Network for the 21st Century. (2009, May 13). Renewables Global Status Report: Energy Transformation Continues Despite Economic Slowdown. *Press Release* . Paris, France: REN21.

Resplendino, J. (2004). First Recommendations for Ultra-High-Performance Concretes and Examples of Application. *International Symposium on Ultra High Performance Concrete*, (pp. 79-89). Kassel.

Ricciotti, R. (2005). Seonyu Footbridge, Seoul. In D. Bennet, *The Art of Precast Concrete* (pp. 156-159). Birkhäuser Basel.

SEI. (2005). *Minimum Design Loads for Buildings and Other Structures.* American Society of Civil Engineering.

Shah, S. P., & Weiss, W. J. (1998). *Ultra High Performance Concrete: A Look to the Future.*

Shutt, C. A. (2004). Precast Helps Projects Attain LEED Certification. *Ascent* , pp. 18-23.

Simiu, E., & Scanlan, R. (1996). *Wind Effects on Structures.* New York: John Wiley & Sons, Inc.

Smith, K. (2000). *WindPACT Turbine Design Scaling Studies Technical Area 2: Turbine, Rotor, and Blade Logistics.* Golden: National Renewable Energy Laboratory.

Sritharan, S. (2009). Use of UHPC for Sustainable Bridges in Seismic Regions. Raleigh.

Sritharan, S., Bristow, B., & Perry, V. (2003). Characterizing an Ultra-High Performance Material for Bridge Applications under Extreme Loads. *Proceedings of the 3rd International Symposium on High Performance Concrete.* Orlando.

Structural Engineering Institute. (2005). *Minimum Design Loads for Buildings and Other Structures.* Structural Engineering Institute of the American Society of Civil Engineers.

Tanaka, Y., Musya, H. O., & Kaneko, O. (2009). Design and Construction of Sakata-Mirai Footbridge Using Reactive Powder Concrete. *1st fib Conference.* Osaka.

Tang, M.-C. (2004). High Performance Concrete - Past, Present and Future. *2004 UHPC Symposium Proceedings* (pp. 3-9). Kassel: Schriftenreihe Baustoffe und Massivbau.

Thomas, D., & Sritharan, S. (2004). *An Evaluation of Seismic Design Guidelines Proposed for Precast Jointed Wall Systems.* Ames: Iowa State University.

Tindall Corporation. (2009). *Anatomy of a Titan*. Retrieved July 7, 2010, from Atlas CTB: http://www.atlasctb.com/anatomy.html

U.S. Department of Energy. (2008, May). *20% Wind Power by 2030.* Retrieved June 12, 2009, from 20percentwind.org

U.S. Department of Energy. (2008, August 27-28). Large Wind: Towers and Foundations. *U.S. Wind Manufacturing Roadmap Workshop: Achieving 20% Wind Energy by 2030* . Washington D.C.: U.S. Department of Energy.

United States Department of the Interior. (2009, September 2009). *Renewable Energy Sources in the United States*. Retrieved June 6, 2010, from The National Atlas of the United States of America: http://www.nationalatlas.gov/articles/people/a_energy.html

Vande Voort, T. L., Suleiman, M. T., & Sritharan, S. (2008). *Design and Performance Verification of UHPC Piles for Deep Foundations.* Ames: Center for Transportation Research and Education, Iowa State University.

Vazquez, T., & Hagen, S. F. (2009). *Codes and Standards for Wind Turbine Foundations: An Overview and Future Outlook.* Chicago.

Veers, P. S., & Butterfield, S. (2001). *Extreme Load Estimation For Wind Turbines: Issues and Opportunities for Improved Practice.* American Institute of Aeronautics & Astronautics.

Vergoossen, R. (2008). Tailor Made Bridge Design with Ultra-High-Peformance Concretes. *Tailor Made Concrete Structures* , 1067-1068.

Vernet, C. P. (2004). Ultra-Durable Concretes: Sturcutre at the Mirco- and Nanoscale. *Materials Research Society Bulletin , 29* (5), 324-327.

Williams, R. (2002, June 19). *A First for DUCTAL, The Concrete of the Future*. Retrieved June 8, 2010, from UBIFRANCE: http://www.infotechfrance.com/cgi-local/affichage_signet_secteur.pl?UNI_ID=8&RUB_ID=54&SS_ID=4152&SEC_ID=26

Wind Energy Planning. (2008, September 2008). *How Wind Turbines Work*. Retrieved July 6, 2010, from Wind Energy Planning: http://www.windenergyplanning.com/how-wind-turbines-work/